International Scientific-Technical and Production Journal

The Paton WELDING JOURNAL

August 2009 # 8

English translation of the monthly «Avtomaticheskaya Svarka» (Automatic Welding) journal published in Russian since 1948

Founders: E.O. Paton Electric Welding Institute of the NAS of Ukraine
International Association «Welding»

Publisher: International Association «Welding»

Address:
E.O. Paton Electric Welding Institute,
International Association «Welding»,
11, Bozhenko str., 03680, Kyiv, Ukraine
Tel.: (38044) 287 67 57
Fax: (38044) 528 04 86
E-mail: journal@paton.kiev.ua
http://www.nas.gov.ua/pwj

State Registration Certificate
KV 4790 of 09.01.2001

Subscriptions:
$324, 12 issues per year,
postage and packaging included.
Back issues available.

CONTENTS

Dear colleagues-welders: professors, teachers and workers of Chair of Welding Engineering of the Admiral Makarov National Shipbuilding University!

On behalf of scientists and workers of the E.O. Paton Electric Welding Institute of NASU and Editorial Board of «The Paton Welding Journal» we cordially congratulate You with the 50th jubilee of Chair of Welding Engineering.

Over many years the specialists of the Chair solve successfully the tasks of improvement of educational level of welders-engineers, perform development and realization of high-efficient technologies not only in shipbuilding, but also in many other branches of industry. During the whole period over 2900 welding production engineers were educated. Among the graduates there are over 80 doctors and candidates of sciences, honored science and technology workers.

Owing to initiative and creative work of the Chair staff under management of scientists-production workers and senior lecturers, such as A.I. Safonov and I.I. Dzhevaga at the first years and Prof. V.F. Kvasnitsky in latest 30 years, the actual scientific trends were formed and branch research laboratories and branches of the Chair at the largest enterprises of shipbuilding and ship machine building were founded.

For specialists education and performance of scientific work the Chair successfully collaborates with leading scientific and educational centers of Ukraine, Russia, Germany, China, actively participates in certification of welding production enterprises at the South of Ukraine.

The scientists and specialists from the E.O. Paton Electric Welding Institute and Editorial Board of Journal wish happiness, welfare and creative success to all staff, graduates and students of the Chair.

Editorial Board

STATUS OF WELDING PRODUCTION AT SHIPBUILDING PLANTS OF UKRAINE

V.F. KVASNITSKY[1], **B.V. BUGAENKO**[1], **Zh.G. GOLOBORODKO**[1], **V.M. ILYUSHENKO**[2], **N.P. ROMANCHUK**[3], **Yu.V. SOLONICHENKO**[3] and **A.N. SHAMRAJ**[3]

[1]Admiral Makarov National Shipbuilding University, Nikolaev, Ukraine
[2]E.O. Paton Electric Welding Institute, NASU, Kiev, Ukraine
[3]OJSC «Vadan Yards «Okean», Nikolaev, Ukraine

It is shown that in spite of economic problems all over the world the shipbuilding enterprises of Ukraine have available the modern efficient technologies and equipment which allows successful production of competitive products at the world market.

Keywords: *shipbuilding, assembly, welding, cutting, parts, sections, blocks, welding consumables, equipment*

The water transport of Ukraine is featured by ships with a life exceeding 20 years and even more. Since the fleet needs updating in the nearest time, it is necessary to build ships for inland navigation as well as for mixed river–sea type. The world shipbuilding market requires also shipbuilding production [1]. However, the world market entry is only possible providing that advanced technologies and equipment are implemented, capable to provide reduction in building terms, required quality and cost effectiveness of ships.

The aim of this work is the analysis (on the example of two plants) of technical and technological status of welding production of shipbuilding in Ukraine, primarily defining the niche of production of this branch at the world market.

The principal technology of shipbuilding depends on the method of hull forming and is defined by design peculiarities of a ship, production capacities of enterprise-manufacturer, program of ships building of this project and also by other factors.

The hulls of modern ships are composed of sheet and shaped rolled stock differed by sizes, shape and materials. The sheet parts make up 85--90 % of ship hull mass. The number of parts for building of one ship can reach several tens of thousands. The principal method of their manufacture is thermal cutting, whose share is about 80 % of the total volume of performed cutting, and the labor intensity is 50 % of the labor consumption for all the volume of works of the hull building shop.

For a long time the principal method of thermal cutting in shipbuilding was air-plasma cutting (APC) with air being used as a plasma gas. The gained experience [2] showed not only the technical-economical advantages of APC, but also its disadvantages. It is known that non-perpendicularity of cut edges for the most popular thickness of metal in shipbuilding can reach 2.5 mm per a side, which considerably influences the volume of deposited metal, productivity and welding quality, the size of angular deformations. In the process of cutting the saturation of metal edges with nitrogen occurs which results in probable formation of pores in welds during automatic submerged-arc welding of parts cut of metal of 5–12 mm thickness. To eliminate mentioned disadvantages a number of methods was used which turned to be low-effective. Today in Ukrainian shipbuilding, in particular in OJSC «Vadan Yards «Okean» (Nikolaev) the same methods and equipment are used as abroad, namely, the plasma cutting under water. The sheet being cut is immersed under water for 4–6 cm depth with plasma arc being in position under water. The machines «Numorex» and «Telerex TXB-10200» are used.

To improve the efficiency and utilization factor the machine «Telerex TXB-10200» is equipped with a portal having two heads of plasma cutters and two basins, which enable simultaneous cutting of symmetrical parts, for example, for left and right boards of a ship. In each basin there are two frames for mounting of sheets that allows working in the mode of a continuous layout. After finishing the cutting in the first basin, the machine moves to the second basin, and the next sheets are mounted in the first basin. The simultaneous cut out of two parts is shown in Figure 1.

The application of underwater plasma cutting requires big investments. In OJSC «Kherson Shipbuilding Plant» (KhSZ) the air plasma cutting with addition of water into plasma (APCAW) is successfully used. The implementation of APCAW was due to the carried out theoretical and experimental investigations which determined the optimal consumption of water supplied to air plasma [3–5].

It was established that while adding of water the partial pressure of nitrogen in plasma decreases due to plasma chemical reactions. The hydrogen being formed increases the intensity of electrical field and decreases the nitrogen content at the cut surface, thus increasing the power characteristics of the arc. The optimal concentration of water vapors in plasma hinders the saturation of edges both with nitrogen and hydrogen, excluding probability of pores formation in welding.

The reduction of plasma arc with water supplied through the tangential channels of optional outer nozzle, provides in APCAW the moving of anode spot into the depth of the cut and decreases the non-perpendicularity of its edges by 2.3–2.5 times. Their roughness 3–5 times decreases (R_z = 0.01–0.02 mm) and is comparable with a milled surface. A part of water from the cooling system of plasmatron is supplied through the radial channels of outer nozzle, forming the air-water shower, which cools the metal in the cut zone allowing the improvement of quality of its edges and precision of parts manufacture. Here the parts deformation is practically absent.


Figure 1. Machine «Telerex TXB-10200» in operation

At shipbuilding enterprises of Ukraine the considerable stock of modernized thermal cutting machines is under the service («Kristall», «Granat», etc.), having updated systems of automation and control. Machines with a modernized plasmatron also operate in OJSC «KhSZ» at the shop area of APCAW.

The cost of a ship is predominantly determined by the condition of assembly-welding production, the labor intensiveness of which is 15–18 % of total labor intensiveness of ship hull building. Moreover, the level of welding production is determined not only by labor intensiveness of actually welding jobs, but also by postweld works. If cleaning of a metal from spatters or also a weld before painting is required or the required roughness can not be achieved in welding, the labor intensiveness of ship hull building increases immensely. Therefore, in Ukraine as well as in the world shipbuilding the methods of welding and welding consumables are perfected.

To reduce metal spattering in shipbuilding welding, a welding solid wire in the mixture of argon and carbon dioxide (18–20 % CO_2) and also flux-cored wires in CO_2 are widely used. The mechanical properties of weld metal and welded joints in welding using wires Sv-08G2S and Sv-10GSNT in the mixture of gases are in compliance with standard requirements and are higher than in CO_2 welding. This is predetermined by considerably lower oxidation potential of shielding gas mixture as compared to CO_2 and higher coefficients of assimilation of alloying elements.

During welding in gas mixtures the coefficient of metal spattering decreases by more than twice. Here, small spatters are formed which do not stick to the surface of a rolled shapes being welded and are easily removed. The mentioned advantages of welding in gas

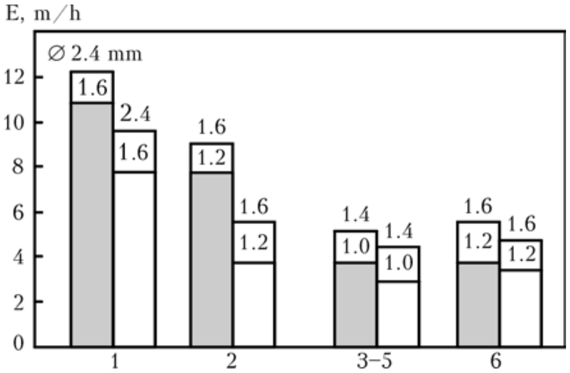

Figure 2. Efficiency of welding of typical ship hull structures (1–6 ---- see the Table) using solid (❐) and flux-cored (■) wire

mixtures are the reason of wide application of this process in shipbuilding. Along with the welding in gas mixtures the flux-cored wire welding becomes ever more applicable.

In shipbuilding of Ukraine the mechanized welding is mainly applied using thin flux-cored wire in CO_2 and also self-shielding wire. The Table shows the types of ship hull structures and most effective methods of their welding applied in Ukraine [6, 7].

The most reasonable is application of automatic welding of butt and fillet welds in flat position for joining of plane sections with a framing of one direction; mechanized and robotic welding of fillet welds in flat and vertical positions for plane sections with a framing of two directions; mechanized and robotic welding of fillet welds in flat, vertical and horizontal positions for open half-volume and volume sections; mechanized and robotiic welding of fillet welds in all spatial positions for closed half-volume and volume sections; mechanized and robotic welding of butt and fillet welds mainly in flat position for frames, basements, small sub-assemblies; mechanized and automatic welding of butt and fillet welds in all spatial positions for blocks of sections and ship hulls on the building berth.

Technical-economic analysis of efficiency of different welding methods was performed in works [8–14]. The productivity of deposition performed using flux-cored and solid wire for welding of structures of different types (Nos. 1–6 according to the Table), is shown in Figure 2.

At the shipbuilding plants of Ukraine the thin flux-cored wire of rutile (AN21, PPs-TMV7, PZ 6110, Megafil 713) and basic (PZ 6130, OK Tubrod 15.06) types of diameters 1.2–1.6 mm are used for manufacture of hull structures. The productivity of CO_2 deposition using these wires is higher as compared with solid wire welding by 2--3 kg/h, and as to the effectiveness it is comparable with automatic submerged-arc welding.

Flux-cored wire of 1.6 mm diameter is recommended for mechanized welding of fillet welds of half-volume sections. To perform welds of majority of ship hull structures in the positions different from flat, the use of flux-cored wire of rutile type of 1.2 mm diameter is most challenged. The application of these wires with rapidly hardened slag not only provides welds with a smooth surface and easy removal of slag, but allows reduction of electrode metal spattering in comparison with CO_2 welding by 3–5 times.

The results of analysis of specific expenses per 1 kg of deposited metal showed that welding in gas mixtures of large-tonnage vessels using solid and thin flux-cored wire provides decrease of cost of deposited metal due to high productivity of welding process and decrease in volume of welds cleaning before painting.

The main method of further increase of welding efficiency is increase of automation level due to replacement of mechanized welding by automatic and robotic process. The experimental works performed together with National Shipbuilding University and «Vadan Yards «Okean» showed advance in application of robotic welding using thin flux-cored wire in manufacture of volume sections [6, 7], however it also implies the solution of number of organizational and technical problems.

If robotization of welding processes in shipbuilding of Ukraine is future prospect, then the automatic submerged-arc welding finds its wide application today. This welding method is most frequently used for manufacture of plane sections with the framing of one direction. At many enterprises the plane sheet panels

Basic types of welded ship hull structures and methods of their welding

No.	Type of structure	Distribution of volumes of welding works as to spatial position, %				Welding method
		Flat	Vertical	Horizontal	Overhead	
1	Plane sections with the framing of one direction	100	--	--	--	A
2	Plane sections with the framing of two directions	70--90	30--10	--	--	M, R
3	Open semi-volume sections	40	55	5	--	M
4	Close semi-volume and volume sections	40	20	10	30	M
5	Frames	60	30	10	--	M, R
6	Blocks of sections, hull	10	30	30	15	A, M

Notes. 1. A ---- automatic; M ---- mechanized; R ---- robotic. 2. The rest 15 % of welded joints (No. 6) are produced using covered electrodes.

are manufactured using mechanized assembly-welding production lines.

In mechanized production line of ESAB company three main positions can be distinguished. At the first one, equipped with a portal with double-arc suspended system A6, the one-sided double-arc welding into the common pool on flux-copper backing of butt joints of sheet panels of thickness from 8 up to 22 mm without edge preparation is performed. Here the first arc is burning at direct current of reversed polarity, whereas the second arc — at alternating current. At the second position the back run of butt joints of sheet panel using automatic machine of A6 system of tractor type at direct current of reversed polarity is performed. At the third position the assembly and welding of framing of main direction with plain sheet panel is performed. Here the framing is supplied to a sheet panel from the store, it is pressed to a sheet panel by a system of hydraulic jacks and fixed on tacks. The T-joint is performed from the middle to the edges using four suspended welding heads of A6 type. The enlargement of sheet panels is performed on the plane stands using automatic welding under flux layer without any backings.

To reduce residual deformations before welding the tensile stresses along the butt of welded sheets are created, that is provided due to transverse shrinkage of run-out and fastening tabs by deposition of transverse beads on them.

In OJSC «KhSZ», to prevent deformation in manufacture of plane sections at the line of ESAB company, the framing of main direction is welded to the steel girder protruding over the plane of sheet panel movement. Due to pressing of framing by hydraulic press, a deflection is formed on the sheet panel, compensating welding deformations.

The welding of plane longitudinal sub-assemblies (stringers, floors, T-girders, etc.) of thickness up to 14 mm is made without edge preparation, while at thickness of more than 14 mm — with edge preparation.

If the possibility of positioning of butts of welded parts of the same thickness into the one line is available the automatic welding is performed under the layer of flux for one pass. If there is no possibility or reasonability of automatic welding application due to curvilinearity or non-flatness, the mechanized welding in mixture of shielding gases (Ar + CO_2) is used for manufacture of sub-assemblies. To decrease labor intensiveness of work for manufacture of volume sections, and also sections manufactured in «beds», the mechanized welding using flux-cored wire with a reversed weld formation using forming ceramic backings (FCB) is used at the enterprises. The manufacture of bottom section of a ship is realized on the floor of the second bottom (Figure 3). All the framing elements are assembled and welded between themselves and floor of the second bottom, thus presetting the shape of contours of the external lining. The latter is formed of the panels and sheets fixed to the mounted framing. For the mechanized welding in shielding gases (Ar + 18 % CO_2) all butts are assembled using FCB which

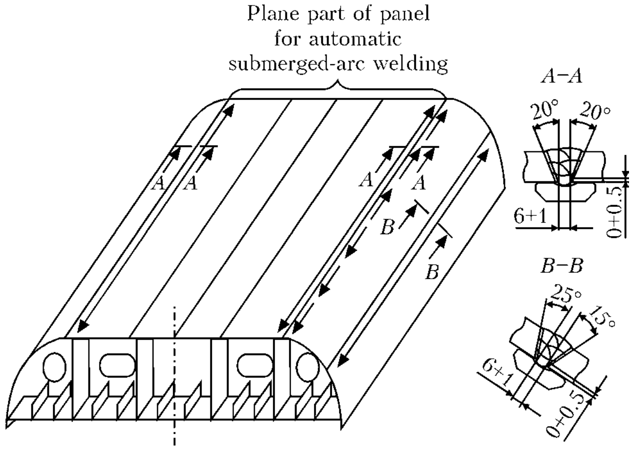

Figure 3. Scheme of welding of external lining of bottom sections of a ship: long arrow — direction of slots welding; short arrow — direction of welds of root passes on forming ceramic backings

provide reverse formation of butt welds. Thus, it eliminates operations on cleaning of root weld and back run of butt joints in closed volume. The welding of framing with the external lining is performed in flat position using a cell method after turning over the section.

The volume board sections of middle part of a ship are assembled at the coke standing «beds» at the lining of the inner board, curvilinear board sections — at the external lining at the standing «beds». During the manufacture of these sections all butt joints are performed using mechanized welding in shielding gases on FCB.

To relieve the inner stresses and to reduce angular deformations, «Vadan Yards «Okean» performs heat treatment of T-joints using special three-flame torch from the smooth side of the section (heating up to 350–400 °C) at the areas of the length of 200 mm with a pitch of 100 mm in the place of mounting the framing directly after its manufacture. The butt joints are heated in the similar way using double-flame torch.

The most critical are site joints during the forming of blocks of sections and hull, in particular, butts and slots of external lining of thickness of 8–30 mm, which were performed for a long time using arc welding. Mechanized welding with a free weld formation 1.3–1.5 times increases the process efficiency, but in positions different from the flat one, the volume of weld pool is limited to prevent its flowing out. The technology of mechanized welding in mixture of shielding gases (Ar +18 % CO_2), implemented at the enterprises using flux-cored wire in combination with FCB, provide high quality of weld formation on face and reversed sides at significant decrease of metal spattering, increase in labor productivity, decrease in labor intensiveness of preparation of welded joints for painting. The FCB are located on the side of framing except of external lining of bottom section where they are positioned on the smooth surface. The FCB are used also during framing welding.

The further increase in welding efficiency in manufacture of ship hull on the berth is provided by the process automation. The shipbuilding enterprises have mastered the welding of vertical site joints using the flux-cored wire and a forced weld formation developed by the Paton Institute [12], and also one-sided welding of horizontal slots in the vertical plane using ceramic backings.

Coming from the specific requirements to automatic welding under site conditions on the berth, the automatic machines traveling directly along the edges being welded or guiding racks have been designed and manufactured. For example, automatic machine A-1150u is designed for welding using flux-cored welding of vertical and inclined butt welds with a forced formation on the metal of 8–30 mm thickness, that is realized using two water cooling shoes along the butt with a curvature of 2 m.

For welding of site slots of external ship lining under the conditions of the berth the Paton Institute has developed the automatic machines AD-119 and AD 330M, which allowed twice increasing the labor productivity and decreasing the labor intensiveness of works due to elimination of gauging of root weld and its post rewelding.

The developed technology is based on the application of multi-pass welding using the flux-cored welding to perform horizontal welds in the vertical plane at one-sided asymmetric edge preparation. Here the reverse weld formation on the ceramic backing positioned on the inner side of external hull lining is provided. The welding is performed using combined way: root and final passes are performed using flux-cored wire of 1.6 mm diameter with a free formation, and filling of a groove is performed using flux-cored wire of 3.0 mm diameter with a semi-forced weld formation. Such technology provides achievement of quality welded joint with a guaranteed weld root penetration and performance of a final pass with minimum undercuts.

The considered welding technologies and equipment are also mastered by other shipbuilding plants of Ukraine. The automatic welding technologies of site welds are high-efficient in building of large-tonnage ships and can provide preference of Ukraine at the world market in the area of shipbuilding.

Nowadays other challenging welding technologies were also developed in Ukraine, in particular, radically new welding processes using combined and hybrid heating sources [13–15] and also underwater welding providing the possibility of production of any large-tonnage vessels while joining their parts afloat, and also platforms of other structures of different purpose [16].

It should be noted that hundreds of welding procedures were certified at shipbuilding enterprises of Ukraine. All welders possess certificates of the qualification societies and confirm them every half a year. All technologies are regulated by technological instructions and introduced into standards of enterprises.

Thus, in spite of economic problems the shipbuilding enterprises existing nowadays in Ukraine have not only preserved their production potential, but also successfully implement the best technologies of modern welding production.

National shipbuilding has available necessary high-efficient technologies, modern equipment, highly-qualified specialists which allows manufacturing, capable to compete at the world market.

1. Egorov, G.V. (2008) About possibilities of entry of Ukraine on world shipbuilding market. *Zbirnyk Nauk. Prats NUKB*, **6**, 3–15.
2. Dragan, S.V., Kvasnitsky, V.V., Romanchuk, N.P. et al. (2004) Welding and cutting processes in shipbuilding of Ukraine. *The Paton Welding J.*, **8**, 2–5.
3. Serbin, S.I., Kvasnitsky, V.V., Goloborodko, Zh.G. et al. (2004) Modeling of gas phase composition in plasma cutting of ship hull steels. *Ibid.*, **8**, 11–14.
4. Kvasnytskyy, V.F., Kvasnytskyy, V.V., Egorov, G.V. et al. (2005) Production technology peculiarities of ships body components from sheet product. In: *Proc. of 12th Int. IMAM Congress on Maritime Transportation and Exploitation of Ocean and Coastal Resources* (Lisboa, Portugal, Sept. 26–30, 2005). London: Taylor and Francis Group, Vol. 1, 935–940.
5. Kvasnytskyy, V.V., Egorov, G.V., Goloborodko, Zh.G. et al. (2008) Influence of plasma cutting methods of the quality of ship hull details and welded constructions. In: *Proc. of 13th Int. IMAM Congress on Maritime Industry, Ocean Engineering and Coastal Resources* (Varna, Bulgaria, Sept. 2–6, 2007). London: Taylor and Francis Group, Vol. 1, 477–482.
6. Kvasnitsky, V.F., Dragan, S.V., Solonichenko, Yu.V. et al. (1998) Efficiency of application of thin flux-cored wires in mechanized and robotic welding in shipbuilding. In: *Abstr. of Papers of Int. Conf. on Welding and Related Processes into the 21st Century*. Kiev: PWI, 52–53.
7. Kvasnitsky, V.F., Dragan, S.V., Gavrilenko, E.D. et al. (1998) Influence of design-technological factors in robotic technology of production of large-sized ship hull structures. *Zbirnyk Nauk. Prats UDMTU*, **8**, 68–79.
8. Kvasnitsky, V.F., Dragan, S.V., Gavrilenko, E.D. et al. (1999) Evaluation of efficiency in application of thin flux-cored wires in welding of ship hull structures. *Avtomatich. Svarka*, **11**, 4–7.
9. Kvasnitsky, V.F., Dragan, S.V., Ivashchenko, G.M. et al. (1999) Economical aspects in application of national and foreign welding consumables for production of ship hull structures. *Zbirnyk Nauk. Prats UDMTU*, **6**, 19–26.
10. Kvasnitsky, V.F., Solonichenko, Yu.V., Dragan, S.V. et al. (2002) Analysis of efficiency of shielded-gas welding technological versions in production of ship hull structures. In: *Proc. of 1st Int. Sci.-Pract. Conf. on Protection of Environment, Health, Safety in Welding Production* (Odessa, Sept. 11–13, 2002). Odessa: Astroprint, 568–575.
11. Kvasnitsky, V.F., Dragan, S.V., Gavrilenko, E.D. et al. (1998) Technological capabilities in efficiency increase of ship hull production. *Zbirnyk Nauk. Prats UDMTU*, **7**, 69–80.
12. Pokhodnja, I.K., Schlepakov, W.N., Iljuschenko, W.M. et al. (1995) Hochleistungsschweissen von Vertikalnaehten mit Zwangsformungj In: *Sondertagung Schweissen in Schiff- und Metallbau mit Kolloqium* (Rostock, 4–5 Mai, 1995). Duesseldorf: DVS, 23.
13. Voropaj, N.M., Ilyushenko, V.M. (2003) Hybrid processes of arc and plasma welding. *Svarshchik*, **2**, 22–27.
14. Voropaj, N.M., Ilyushenko, V.M., Mishenkov, V.A. (2005) Technological capabilities of the processes of gas-shielded pulsed twin-arc welding (Review). *The Paton Welding J.*, **7**, 38–42.
15. Shelyagin, V.D., Krivtsun, I.V., Borisov, Yu.S. et al. (2005) Laser-arc and laser-plasma welding and coating technologies. *The Paton Welding J.*, **8**, 44–49.
16. Gretsky, Yu.Ya., Maksimov, S.Yu. (1997) Technological processes of underwater welding and cutting of steels with flux-cored wires. In: *Proc. of ASM Int. European Conf. on Welding and Joining Science and Technology* (Madrid, Spain, March, 10–12, 1997), 165–179.

PECULIARITIES OF FORMATION OF STRESS-STRAIN STATE IN DIFFUSION BONDS BETWEEN DISSIMILAR MATERIALS

V.I. MAKHNENKO[1] and **V.V. KVASNITSKY**[2]
[1]E.O. Paton Electric Welding Institute, NASU, Kiev, Ukraine
[2]NTUU «Kiev Polytechnic Institute», Kiev, Ukraine

Stress-strain state (SSS), allowing for plastic creep strains, in cylindrical parts of metals with different physical-mechanical properties in diffusion bonding was studied by computer modelling based on the finite element method. The mechanisms of creep in diffusion bonds, as well as formation of SSS in them, were established.

Keywords: *diffusion bonding, dissimilar materials, stress-strain state, plastic strain, cylinder–cylinder assembly, sleeve–sleeve assembly, stagnation zone*

Parts made by diffusion bonding in vacuum [1, 2] are widely applied in machine building and other industries. This joining method makes it possible to produce components and assemblies with unique design and performance characteristics. Traditionally, selection of process parameters is based on a uniform distribution of the force of compression over the entire joining area. But in fact, as follows from study [3], in the case of aluminium strip to silicon crystal bonding the scheme of the stressed state and its components are different in different zones of the bond, this affecting the bond formation conditions. The most favourable conditions for activation of the mating surfaces of pieces and their bonds occur in the zone of tangential stresses and shear strains [3]. As shown in studies [4–7], diffusion bonding with thermal cycling is an efficient method to induce tangential stresses and localise plastic strains in the bond when joining metals with different physical-mechanical properties [8]. The above studies are based on modelling of the stress-strain state (SSS) of cylinder--cylinder (C--C), sleeve–sleeve (S–S) and sleeve–flange assemblies under elasticity and instantaneous plasticity conditions, where the strain values are independent of time [9]. Under real conditions of diffusion bonding there are also the creep strains that affect SSS of an assembly.

The purpose of this study was to investigate SSS of the C–C and S--S assemblies in diffusion bonding allowing for the creep strains, as well as to establish the general mechanisms of different types of strains and their effect on formation of the diffusion bonds.

SSS in cylindrical assemblies was analysed from the results of computer modelling by the finite element method. The equation of creep rate under diffusion bonding conditions was preliminarily determined to model SSS with allowance for the creep strains. Reported [10, 11] is a number of equations to determine the creep stage.

Strain diagrams given in [10] were used to establish the creep mechanisms, and experimental studies were carried out under uniaxial loading conditions to determine the creep parameters by the temperature perturbation method [11]. It was found out that under certain conditions of diffusion bonding the creep actually begins from the second stage, and its rate can be determined from the following equation:

$$\dot{\varepsilon} = Bp^m \exp\left(-\frac{\Delta H_n}{RT}\right), \qquad (1)$$

where B and m are the coefficients for a given material; p is the effective stress (compression pressure); ΔH_n is the creep activation energy; T is the temperature; and R is the universal gas constant.

At a constant temperature, equation (1) can be simplified to $\dot{\varepsilon} = C_1 p^{C_2}$, where C_1 and C_2 are the coefficients. It was experimentally established that $m = 3.5$–4.6 under diffusion bonding conditions for metals under investigation (armco iron, steels 10854, 12Kh18N9T, and heat-resistant alloys), this evidencing the presence of the dislocation creep and corresponding to the strain diagrams [10].

As shown in studies [5–7], a complex stressed state forms within the bond zone between dissimilar materials. For these conditions, the creep rate equation expresses the Mises--Hankey theory of general deformation, which is based on the Mises law of flow and equivalent stresses determined by using the known equation [12].

It is impossible to conduct creep tests in diffusion bonding of dissimilar materials. However, as shown in study [12], in many cases it is possible to use results of uniaxial loading tests to determine creep under conditions of the complex stressed state and at variable stresses and temperatures.

The effect of cyclic loading depends upon the maximal stress time to cycle period ratio. Acceleration of the creep strain at variable stresses, compared with creep at a constant stress, was found to take place with decrease in the above ratio due to reduction of the maximal stress time or increase in the loading cycle period [12]. The effect of cyclic loading on the creep rate is estimated by coefficient ψ, which is a ratio of the creep rate relative to the «net» loading time in creep with periodic loading to the creep rate at a constant stress. The experiments proved the strain dependence of coefficient ψ. For example, at a strain of more than 0.1 % per loading cycle, its value is close to one. As follows from study [12], at a high temperature and short period of variations in stress, even in the case where a mean stress is superimposed by a sinusoidal cyclic stress (repeated-stress cycle), the creep curve is the same as in the case of static creep. Results of the creep tests [12] of low-carbon steel, nickel alloy Nimonic 75 and other metals under conditions of uniaxial loading and complex stressed state caused by tension and torsion show that the creep curve is the same independently of the tensile stress to torsion stress ratio.

In diffusion bonding with thermal cycling, the creep strain occurs at a variable temperature and variable stress. The effect of variations in the above values on the creep rate is characterised by the internal state parameter, which is determined by creep strain ε and described by the mechanical equation of state of solid [12] $\dot{\varepsilon} = f(p, T, \varepsilon)$, i.e. the creep rate at any time moment is determined by the stress, temperature and strain at the given time moment.

Based on the theory of strain and time hardening, there are two approaches to a specific writing of the mechanical equations. As to the character of variations in diffusion bonding parameters, we chose the equation for time hardening, which has the following form for the first stage of creep:

$$\dot{\varepsilon} = C_1 p^{C_2} t^{C_3} \exp\left(-\frac{C_4}{T}\right), \qquad (2)$$

where $C_1 > 0$, C_2 and C_3 are the coefficients determined from the experimental curves of creep of a material; $C_4 = (\Delta H_n/R)$; and t is the strain time.

The values of strain at the first and second stages of creep, proceeding from expressions (1) and (2), are determined from the following equation:

$$\varepsilon = C_1 p^{C_2} \frac{t^{C_3+1}}{C_3+1} \exp\left(-\frac{C_4}{T}\right) + C_5 p^{C_6}\, t \exp\left(-\frac{C_7}{T}\right), \qquad (3)$$

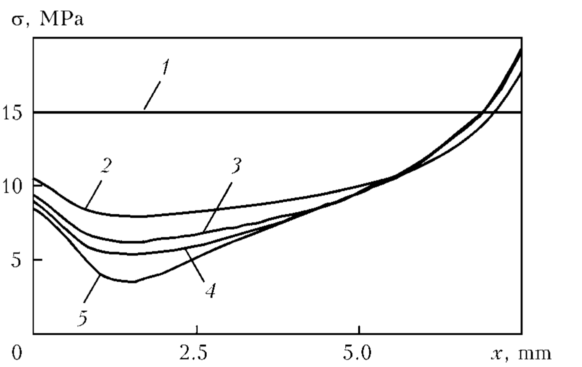

Figure 1. Diagrams of distribution of equivalent stresses along the bond in material 1 in loading by compression pressure of 15 MPa in 0 (*1*), 30 (*2*), 60 (*3*), 90 (*4*) and 300 (*5*) s after loading

where $C_1 > 0$, C_2, C_3, $C_5 > 0$ and C_6 are the coefficients determined from the experimental curves of creep of a material; $C_4 = (\Delta H_{n(1)}/R)$; and $C_7 = (\Delta H_{n(2)}/R)$.

Coefficients C_5–C_7 for the steady-state stage of creep in equation (3) were determined by the temperature perturbation method. As the energy of activation of a high-temperature creep is identical at the first and second stages [13], coefficient C_4 was assumed to be equal to C_7. Values of the rest of coefficients C_1–C_3 were determined by processing the creep curves.

Calculations of SSS were made by using equations (1) and (3) for the cases of loading of the S–S assembly by a constant pressure of 15 MPa, thermal cycling and pressure with thermal cycling. Combination of the materials to be joined was such that the creep process occurred only in the upper piece (1). The creep rate in this piece was determined from equation (1) at T = 1373 K. Values of the coefficients were taken from the experimental data: $C_1 = 2\cdot10^{-31}$ and $1\cdot10^{-31}$ (models 1 and 2, respectively), and C_2 = 3.65.

Fields of radial, axial, circumferential, tangential and equivalent stresses, as well as plastic strains, were investigated for both models and all variants of loading. It was found that the creep rates at loading with a constant pressure of 15 MPa form a complex stressed state in one of the materials being joined, both in the upper and lower non-deformed piece. Radial, circumferential and tangential stresses form and grow, and particularly near the bond, their maximal values reaching the level of the applied axial ones as early as within the first minutes of holding. Uniformity of axial stresses is also markedly violated. In general, they decrease in both materials, but only in a small zone on the external surface of material 2 [5–7] they increase 2–2.5 times. The fields of all the stresses rapidly stabilise, and their character remains almost unchanged during subsequent holding.

The field of equivalent stresses also changes according to individual components. As seen from the diagrams of distribution of equivalent stresses (Figure 1), in material 1 the equivalent stresses markedly decrease in a major part of the bond as early as within the first minute of holding, this decrease being especially pronounced in the internal part of the bond at a distance of about 1/4 of thickness of the sleeve from its internal surface. In material 2, on the contrary, they grow in a major part of the bond to a level which is 2 times or more in excess of nominal values of the equivalent stresses, reaching the maximal values near the internal and external edges of the bond.

To compare the SSS modelling results with the results obtained by using equations (1) and (3), Figure 2 shows time variations in equivalent and tangential stresses at a point located at a distance of 5 mm from the internal surface of the sleeve and 0.2 mm from the bond in material 1. It can be seen from the Figure that stresses differ in value only within the first minute, further on they fully coincide. Therefore, for a time of impact of the stresses equal to more

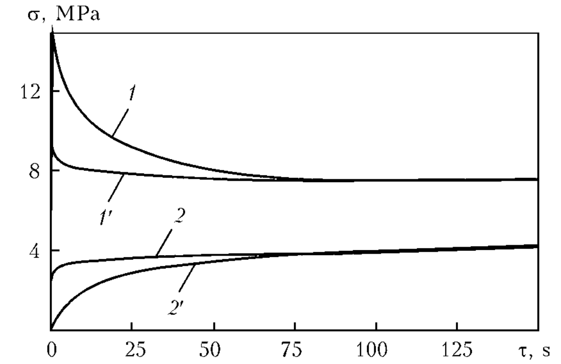

Figure 2. Variations of equivalent (curves *1*, *1′*) and tangential (curves *2*, *2′*) stresses with time in central part of the bond according to equations (1) (curves *1*, *2*) and (3) (curves *1′*, *2′*)

than 1.0–1.5 min, it is possible to use a simpler equation to reduce the calculation time. The equivalent stresses form a complex field of plastic creep strains (Figure 3).

Unlike the stress fields, the strain field changes during the entire holding time. However, its main peculiarity persists — plastic strains develop in material 1 mainly at a distance from the bond. A point of concentration of strains forms at the external edge of the bond during holding, the zone of increased strains near this point gradually increases, but there are hardly any plastic strains in the major part of the bond. It is reported [13] that one of the methods to localise plastic strains within the bond zone in solid-state joining is to increase the strain rate. In diffusion bonding with its low-intensity force effect, such method cannot be realised at a low strain rate ($1\cdot10^{-6}$ – $1\cdot10^{-4}$ s^{-1}). Analysis of SSS with allowance for instantaneous plastic strains shows that thermal cycling is an efficient method for localisation of plastic strains within the bond zone [7]. The fields of instantaneous plastic strains, allowing for instantaneous plasticity, in the S–S assembly loaded by pressure, thermal cycling and pressure with thermal cycling are shown in Figure 4.

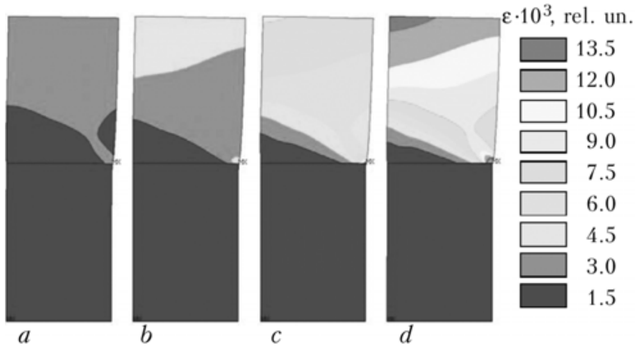

Figure 3. Field of plastic creep strains ε in loading with compression at different time moments after loading: *a* — 60; *b* — 90; *c* — 180; *d* — 300 s

It can be seen from the Figure that thermal cycling without and with pressure provides the distribution of stresses in height of the pieces joined that is close to the ideal one. Also, it leads to a more uniform distribution of plastic strain in the bond, compared with compression at a constant temperature. However, SSS for the C–C assemblies under thermal cycling conditions is characterised by a point with zero tangential stresses present in the bond, and by a zone with minimal equivalent stresses [4, 6, 7] and minimal plastic strains (Figure 4, *b*) present near the above point. It is suggested that the point and zone near it should be called the stagnation point and zone, in analogy with the terminology used in the theory of hot pressure working of metals [11]. Formation of plastic strains in this zone is hindered, and absence of shear strains excludes any strain activation of the mating surfaces [3]. Tangential stresses in bonding of cylinders are equal to zero at the centre of a cylinder, and in bonding of sleeves they are equal to zero near the internal surface. The character of the fracture surface in mechanical tests of the bonded specimens is indicative of the fact that their fracture begins particularly in these zone. As seen from Figure 5, *a*, the fracture surface of specimens of the C–C assembly made from dissimilar materials has a conical shape

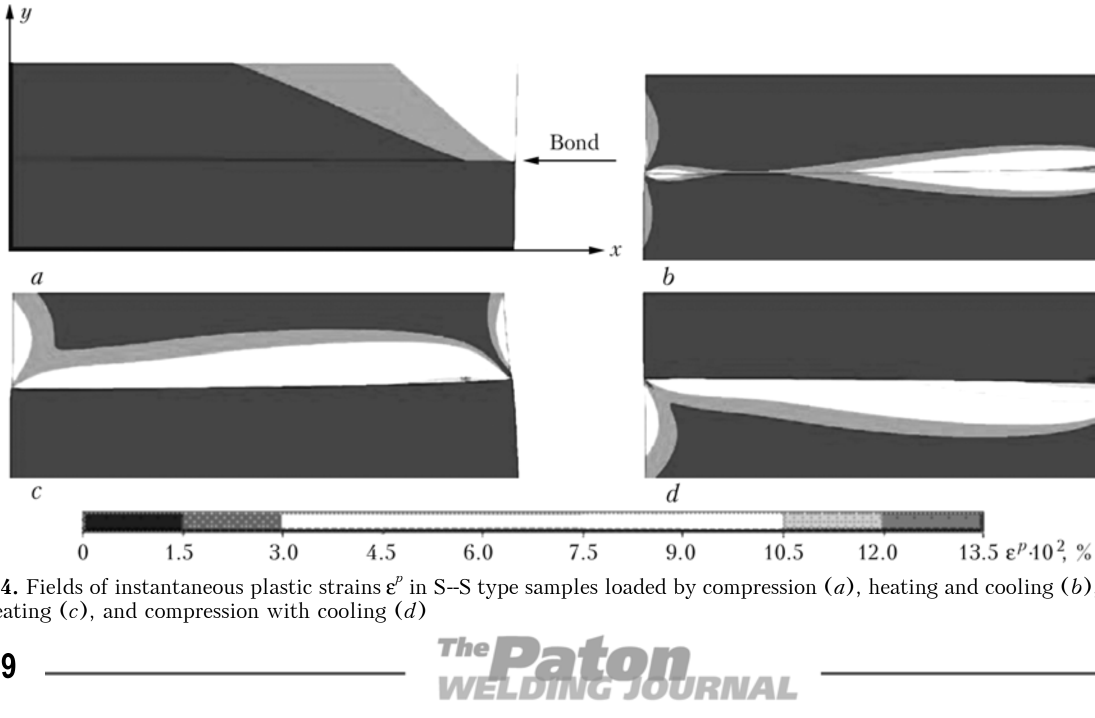

Figure 4. Fields of instantaneous plastic strains ε^p in S–S type samples loaded by compression (*a*), heating and cooling (*b*), compression with heating (*c*), and compression with cooling (*d*)

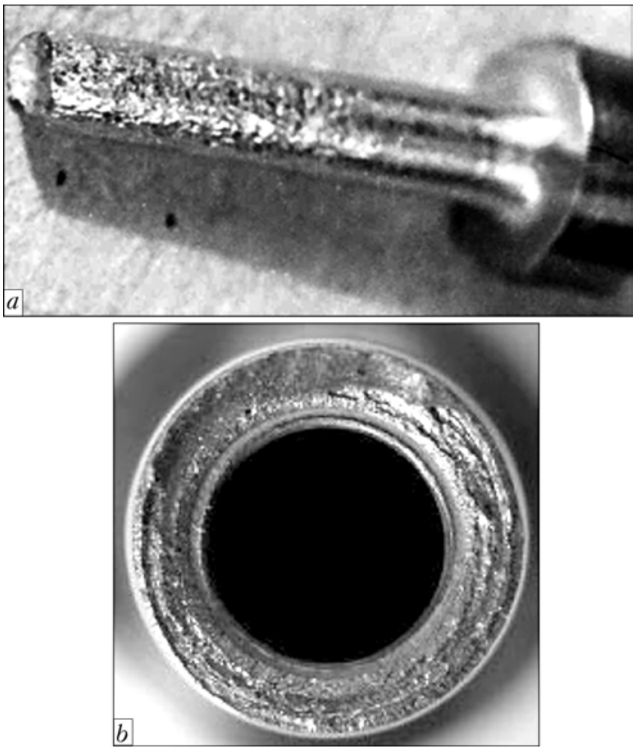

Figure 5. Character of fracture surfaces on bonded samples of cylinders (*a*) and sleeves (*b*)

with an apex on the specimen axis, and that of the sleeves has the form of a strip near the internal surface (Figure 5, *b*). The fracture develops from the strip to the external and internal surfaces with a tear in a less strong metal.

The most uniform distribution of plastic strains in the bond is provided by compression combined with thermal cycling (see Figure 4, *c, d*), which provides the full-strength bonds with a fracture occurring in tests in a less strong metal. Modelling of SSS allowing for instantaneous plastic strains shows that plastic strains reach their highest values in compression combined with thermal cycling in a case where the materials joined have close yield stress values. In this case the plastic strains propagate in the bond almost uniformly, being localised during heating and cooling in turn in one and the other material.

Modelling of SSS of cylindrical assemblies allowing for creep strains proved the mechanisms of its formation established in solving the elasticity and instantaneous plasticity problems. A variant of holding of pieces of dissimilar materials at a bonding temperature and constant pressure does not provide formation of plastic strain in the entire bond. Moreover, the creep rate in material 1 within the bond zone is much lower than at a distance from it, this leading to increased general strains of the bonded assembly. The fields of strains for variants of thermal loading and

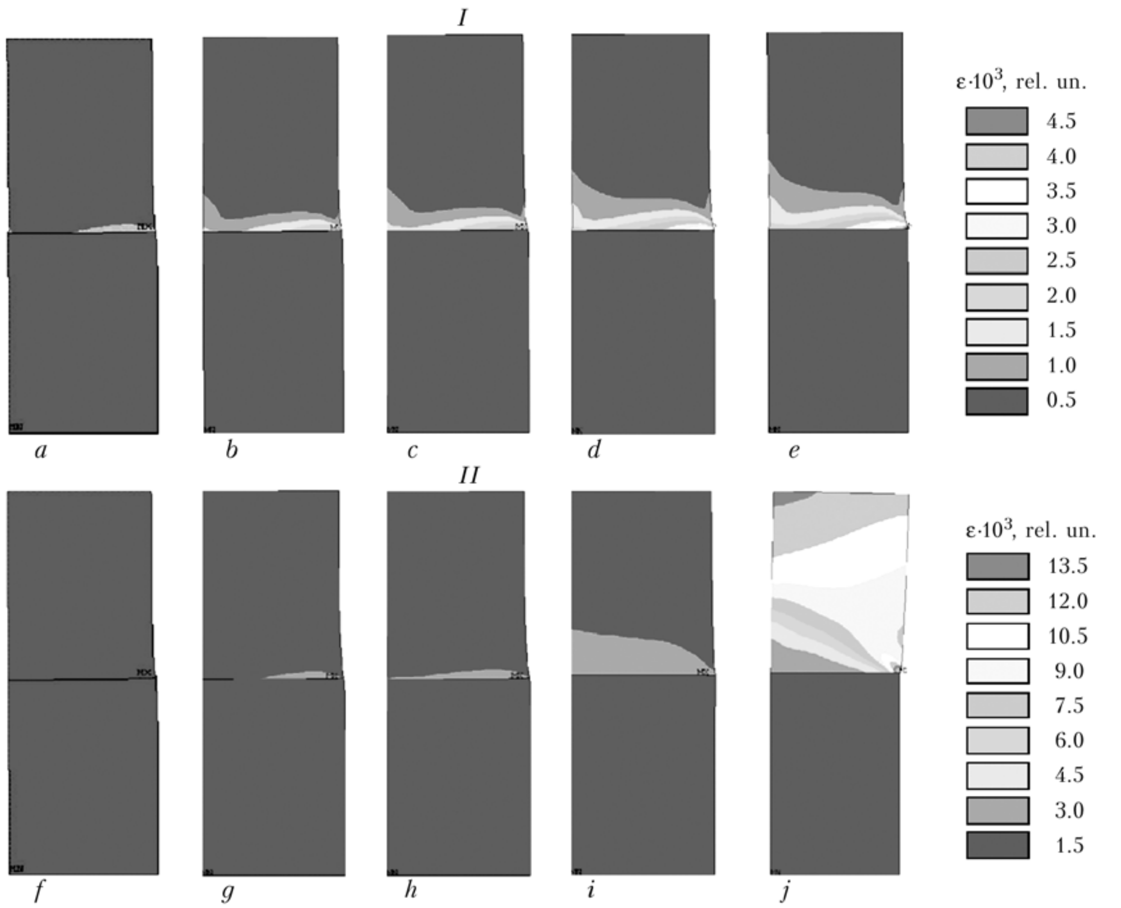

Figure 6. Fields of creep strains ε under thermal (*I*) and combined loading by compression and increase in temperature (*II*) at different time moments after loading: *a, f* ---- 0; *b, g* ---- 1; *c, h* ---- 2; *d, i* ---- 30; *e, j* ---- 300 s

compression with thermal cycling, allowing for creep strains, are shown in Figure 6.

The level of equivalent stresses in both materials decreases in thermal loading as a result of creep of material 1. Plastic creep strains are concentrated in material 1 near the bond, and with time they cover an increasingly wider zone (Figure 6, *a*).

Under combined loading by compression and heating, the strains in the first seconds are also concentrated near the bond (Figure 6, *b*), and they reach their maximal values during 1 min, their distribution in this case being almost uniform. In long-time holding (for 300 s), the creep strains propagate in the entire height of a specimen, their values growing with distance from the bond.

As proved by the investigation results, the creep strains increase the level of plastic strains both in thermal and combined loading by compression and heating. In thermal cycling, they level the distribution of strains in the bond.

Therefore, the calculation results showed that the combined loading by compression and thermal cycling is indicated only in short-time loading, where the instantaneous plasticity strains are distributed along the bond almost uniformly, thus providing formation of a physical contact between the materials joined over the entire bond. The initial stresses, when they decrease due to creep of a material, should not be restored. At the holding stage, it is better to apply purely thermal loading, which provides not only localisation of plastic creep strains near the bond, but also their sufficiently uniform distribution over its entire surface area.

CONCLUSIONS

1. Modelling of SSS allowing for creep strains in diffusion bonding of dissimilar materials showed persistence of the main mechanisms of its formation established for the stages of elastic deformation and formation of short-time (instantaneous) plasticity strains, as well as some increase in the level of strains.

2. In terms of SSS, combined loading by compression and increase in temperature is most efficient in the initial period of formation of the bond, where plastic strains are distributed almost uniformly along the bond.

3. At the holding stage, it is better to apply a low compression pressure and thermal loading, which provide not only localisation of plastic strains near the bond, but also their sufficiently uniform distribution over its entire surface area. The holding time and compression pressure values should be selected with allowance for properties of the materials being joined (creep resistance).

1. Lyushinsky, A.V. (2006) *Diffusion bonding of dissimilar materials*. Moscow: Akademiya.
2. Kireev, L.S., Peshkov, V.V., Selivanov, V.F. (2003) *Physical chemistry of the process of production of titanium-based porous compact materials*. Kiev: PWI.
3. Krasulin, Yu.L., Nazarov, G.V. (1976) *Pressure microwelding*. Moscow: Metallurgiya.
4. Kuznetsov, V.D., Kvasnitsky, V.V., Ermolaev, G.V. et al. (2007) General principles of stressed state formation in diffusion bonding of cylindrical shape parts. *Zbirnyk Nauk. Prats NUKB*, **6**, 62--73.
5. Makhnenko, V.I., Kvasnitsky, V.V., Ermolaev, G.V. (2008) Effect of physical-mechanical properties of the materials joined and geometry of the parts on distribution of stresses during diffusion bonding in vacuum. *The Paton Welding J.*, **1**, 2--8.
6. Makhnenko, V.I., Kvasnitsky, V.V., Ermolaev, G.V. (2008) Stress-strain state of diffusion bonds between metals with different physical-mechanical properties. *Ibid.*, **8**, 2--6.
7. Makhnenko, V.I., Kvasnitsky, V.V. (2009) Stress-strain state of assemblies of the cylindrical shape in diffusion bonding. *Ibid.*, **2**, 2--7.
8. Kvasnytsky, V.V., Matvienko, M.V., Ermolaev, G.V. et al. *Method of diffusion bonding of materials*. Pat. 81583 Ukraine. Int. Cl. B 23 K 20/14. Publ. 10.01.2008.
9. Makhnenko, V.I. (1976) *Computational methods for analysis of kinetics of welding stresses and strains*. Kiev: Naukova Dumka.
10. Chapek, J. (1987) *Creep of metallic materials*. Moscow: Mir.
11. Garofalo, F. (1968) *Principles of creep and long-term strength of metals*. Moscow: Metallurgiya.
12. Taira, S., Otani, R. (1986) T*heory of high-temperature strength of materials*. Moscow: Metallurgiya.
13. Markashova, L.I., Arsenyuk, V.V., Grigorenko, G.M. (2002) Peculiarities of plastic deformation of dissimilar materials in pressure joining. *The Paton Welding J.*, **5**, 9--13.
14. Unksov, E.P. (1955) *Engineering methods of calculations of forces in plastic working of metals*. Moscow: Mashgiz.

TECHNOLOGY OF AUTOMATIC SUBMERGED-ARC WELDING AND CLADDING BY LOW-DENSITY CURRENT

S.V. DRAGAN[1], **Yu.A. YAROS**[1] and **A.A. YAROS**[2]
[1]Admiral Makarov National Shipbuilding University, Nikolaev, Ukraine
[2]SPB «AMITI», Nikolaev, Ukraine

The paper describes the results of application of power sources with a combined external volt-ampere characteristic for narrow-gap welding of plates and repair cladding of freight car wheel flanges.

Keywords: *arc welding, cladding, power source, process stability, current density, combined volt-ampere characteristic, technology, metal structure*

Substantiation of the possibility of performing automatic submerged-arc welding and cladding by low-density current. Automatic submerged-arc welding and cladding of steel structures is one of the leading processes in fabrication and repair of steel structures and machine parts.

Automatic welding can be performed in a broad range of currents, using local equipment and different engineering solutions aimed at arc length stabilization and improvement of the stability of operation of «power source–arc–weld pool» system (PS–A–WP) [1]. However, application of electrode wire of 4--5 mm diameter and welding modes with current density below 40 A/mm^2 aggravates the problem of arc length stabilization. For each wire diameter d_{el} minimum admissible values of current I or current density j were established (Table), at which it is possible to achieve a stable arcing process at application of standard welding equipment. At the same time, it is possible to perform automatic welding in modes with current density below the values given in the Table, thus opening good prospects for application of large diameter electrode wire instead of thin wire.

Application of large diameter wires and low-density welding current is rational at automatic narrow-gap submerged-arc welding (pressure on the weld pool is reduced), in fabrication of complex 3D structures (residual welding deformations are reduced), as well as at performance of cladding operations (base and clad metal mixing is reduced) [2]. Lowering of current density and increase of electrode diameter are also favourable for current-conducting tip resistance, thus reducing the equipment operation costs. Application of 4–5 mm electrode wires instead of 2–3 mm wires for welding is cost-effective due to the low cost of larger diameter wires, irrespective of their grade, as manufacture of 5 mm wire from the rolled bar does not include such a labour-consuming operation as high-cycle «hot drawing», which is compulsory for thin wires.

So, for instance, the cost of 1 t of 2 mm welding wire of Sv-08A (Sv-10Kh2M) grade is equal to approximately 4.08 (8.96); 3 mm — 3.84 (8.43); 4 mm — 3.78 (7.92); 5 mm — 3.72 (7.84) thou UAH [3].

Arc process stability in low-density current welding can be essentially increased by application of rectifiers with a combined external volt-ampere characteristic [4]. The electrode wire feed rate is unchanged, and is determined by the specification, while arc voltage is controlled by adjustment of welding circuit voltage and resistance. Rectifiers of VDU25 series with a combined external volt-ampere characteristic (Certificate of compliance # UA1.012.0165143--06) accommodate a controllable rectifier block, assembled as a six-phase circuit of current rectification with a paralleling reactor, which ensures a low welding current ripple factor and high accuracy of welding voltage stabilization. The adjustable combined external characteristic provides optimum welding modes and high dynamic properties of the sources [5].

The process of automatic submerged-arc welding or cladding at low-density current using rectifiers with a combined external characteristic is performed as follows. The source is set up so as to ensure arcing at working values of voltage and current, i.e. so that voltage U in point A (point of transition from the

Admissible values of current (density) depending on electrode wire diameter

Kind of current, arc stabilization principle	Electrode wire diameter, mm			
	2.0	3.0	4.0	5.0
Alternating current, automatic regulation	290 (92.3)	400 (56.6)	530 (42.2)	680 (34.7)
Alternating current, self-regulation	220 (70.0)	330 (46.7)	420 (33.4)	550 (28.0)
Direct current	160 (51.0)	220 (31.1)	320 (25.5)	450 (22.3)

steeply-falling to the flat part of the combined external characteristic) was by 14–21 % lower than working voltage U of the welding process (Figure 1). The welding process starts after ignition of the welding arc by short-circuiting of the electrode on the item and achievement of working values of voltage U and current I.

However, the arising voltage fluctuations in the range from U_{w1} to U_{w2} can lead to the respective current changes. So, at voltage increase from U_w up to U_{w1} (up to 10.5 %) welding current drops from I_w to I_{w1}, and at voltage lowering from U_w to U_{w2} current rises up to U_{w2}. As arc power in the range of working voltages and currents is applied in the steeply-falling part of the external characteristic, current fluctuations are small. This essentially reduces the variation of the depth of base metal penetration and improves the clad layer formation. At development of disturbances and lowering of arc voltage by 21 % and more (for instance, from U_w to U_{w3}), which may lead to welding process disturbance and beginning of short-circuiting mode, the power to the arc is fed in the flat part of the external characteristic. As a result, current rises from I_w up to I_{w3}, the process of arc self-regulation is intensified, i.e. electrode wire melting rate rises, the arc becomes longer and the set working voltage U is restored. At the same time, current is automatically decreased to value I. Thus, an abrupt pulsed increase of current stabilizes the welding process, preventing the short-circuiting mode and improving the quality of weld formation [6].

Narrow-gap welding of large-sized panels. Automatic narrow-gap submerged-arc welding by low-density current of 20--25 mm thick panels is promising in fabrication of large-sized ship and mechanical engineering structures. Compared to the widely used welding into an X-shaped groove, this process has the following obvious advantages:

• elimination of the operation of two-sided beveling of the abutted plate edges from the technological process;

• absence of labour-consuming additional operations, associated with reduction of the longitudinal welding deformations by panel pre-tension before welding both from one, and the other side (rigid attachment of the plates to the bench, heating of stretch straps, their removal and re-mounting after the panel has been turned over);

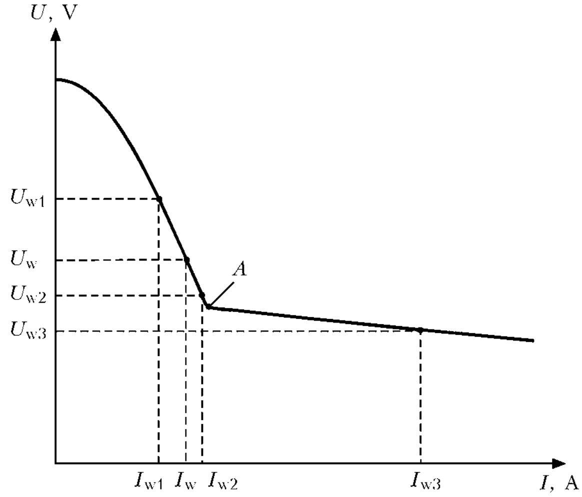

Figure 1. Combined external characteristic of the power source at arc length variations

• reduction of transverse welding deformations of the panel as a result of the possibility of free expansion of the metal across the weld axis.

One of the conditions for producing a sound weld in automatic narrow-gap welding is the stability of the arcing process during the arc migration from one of the edges being welded to the other with periodical shortening of the arc with edges melting and weld pool formation. To ensure a continuous running of the welding process, PS–A–WP system should have a high stability at arc length variations. Arc pressure on the weld pool should be minimum to eliminate the possibility of the molten metal flowing out of the gap [7].

The complexity of simultaneous fulfillment of the above conditions when batch-produced equipment is used, limits the application of narrow-gap welding in industry, despite its advantages. Power sources with flat and drooping characteristics do not provide welding current stability at the change of arc length in operation with standard automatic machines, thus leading to development of lack-of-fusion on one of the edges, due to interruption of the process of arc migration (Figure 2, *a*).

Specialized automatic machines fitted with the mechanism of transverse oscillation of welding wire, which stabilizes the arc length and welding current, respectively, are usually mounted on welding gantries. Mounting of such a mechanism on tractor-type automatic machines, applied in shipbuilding, is difficult,

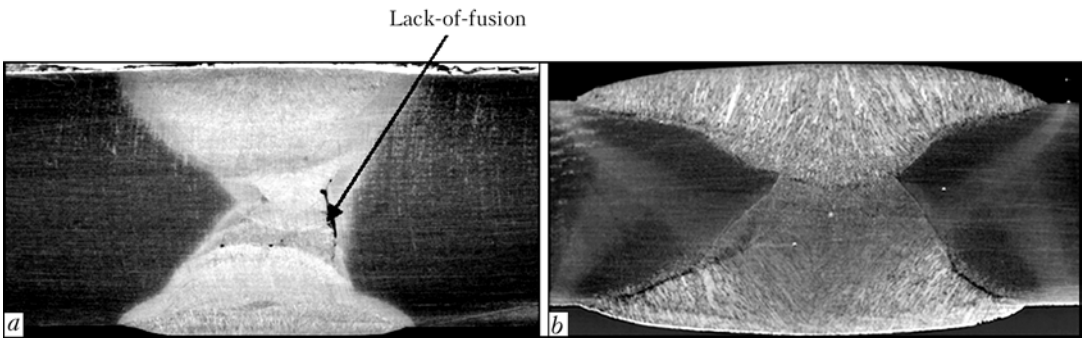

Figure 2. Macrosections of the joints made by narrow-gap welding with application of standard equipment (*a*) and power source with a combined external characteristic (*b*)

because of limitations on weight and overall dimensions.

Power sources with a combined external characteristic provide a high elasticity of the arc and welding current stabilization in the working part and stable operation of PS–A–WP system in the low-density current range, thus promoting a lowering of welding arc pressure and prevention of weld pool running out.

The bench for narrow-gap welding applied in fabrication of large-sized panels, is a light-weight (due to absence of a high rigidity requirements) framed metal structure with 10 mm deck. A 120 mm wide slot is envisaged along the weld axis for placing the trough with the flux.

The developed technology of automatic narrow-gap welding of panels from 3sp1 (killed) steel 20 mm thick using AN-348A flux and Sv-08A wire of d_{el} = = 5 mm with application of VDU25-1202 rectifier with a combined external characteristic and TS-77 welding tractor envisages the following sequence of work performance: mounting the trough with the flux backing; mounting the plates to be welded with 4 mm gap and its fixation with technological straps; mounting the tractor guide rail and adjustment of tractor motion; welding the first weld in the following mode: I_w = 450–460 A (j = 22.9–23.4 A/mm^2), U_w = 31–32 V, v_w = 20 m/h; item turning over; weld root cleaning with a pneumatic tool; re-mounting of the tractor guide rail with the tractor and adjustment of tractor motion; welding the second weld in the following mode: I_w = 890–900 A (j = 45.4–45.9 A/mm^2), U_w = 33–34 V, v_w = 30 m/h.

Samples welded by the above technology were subjected to metallographic investigations and mechanical testing: static tension, bending and hardness measurement. Mechanical characteristics of weld metal (average values over five measurements) were as follows: σ_t = 472 MPa; σ_y = 294 MPa; δ_5 = 28.5 %; ψ = = 68.2 %; impact toughness value KCU for root weld metal at +20 °C was 217 J/cm^2.

Hardness of welded joint metal for the root weld was HV10–184 (weld); HV10–18 (HAZ metal); HV10–179 (base metal); for the facing weld: HV10–194 (weld); HV10–182 (HAZ metal); HV10–179 (base metal).

Results of metallographic analysis and mechanical testing of the welded joint showed the following;

• the joint has no cracks, slag inclusions, lacks-of-fusion on the edges (Figure 2, *b*) or other defects, which confirms the stability of the arc migration from one of the edges being welded to the other when powering the arc by low-density current from a source with a combined external characteristic;

• at tensile testing of the welded joint all the samples failed in the base metal, at testing for static bending in the longitudinal and transverse direction in a 30 mm mandrel the samples withstood a bending angle of 100° without cracking; weld metal has a ferrite-pearlite structure, HAZ length is 4–6 mm; geometrical dimensions of the weld, mechanical characteristics and structure of the welded joint metal meet the requirements of SNiP III-18–75 and SNiP 3.03.01–87 and specifications.

Developed equipment and technology of automatic welding of up to 25 mm thick panels, providing a sound weld formation without preliminary rigid fastening of the plates being welded, have been introduced at MK MONTAZh (Krivoj Rog).

Cladding freight car wheel flanges. The most rapidly wearing elements of freight car wheel pairs are flanges of all-rolled wheels made from 65G steel. For their reconditioning, repair factories apply the technology of automatic twin-arc submerged-arc cladding with preheating up to 200 °C with 2 mm solid wires. A feature of this technology is welding into two pools, when the second arc remelts the bead deposited by the first arc, without any direct contact of the arc with the base metal.

Cladding is performed in the following mode: current of the first arc I_{cl1} = 190–250 A; that of the second arc I_{cl2} = 290–330 A; each arc voltage U_a = 30–34 V; cladding rate v_{cl} = 24–25 m/h; cladding step is 4.5 mm [8]. The above parameters of the mode correspond to arc current density j = 60–100 A/mm^2. When such a mode is used, base metal penetration depth reaches 3–4 mm. In addition, because of the intensive heat evolution into the wheel mass, there is a high probability of formation of quenching structures with a high hardness, and, hence, of cracks or tears in the clad layer metal, inadmissible by the wheel service requirements [8, 9]. On the other hand, machining of the clad surface also becomes more difficult.

The required properties of the clad metal and HAZ at a simultaneous reduction of the cladding process cost can be ensured by application of larger diameter electrode wire at preservation of the currently used mode parameters.

Application of cladding by current of less than 40 A/mm^2 density allows lowering both the penetration depth and the extent of base metal dilution by the clad metal at a simultaneous improvement of the clad metal structure.

In order to develop the commercial technology we studied the quality of automatic submerged-arc bead deposition by low-density current with 4 mm Sv-08KhM wire and AN-348A flux on 65G steel plate samples 5 mm thick.

Cladding was performed in a welding station fitted with TS-77 tractor and VDU25-630K rectifier with a combined external characteristic. Beads were deposited in the following mode: I_{cl} = 220–230 A (j = 17.5–18.3 A/mm^2), U_a = 31–32 V, v_{cl} = 24 m/h. Experiments were conducted with initial condition variation.

Variant 1. Deposition of one bead with intensive heat removal into water. This variant simulates the technology of wheel flange cladding and models heat removal in the radial direction. Before deposition the sample-plate was fastened on a special bench so that its lower surface was immersed into water.

Variant 2. Deposition of one bead with base metal preheating to temperature T = 250–300 °C.

Variant 3. Successive deposition of two beads with shifting by one step over the metal preheated up to T = 250–300 °C (close to the actual conditions of operation of an industrial cladding machine).

Study of the macro- and microstructure of the transverse sections led to establishment of the following regularities:

• at deposition by variant *1*, quenching cracks initiate in the HAZ metal because of the high cooling rate (Figure 3, *a*) and an insignificant penetration of base metal in the weld peripheral regions is observed. Deposited bead width reaches 16 mm, penetration depth is 2.6 mm;

• application of preheating (variant *2*) leads to a greater width of the deposited bead and base metal penetration depth by 10--15 % (Figure 3, *b*). However, the penetration depth still turns out to be 30--40 % less than with the currently applied industrial technology. Deposition of the second bead on the surface of the plate preheated by previous deposit (variant *3*) does not increase the depth of base metal penetration (Figure 3, *c*);

• at successive deposition of two beads the metal structure of the second bead (Figure 4, *a*) is medium-grained sorbite, line of fusion of the second bead with the first one (Figure 4, *b*) is characterized by transition from medium-grained sorbite to fine-grained one. Structure of the metal deposited by the first arc (Figure 4) is fine-grained sorbite, tempered by the second arc, line of fusion of the first bead with the base metal (Figure 4, *d*) has a graded structure: from fine-grained sorbite to pearlite-sorbite structure;

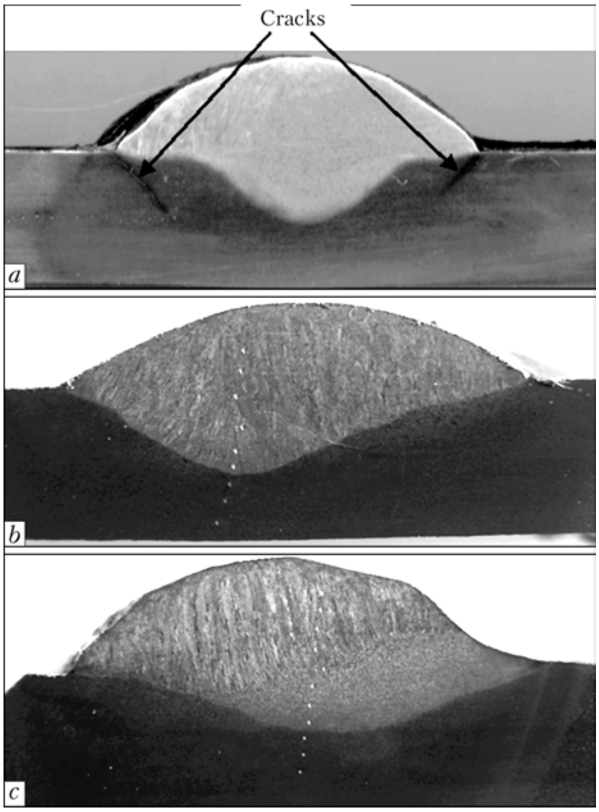

Figure 3. Macrosections of bead cross-sections under different cladding conditions: *a* ---- without preheating; *b* ---- with preheating; *c* ---- successive deposition of two beads

• measurement of metal hardness at different variants of cladding confirms the results of metallographic investigations. Deposited metal hardness for variant *1* is equal to *HV*5–440; *2* ---- *HV*5--270; *3* ---- *HV*5–240; for HAZ metal for variant *1* ---- *HV*5–630; *2* ----

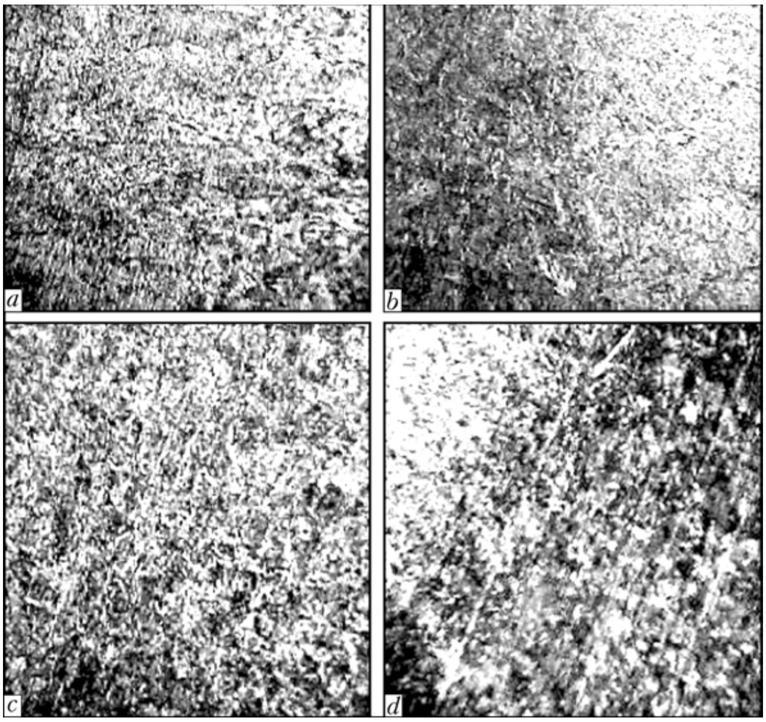

Figure 4. Metal microstructure at successive deposition of two beads: *a* ---- deposited metal of the second bead; *b* ---- fusion line of the first and second bead; *c* ---- metal of the first bead; *d* ---- fusion line of the first bead and base metal (×170)

*HV*5--300; *3* ---- *HV*5--250; base metal hardness for all the deposition variants is the same and is equal to *HV*5--240.

When cladding is performed without preheating (variant *1*) the deposited metal develops hardness, which is higher than that of the base metal more than 1.5 times; HAZ metal demonstrates a considerable hardening with its abrupt lowering at transition to the base metal. At deposition on preheated metal (variant *2*) a lowering of hardness in the deposited metal is observed and the hardened metal zone in the HAZ is preserved. Deposition of two beads with one-step shift (variant *3*) ensures a practically complete equalizing of the deposited and base metal hardness in the deposition zone.

Metal hardness obtained in variant *3* does not hinder further mechanical treatment of the clad layer of reconditioned wheel flanges and meets the requirements made of the service conditions of the wheel pair. Thus, the third variant of cladding technology by current of less than 40 A/mm^2 density, is admissible for commercial application.

The pilot-production technology and batch of power sources with a combined volt-amphere characteristic included into KT 068 units (developer is Design Office of «Ukrzaliznytsa», Kiev) for reconditioning railway car wheel pairs, have been introduced into production in «Ukrzaliznytsa» repair enterprises.

CONCLUSIONS

1. Technology of automatic submerged-arc welding and cladding by low-density current (17--24 A/mm^2) using power sources with a combined external characteristic was developed for fabrication of large-sized panels and reconditioning worn wheel pairs of railway freight cars.

2. Replacement of welding with a two-sided edge preparation by narrow-gap welding of up to 25 mm thick panels ensures sound weld formation without rigid pre-fixing of the sheets to be welded and achievement of joint properties meeting the SNiP specification requirements.

3. Cladding of freight car wheel flanges by two 4 mm electrode wires allows obtaining base metal properties satisfying the requirements of subsequent machining of the surface and conditions of wheel pair service.

1. (1974) *Technology of fusion electric welding of metals and alloys*. Ed. by B.E. Paton. Moscow: Mashinostroenie.
2. Ryabtsev, I.A. (2004) *Surfacing of machine and mechanism parts*. Kiev: Ekotekhnologiya.
3. (2006) *Welding production in Ukraine in 1990--2005 (economical-statistical review)*. Kiev: Ekotekhnologiya.
4. Dragan, S.V., Yaros, Yu.O., Yaros, O.O. et al. *Rectifier for submerged-arc welding and surfacing*. Pat. 30840 Ukraine for utility model. Publ. 11.03.2008.
5. Dragan, S.V., Yaros, Yu.A. (2008) Ensuring the stability of submerged-arc welding process at low current density. *The Paton Welding J.*, **1**, 26--29.
6. Dragan, S.V., Yaros, Yu.O., Yaros, O.O. et al. *Method of submerged-arc surfacing*. Pat. 30841 Ukraine for utility model. Publ. 11.03.2008.
7. (1960) *Process of base metal melting in welding*. Ed. by I.I. Rykalin. Moscow: AN SSSR.
8. (2003) *Equipment for repair by welding and surfacing of rolling stock parts and assemblies*: Catalogue-reference book. Kiev: PKTB Podv. Sost.
9. Ryabtsev, I.A., Kondratiev, V.N. (1999) *Mechanized arc surfacing of metallurgical equipment parts*. Kiev: Ekotekhnologiya.

INFLUENCE OF THE RATIO OF DIMENSIONS OF CYLINDRICAL PARTS FROM DISSIMILAR MATERIALS ON THEIR STRESS-STRAIN STATE IN DIFFUSION WELDING*

V.F. KVASNITSKY[1], **M.V. MATVIENKO**[1], **G.V. ERMOLAEV**[1], **A.V. LABARTKAVA**[1] and **V.D. KUZNETSOV**[2]
[1]Admiral Makarov National Shipbuilding University, Nikolaev, Ukraine
[2]NTUU «Kiev Polytechnic Institute», Kiev, Ukraine

Computer simulation based on finite element method was used to study the influence of the ratio of dimensions (radii and height) of cylindrical parts of the type of cylinders and bushings from dissimilar materials on the stress-strain state in the butt zone in diffusion welding, allowing for plastic deformations under the conditions of loading by compression and thermal cycling, and to establish the regularities of its formation.

Keywords: *diffusion welding, dissimilar materials, stress-strain state, plastic deformation, cylinder–cylinder component, bushing–bushing component, relative radius, relative height, computer simulation, stagnation point*

The main regularities of formation of stress-strain state (SSS) in vacuum diffusion welding of components from dissimilar materials are given in [1–4]. It is established that welding of blanks with different physico-mechanical properties leads to formation of a bulk stressed state, promoting localizing of plastic deformations in the butt zone. The most effective method to localize deformations is thermal cycling.

Bulk stressed state is due to the difference in rigidity, strength and coefficients of linear thermal expansion (CLTE) of the materials being joined. Stresses and strains are non-uniformly distributed along the butt joint. The most unfavourable for joint formation is the so-called stagnation zone with zero tangential stresses, minimum equivalent stresses and plastic deformations, as deformation-induced activation of the surface in it is eliminated [5]. The position of this zone needs to be known, when designing blanks for dissimilar material components to be welded by diffusion process. During earlier research [6] the influence of the combination of the materials being joined and loading modes on SSS was studied on models of the type of cylinder–cylinder (C–C), bushing–bushing (B–B) and bushing–flange. Model dimensions (radius and height) and position of the stagnation zone remained constant. It is obvious that the size and position of this zone can change at the change of the ratio of the part dimensions. Therefore, studying the degree of the influence of the geometrical factors on the earlier established regularities is urgent.

The purpose of this work is establishing the influence of the main dimensions of cylindrical parts of C–C and B–B type on the SSS at diffusion welding of dissimilar materials.

Investigations were performed by the method of computer simulation using ANSYS program package. Components and models, the shape and size of which were similar to those used in previous studies [1–4] were considered. Moduli of elasticity and strength of materials were taken to be the same ($E_1 = E_2 = 1\cdot10^5$ MPa), yield points were selected on such a level that plastic deformations ran in both the parts (on the level below the maximum equivalent ones, found in an elastic solution, i.e. $\sigma_{y1} = \sigma_{y2} < \sigma_{eq}^{max}$). Modulus of hardening at plastic deformation was taken to be zero for all the materials. CLTE for all the materials being joined in all the variants differed 2 times ($\alpha_1 = 10\cdot10^{-6}$; $\alpha_2 = 20\cdot10^{-6}$ 1/deg).

In C–C and B–B type components thermal loading (heating by 100 °C) in an unrestrained state was considered, as it is the main cause for appearance of tangential stresses in the butt joint and presence of stagnation point and zone is the most pronounced. In order to generalize the obtained regularities, the results were compared with the variant of simultaneous loading by compression (40 MPa) and thermal cycling (±100 °C).

Proceeding from the ratio of the main dimensions (inner radius, thickness and height of the bushing) the cylindrical components were conditionally divided into three groups: bushings (height is greater than the radius and thickness, i.e. the prevailing dimension is height), flat rings — discs (thickness is much greater than the inner radius and height, i.e. the prevailing dimension is thickness), and thin rings (inner radius is much greater than the height and thickness, i.e. the prevailing size is the inner radius).

Accordingly, the dimensions of components C–C and B–B were varied within the following ranges: bushing inner radius *r* from 0 (cylinder) up to 450 mm;

*V.V. Kvasnitsky, Cand. of Sci. (Eng.), studying for his Doctor's degree, participated in the work.

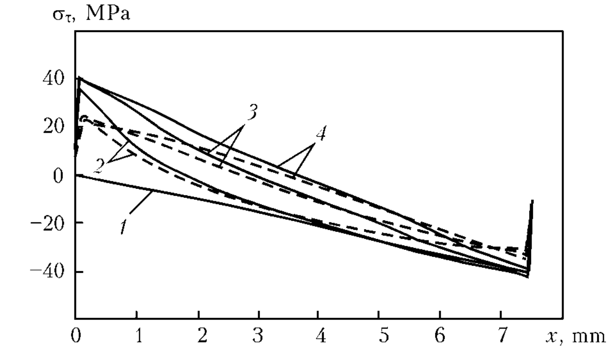

Figure 1. Epures of tangential stresses in the butt at h = 12 mm: *1* --- cylinder welding $r(r/b)$ = 0 (0); *2*--*4* --- bushing welding at $r(r/b)$ = 2.5 mm (0.33), 15 (2.0) and 100 (13.3), respectively, at loading by thermal cycling (solid curves) and compression and thermal cycling (dashed)

bushing height h from 1 to 20 mm, bushing thickness (difference between the inner and outer radii) $b = R - r$ from 4.5 up to 20 mm. Here, the ratio of dimensions changed within the following ranges: r/b from 0 up to 90 (thin ring) at h/b from 0.13 (flat ring) up to 2.7 (0.13, 0.67, 1.6 and 2.7).

Influence of relative radius. Ratio of inner radius to bushing thickness r/b was studied at constant bushing thickness b = 7.5 mm, height h = 1, 5, 12 and 20 mm, and radius r from 0 (cylinder) up to 200 mm (ring). Fields of axial, tangential, equivalent stresses and plastic deformations at heating were investigated.

Analysis of the results showed that the nature of tangential stress distribution along the butt at variation of inner radius is constant (Figure 1). Stresses decrease almost linearly from the maximum near the outer surface to zero in the stagnation point and then increase again after sign change closer to the inner surface. Maximum stresses near the outer surface are preserved at increase of inner radius from 0 (C--C component) up to 100 mm (B--B component), and near the inner surface the stresses first rise at increase of the relative radius up to 2 and then remain constant. The position of the stagnation point along the butt length (bushing thickness) x/b changes from 0 (in the cylinder) up to 0.45 (at r/b = 13), i.e. at increase of the inner radius the stagnation point shifts from the cylinder center at $r(r/b)$ = 0 closer to bushing mid-thickness (3.75 mm).

At loading by compression with thermal cycling, the nature of distribution of tangential stresses in the butt joint changes insignificantly, their level decreases, and stagnation point moves to the left only slightly (fractions of a millimeter).

At the change of inner radius the nature of distribution of plastic deformations along the butt joint changes (Figure 2). At its increase the deformations at the outer surface gradually decrease, and near the inner surface they increase. In samples of C--C type plastic deformations are absent, they appear already at inner radius of 1 mm ($r/b > 0.13$) and noticeably increase with increase of the radius.

With greater distance from the inner and outer surfaces, plastic deformations decrease to zero. Stagnation zone (zero plastic deformations) changes only slightly with increase of the radius, remaining at about 4 mm (0.55b) at all the radii.

At the change of heating to cooling the axial stress fields are mirrored relative to the butt line, those of tangential stresses reverse their sign, while fields of equivalent stress and plastic deformations do not change.

At simultaneous loading by compression and thermal cycling plastic deformations increase along the entire butt joint from the side of the material with

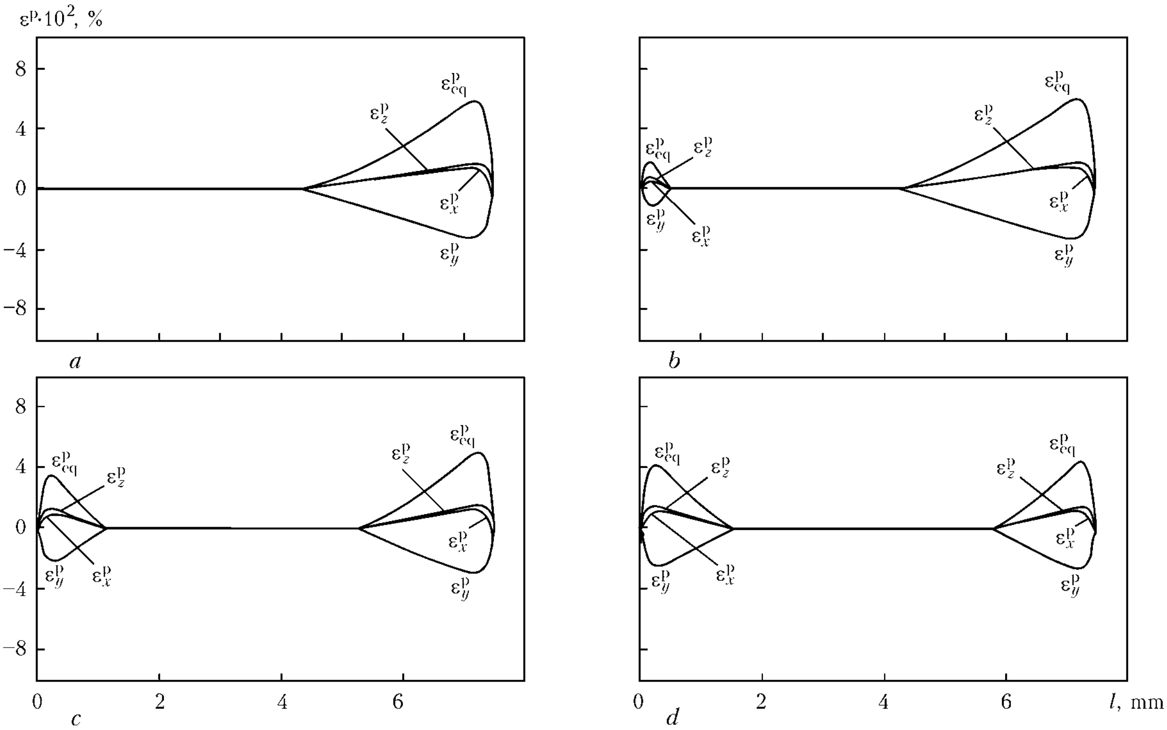

Figure 2. Epures of plastic deformations in the butt joint at $r(r/b)$ = 0 (a), 2.5 (0.33) (b), 15 (2.0) (c) and 100 mm (13.3) (d)

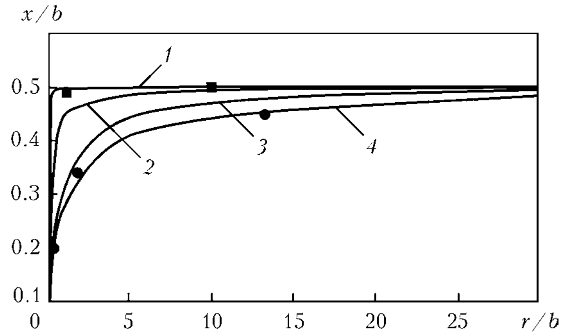

Figure 3. Dependence of the position of stagnation point on bushing relative radius r/b at the height: *1*, ■ — h = 1 mm (h/b = 0.13); *2* — 5 (0.67); *3*, ● — 12 (1.6); *4* — 20 (2.67)

smaller CLTE at heating and that with larger CLTE at cooling. From the side of the second material, plastic deformations decrease to zero at heating in the material with a higher CLTE and at cooling — in the material with smaller CLTE, respectively.

Figure 3 shows the graphs of dependence of the position of stagnation point (zero tangential stresses) relative to the bushing inner surface along the butt joint length on the relative radius at different relative height of the bushing h/b at loading by thermal cycling. For comparison, the position of stagnation points at simultaneous loading by compression and thermal cycling is shown. As can be seen from the Figure, at r/b = 0 (cylinder without inner surface) the stagnation point is exactly on the axis (in the butt joint center), i.e. ratio x/b is equal to zero. In the presence of a bore of even a small radius inside the cylinder the stagnation point is shifted farther from the axis (from the inner surface) the faster, the smaller the relative height.

At a small relative height (h/b = 0.13), i.e. in a component of flat disc type, even at relative radius h/b = 0.2, the relative distance from the inner surface x/b reaches 0.5, i.e stagnation point moves closer to mid-thickness.

At large relative heights (h/b from 0.67 to 2.67) stagnation point is also shifted closer to mid-thickness, but to a smaller degree. At r/b = 1 ratio x/b is equal to 0.45, 0.33 and 0.3 at relative heights of 0.67, 1.6 and 2.67, respectively.

Further increase of inner radius, i.e. transition from the bushing to the ring, continues to gradually shift the stagnation point from the inner surface to mid-thickness, and the stronger, the smaller the relative height of the bushing. At relative radius $r/b >$ > 40 position of stagnation point x/b = 0.5, practically at all the heights.

At simultaneous loading by compression with thermal cycling the position of stagnation points practically does not change in a flat disc (see Figure 3, curve *1*) and somewhat shifts towards bushing axis (Figure 3, curve *3*), i.e. application of a compressive force has an influence similar to increase of bushing height.

Influence of relative height. Ratio of bushing height to its thickness, h/b, was studied at constant

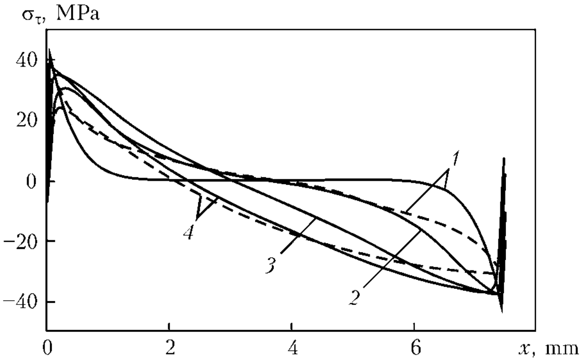

Figure 4. Epures of tangential stresses in the butt joint in welding of bushings: *1* — r = 8 mm, $h(h/b)$ = 1 mm (0.13); *2* — 3 (0.4); *3* — 7.5 (1.0); *4* — 15 (2.0) at loading by thermal cycling (solid curves) and compression and thermal cycling (dashed)

bushing thickness b = 7.5 mm, height from 1 to 20 mm and radii r = 3, 8 and 50 mm.

Analysis of epures of tangential stresses (Figure 4) shows that the level of maximum stresses both near the inner and the outer surfaces changes only slightly at all the heights. However, the nature of distribution along the butt changes from abruptly non-uniform with a large stagnation zone (zero tangential stresses) at a small height (h/b = 0.13) to a value close to a linear one at large heights ($h/b > 1$). The Figure also clearly shows the shifting of the stagnation point (zero tangential stresses) and its removal from bushing mid-thickness with increase of relative height.

Plastic deformation zone changes considerably with increase of relative height of the bushing and deformation level also changes. Relative extent of the stagnation zone decreases from 0.9 at h/b = 0.13 to 0.65 at $h/b > 1$.

At simultaneous loading by compression and thermal cycling distribution of tangential stresses changes noticeably only at a small relative height (see Figure 4, curves *1*). Zone with zero tangential stresses disappears, stress peaks near the bushing surfaces become somewhat smaller, and the epure takes on the shape characteristic for bushings of a large relative height. Thus, the conclusion about application of a compressive force being equivalent to increase of the bushing relative height is confirmed.

Figure 5 shows the graphs of dependence of stagnation point position (relative to bushing inner sur-

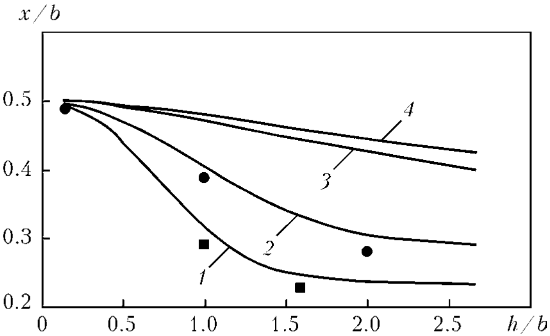

Figure 5. Dependence of the position of stagnation point on relative bushing height h/b: *1*, ■ — $r(r/b)$ = 3 mm (0.4); *2*, ● — 8 (1.07); *3* — 35 (4.67); *4* — 50 (6.67)

face) along the butt joint length on relative height at different inner radii of the bushing. Respective values for the variant of loading simultaneously by compression and thermal cycling are also shown there by dots for comparison. As is seen from the Figure, position of stagnation point at low relative height ($h/b = 0.1$ – 0.2) only insignificantly depends on radii and thickness and is close to 0.5. At medium and large relative heights ($h/b > 0.2$) relative distance from the bushing inner surface to stagnation point depends both on the relative height and relative radius, decreasing with increase of relative height and increasing with increase of relative radius. At simultaneous loading by compression and thermal cycling, the stagnation point, similar to previous cases, shifts closer to the inner surface.

Thus, analysis of simulation results allows establishing the following main regularities of the influence of the ratio of dimensions (radius, height and thickness) of cylinders and bushings on SSS of dissimilar material joints in diffusion welding at heating (cooling).

The nature of the fields of stresses and plastic deformations changes at increase of relative inner radius of the bushing. At small radii, plastic deformations are concentrated near the butt joint in its half adjacent to the outer surface and uniformly cover both the materials. Increase of the radius leads to appearance of the second field of plastic deformations in the half of the butt adjacent to the bushing inner surface. At increase of inner radius, the plastic deformation zone near the outer surface is somewhat decreased, and near the inner surface it is increased. Stagnation zone changes only slightly with increase of relative radius, remaining equal to about 4 mm (0.53) at all the radii.

Nature of distribution and level of tangential stresses along the butt joint does not change at increase of inner radii, but stagnation point shifts from the cylinder center closer to the bushing mid-thickness. At small relative height ($h/b = 0.13$), i.e. in a component of the type of a flat disc, even at small relative radii ($r/b = 0.5$) stagnation point becomes closer to mid-thickness. At large relative heights stagnation point shifting closer to mid-thickness is also found, but to a smaller degree. Further increase of inner radii, i.e. transition from bushing to ring, continues to gradually shift the stagnation point from the inner surface to mid-thickness, and the stronger, the smaller the relative height of the bushing.

Fields of tangential stresses retain their symmetry relative to the butt at all heights. However, skew symmetry relative to mid-thickness is preserved only at small relative height, being disturbed with greater height.

Fields of plastic deformations somewhat change, with height increase the plastic deformation zone increases to a greater extent near the outer surface.

Level of maximum tangential stresses both near the inner and the outer surface changes only slightly at all the heights. Nature of distribution along the butt changes from abruptly non-uniform with a large stagnation zone (zero tangential stresses) at a small height ($h/b = 0.13$) to that close to the linear one at large heights ($h/b > 1$). Stagnation point shifting and its removal from bushing mid-thickness occur with increase of relative height.

Stagnation point position at a small relative height ($h/b = 0.1$--0.2) only slightly depends on radius and thickness and is close to 0.5. At medium and large relative heights ($h/b > 0.2$) relative distance from the bushing inner surface to stagnation point depends both on relative height, and on relative radius, decreasing with increase of relative height and increasing with increase of relative radius.

At simultaneous loading by compression and thermal cycling, the established regularities are preserved, but stagnation point somewhat shifts to the side of the bushing inner surface, i.e. the influence of the compressive force is similar to increase of bushing relative height.

CONCLUSIONS

1. Position of stagnation point and size of stagnation zone depend on the ratio of dimensions (inner radius, thickness and height) of cylindrical components from dissimilar materials, which should be taken into account in design of parts to be joined by diffusion welding.

2. In components of the type of disc and thin ring stagnation point is located in the butt middle part close to mid-thickness.

3. With decrease of relative inner radius and increase of relative height of bushings being welded the stagnation point shifts from mid-thickness to bushing inner surface. At joining of cylinders it is located in the butt joint center.

4. Minimum value of stagnation zone in joints of cylindrical parts is provided by diffusion welding at simultaneous compression and thermal cycling.

1. Makhnenko, V.I., Kvasnitsky, V.V. (2009) Stress-strain state of assemblies of cylindrical shape in diffusion bonding. *The Paton Welding J.*, **2**, 2–7.
2. Makhnenko, V.I., Kvasnitsky, V.V., Ermolaev, G.V. (2008) Stress-strain state of diffusion bonds between metals with different physical-mechanical properties. *Ibid.*, **8**, 2--6.
3. Makhnenko, V.I., Kvasnitsky, V.V., Ermolaev, G.V. (2008) Effect of physical-mechanical properties of the materials joined and geometry of the parts on distribution of stresses during diffusion bonding in vacuum. *Ibid.*, **1**, 2--8.
4. Kvasnitsky, V.V., Ermolaev, G.V., Matvienko, M.V. (2008) Effect of plastic deformation on stress-strain state in diffusion bonding of dissimilar metals as applied to cylinder--cylinder and bushing--bushing assemblies. *Zbirnyk Nauk. Prats. NUKB*, **1**, 100--107.
5. Krasulin, Yu.L., Timofeev, V.I., Kharlamov, Z.I. et al. (1967) Calculation of contact stresses in pressure welding of wire to plate. *Fizika i Khimiya Obrab. Materialov*, **5**, 61--66.
6. Kuznetsov, V.D., Kvasnitsky, V.V., Ermolaev, G.V. et al. (2007) General principles of stressed state formation in diffusion bonding of cylindrical shape parts. *Zbirnyk Nauk. Prats NUKB*, **6**, 62--73.

INFLUENCE OF WELDING AND POST-WELD HEATING ON STRUCTURAL TRANSFORMATIONS AND PROPERTIES OF HAZ OF WELDED JOINTS ON HARDENING STEELS

Yu.M. LEBEDEV
Admiral Makarov National Shipbuilding University, Nikolaev, Ukraine

Experimental investigations of influence of welding and post-weld heating on hardness and impact toughness of simulated high-temperature areas of heat-affected zone (HAZ) of joints on low-carbon high-strength steels and medium-carbon 40Kh steel were carried out. Peculiarities of phase transformations in these steels were studied. It is determined that the most effective is fast post-weld heating of HAZ metal in a temperature interval, corresponding to intercritical interval of A_{C1}–A_{C3}.

Keywords: *heat-affected zone, high-strength hardening steels, post-weld heating, diagrams of thermal-kinetic transformation of HAZ austenite, hardness, impact toughness*

Martensite structure, tending to delayed fracture and formation of cold cracks, is formed in a heat-affected zone (HAZ) during welding of low- and medium-alloy steels. Product preheating allows preventing or limiting the hardening of HAZ metal at given welding or cladding modes, however, it complicates welding engineering procedure and increases product cost. Appropriateness of using this operation in steel welding should be proved in each particular case. Analysis of the possibility of HAZ hardening and calculation of minimum heating temperature, at which cold crack formation is eliminated, can be done using results obtained in work [1]. Time of metal cooling in the range from critical point A_{C3} up to temperature of the start of martensite transformation M_s at a given welding or cladding mode should be determined for that.

Time of cooling of HAZ metal in specified temperature interval in single-pass welding or cladding on a massive body can be calculated by the following formulas:

$$\Delta t_w = \frac{q_{h.i}^2}{4\pi\lambda c\gamma v^2\delta^2}\left(\frac{1}{(M_s - T_0)^2} - \frac{1}{(A_{C3} - T_0)^2}\right), \qquad (1)$$

$$\Delta t_{cl} = \frac{q_{h.i}^2}{2\pi\lambda v}\left(\frac{1}{M_s - T_0} - \frac{1}{A_{C3} - T_0}\right), \qquad (2)$$

where $q_{h.i}$ is the heat input; λ is the heat conductivity coefficient; T_0 is the item initial temperature; v is the welding (cladding) speed; $c\gamma$ is the volumetric heat capacity; δ is the thickness of plates being welded at single-pass welding.

Values of critical points depend on steel composition, which for low-alloy steel can be determined by following dependences:

$$A_{C3}\ [^\circ C] = 910 - 229\ C + 32\ Si - 25\ Mn - 8\ Cr - 18\ Ni + 2\ Mo + 117\ V - 24\ Cu + 7\ W - 120\ B;$$

$$M_s = 520 - 380\ C - 18.4\ Mn - 12\ Cr - 8.2\ Ni - 21.5\ Mo - 170\ V + 6.6\ Zr + 500\ Ti$$

(content of all elements is given in weight percent and root-mean-square deviation is equal to ±15 °C).

Practical experience of welding operations and results of analysis of steel weldability showed that cold cracks in the HAZ can appear at martensite content above 50 vol.%.

Time of HAZ cooling from critical point A_{C3} to M_s, when 50 vol.% of martensite forms, also depends on steel composition and is calculated by formula

$$\Delta t_{0.5M} = (9\ C)^{1.45} \cdot 10^n,$$

where $n = 0.48(Si - 0.3) + 0.73(Mn - 0.6) + 0.75(Cr - 0.15) + 0.32(Ni - 0.15) + 0.63\ Mo + 1.14\ V$ is the exponent, depending on the content of alloying elements in steel.

If cooling time in welding or cladding is less than $\Delta t_{0.5M}$, then 50 vol.% of martensite is formed in HAZ, and preheating is necessary in order to prevent cold cracks. Minimum preheating temperature T_{pr}, at which 50 vol.% of martensite is contained in the HAZ metal, for the case of cladding on a massive body is calculated from condition $\Delta t_{cl} = \Delta t_{0.5M}$ by the following equation:

$$T_{pr} = \frac{A_{C3} + M_s}{2} - \sqrt{\left(\frac{A_{C3} + M_s}{2}\right)^2 + \left(\frac{q_{h.i}(A_{C3} - M_s)}{2\pi\lambda\Delta t_{0.5M}}\right) - A_{C3}M_s}.$$

Minimum temperature of preheating T_{pr}, at which 50 vol.% of martensite is formed in the HAZ metal in single-pass welding, can be calculated by equation (1), substituting $\Delta t_{0.5M}$ value instead of Δt_w, if it is larger than Δt_w, and solve it by the method of half-division considering that $T_{pr} < M_s$.

Preheating significantly complicates and raises the price of welding (cladding) procedure, and can have a negative influence on ductility of steel welded joints because of the increase of the period of HAZ being at high temperature. This results in grain growth in the overheated zone. If mechanical properties of the joints do not satisfy normative requirements, then an additional procedure — heat treatment — is required. Besides, preheating can not be used for all types of welded structures. Local post-weld heating is used during manufacturing of higher-strength steel welded structures with the aim of eliminating formation of cold cracks. It promotes martensite decomposition in the HAZ or results in recrystallization with generation of other structural components of steel. Local heating can be realized with the help of different heat sources, including welding ones. In the last case heat treatment (or heating) operation is carried out in the process of welding proper. Short beads welding [2], transverse bead weave welding, twin-arc welding with shifted arcs [3--5], modulated current welding [6, 7], welding with application of pulsed-arc power sources etc. [8] can be named as such methods of autoheat treatment. Similar technology of post-weld heat treatment is easily implemented during welding of sheet structures of high-strength steels with further or concurrent heating of the joint by a nonconsumable electrode arc [9, 10].

As the high-temperature areas of HAZ with coarse-grained structure of overheated metal are the weakest point in the welded joints, during performance of post-weld heating or heat treatment their mode should provide at least a partial correction of overheating effects and promote achievement of a satisfactory complex of mechanical properties in the specified zones. In the case of steel quenching during welding, the primary task is creation of such conditions of formation of welded joints at which the possibility of cold crack formation is eliminated. Effective control of the structure of different areas of welded joints at the impact of reheating by welding or special sources can be realized in full scale in the case of previously known metal behavior under the conditions of change of temperature-time characteristics of such heating. Wide introduction of post-weld heating in welding of hardening steels is prevented by the fact that processes of structural transformations in HAZ metal at specified heating and their influence on mechanical properties of steels is virtually not studied.

The aim of the present study is investigation of influence of temperature of initial and post-weld heating on structural transformations of high-temperature areas of HAZ as well as on its mechanical properties for the range of a number of high-strength steels.

Influence of different temperature modes of welding heating on the change of metal structure and properties of simulated areas of HAZ of welded joints from high strength steels with different alloying was investigated. Heating of 10 × 10 mm section samples with a semi-circular cut designed for impact toughness tests (type 1 to GOST 9454--78) is performed with passing current in ASA-30 machine for butt resistance welding, specially refitted for this purpose. Temperature was controlled with the help of chromel-alumel thermocouple, welded by a capacitor discharge to the surface of middle part of heated samples. Simultaneously, thermal cycle of heating–cooling was recorded by oscillograph N-700 at visual inspection. Distance between the clamps was equal to 35 mm. Heating of billets was performed with average speed of about 100 °C/s and cooling — in clamps of the device in air. After impact bend testing the samples were subjected to metallographic analysis.

In 40Kh steel with initial ferrite-pearlite structure significant change of strength properties takes place after high speed heating of samples up to the temperature somewhat below critical point A_{C1} or intercritical interval A_{C1}--A_{C3}. Heating up to such a temperature led to significant increase of values of impact toughness KCU from 18 up to 43--65 J/cm^2 and certain lowering of hardness from HV 260 to 230 (Figure 1, *a*). After heating above critical point A_{C3} the impact toughness decreases to values below those of the initial metal and hardness notably increases. Maximum hardness value HV 580 is observed after heating up to 1100 °C. At that impact toughness of metal drops to KCU = 11 J/cm^2. Further increase of heating temperature up to 1375 °C has practically no influence on the specified indices.

Structural changes of 40Kh steel visible in optical microscope take place only after its heating above critical point A_{C1}. Thus, heating in intercritical interval up to 790 °C and further cooling with speed w_{550} = = 15 °C/s leads to pearlitic transformation of generated austenite. The volume fraction of free hypoeutectoid ferrite, located in the form of very thin interlayers along some boundaries of former austenite grains, is significantly reduced in comparison with the initial structure. Such heating promotes some grain size refinement. Pearlitic transformation also takes place after cooling of 40Kh steel from 825 °C virtually without any hypoeutectiod ferrite precipitation from austenite.

Higher heating temperature results in a change of transformation mechanism of overcooled austenite. So, austenite undergoes bainite-martensite transformation after heating up to 900 °C and hardness of metal with such a structure is equal to HV 390. Completely martensite transformation is observed after heating 40Kh steel up to 1100 °C and higher.

Influence of post-weld heating on impact toughness and structural transformations was investigated on samples of simulated HAZ with high-temperature areas of 40Kh steel, i.e. those which underwent heating up to 1250 °C. For this purpose samples after heating up to 1250 °C were cooled down to 200 °C. Here, austenite underwent martensite transformation beginning from temperature M_s = 340 °C. Metal struc-

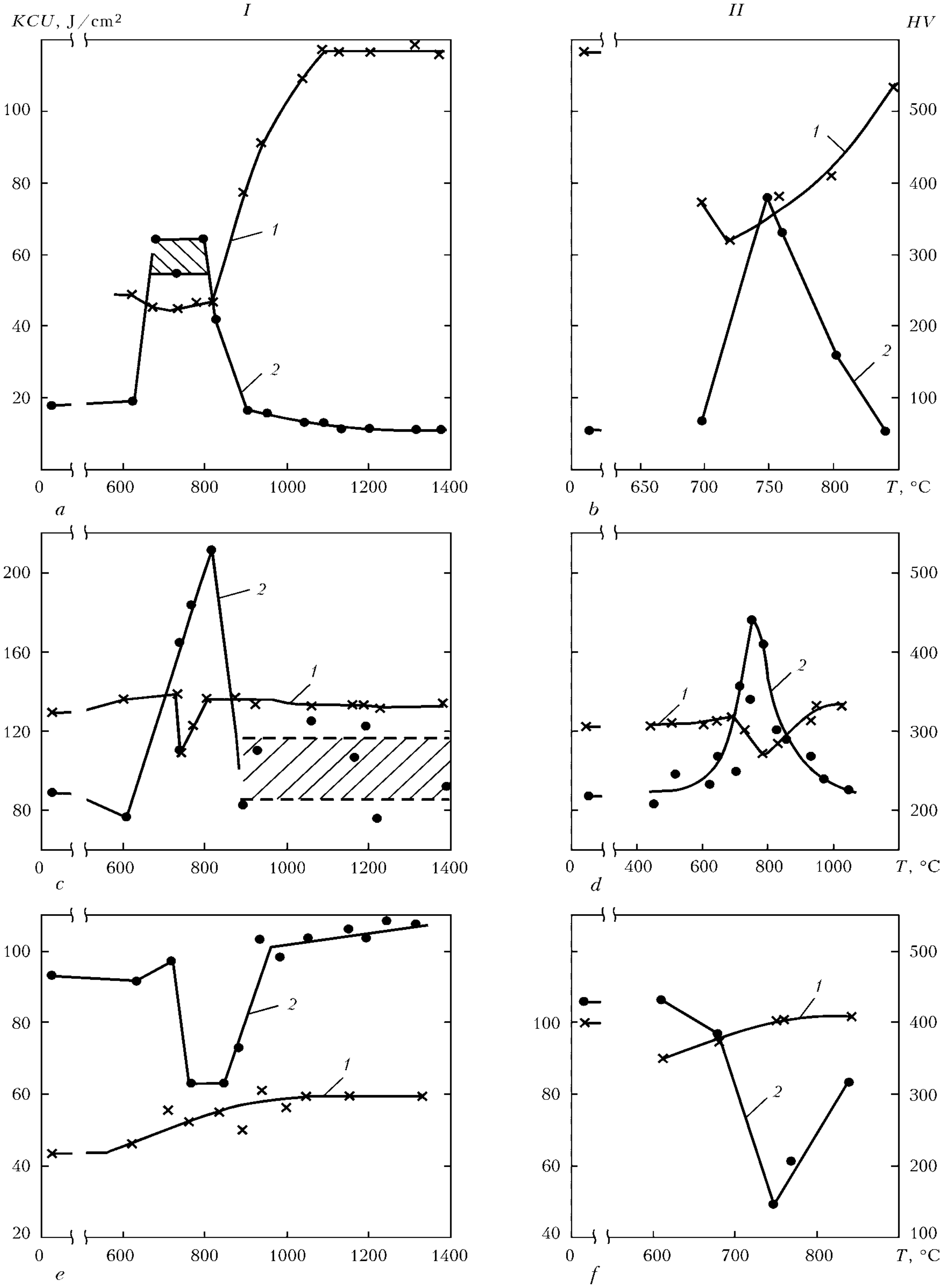

Figure 1. Influence of temperature of fast heating on hardness (*1*) and impact toughness (*2*) of samples from 40Kh (*a, b*), 07Kh3GNM (*c, d*) and 14KhGNMDFB (*e, f*) steels: *I* ---- heating in as-delivered state; *II* ---- second heating after heating up to 1300 °C

ture consisted approximately of 75 vol.% of martensite and 25 vol.% of austenite after cooling to 200 °C. Presence of one fourth of ductile austenite in the structure provides satisfactory metal resistance to cold crack formation. Then reheating was carried out for the purpose of martensite temper or recrystallization of metal structure. Influence of temperature of such post-weld heating on change of impact toughness of simulated high-temperature HAZ of 40Kh steel is shown in Figure 1, *b*.

As follows from this Figure, post-weld heating from 200 up to 700 °C allows achieving *HV* 375 hardness instead of *HV* 590 in high-temperature areas of HAZ of 40Kh steel samples at cooling only by the welding thermal cycle. Sample structure after cooling from reheating temperature of 700 °C consists of troostite and secondary sorbite with separate inclusions of martensite (about 5 vol.%), which is formed at the final stage of cooling from remaining austenite. In spite of presence of visible temper transformations, however, such a reheating below critical point A_{C1} does not allow achieving high indices of HAZ toughness. In this case the impact toughness is equal to KCU = 13 J/cm^2 that, approximately, corresponds to similar indices for hardened HAZ area.

Heating from 200 up to 725 °C lowers 40Kh steel hardness to HV 320 and increases impact toughness up to KCU = 50 J/cm^2. After such a reheating the volume fraction of martensite decreases in metal structure, its inclusions having significantly smaller sizes in comparison with those after heating up to 700 °C.

Post-weld heating in intercritical temperature interval up to 745 and 770 °C results in increase of impact toughness indices up to KCU = 75 and 64 J/cm^2, correspondingly, at metal hardness HV 365 and 375. Further increase of post-weld heating temperature notably lowers impact toughness and increases hardness. Thus, after heating up to 800 °C hardness rises up to HV 400 and impact toughness drops to KCU = 31 J/cm^2. After heating up to 840 °C these indices change to HV 545 and KCU = 8 J/cm^2. In the latter case 40Kh steel structure consists of fine-needled martensitic areas of bainite.

07Kh3GNM steel in the initial state after normalizing has a structure of fine-needled martensite with impact toughness KCU = 80 J/cm^2 and hardness HV 340. Heating of such a steel by welding thermal cycles leads to increase of impact toughness starting from the temperature above 600 °C (Figure 1, *c*). It is especially noticeable at heating in intercritical temperature interval A_{C1}--A_{C3}. In comparison with initial state the impact toughness rises more than 2 times, maximum value of KCU = 210 J/cm^2 is obtained after heating up to 825 °C. Heating in intercritical temperature interval also results in insignificant (up to HV 270--300) hardness reduction.

Further increase of heating temperature above critical point A_{C3} reduces the impact toughness on average to KCU = 100 J/cm^2 and increases hardness of 07Kh3GNM steel up to the level of hardness values in the initial state.

Post-weld heating for low carbon 07Kh3GNM and 14KhGNMDFB steels with high temperature of martensite transformation M_e was carried out after martensitic transformation of austenite has been practically completed. Cooling of billets was carried out to the temperature of 250 °C after first heating up to 1300 °C.

At subsequent heating of quenched samples of 07Kh3GNM steel significant structural changes were discovered after heating above 600 °C. Thus, heating up to 700 °C results in elimination of martensite orientation. Significant grain refinement along the boundaries of the former initial structure and intensification of structure contrast at microsection etching take place after heating in intercritical temperature interval up to 750 °C, that is, probably, induced by inhomogeneity of metal volumes on carbon. Heating up to 793 °C leads to bainite net precipitation along the boundaries of former initial grains and process of recrystallyzation after heating up to 825 °C promotes generation of extra fine-grain structure. Only the martensite transformation takes place after heating up to the temperature above critical point A_{C3} and further cooling of 07Kh3GNM steel austenite.

Post-weld heating of 07Kh3GNM steel billets from 250 °C up to the temperature below critical point A_{C1} does not result in noticeable change of hardness and impact toughness of metal in comparison with these indices of steel quenched from 1300 °C. Microstructure of tempered steel retains martensite orientation. Significant changes of strength properties take place after heating hardened steel in intercritical temperature interval (see Figure 1, *d*). After heating up to 768--800 °C impact toughness increases ($KCU \approx$ ≈ 170 J/cm^2) that almost 2 times exceeds values of this index in hardened steel. Metal hardness somewhat decreases after such a heating. It has a minimum value (HV 265) after heating up to 790 °C. After such heating the metal structure, even though it retains grain orientation of hardened steel, corresponds to a greater degree to bainite structure. Post-weld heating up to 830 °C also restores the structure of initial hardened steel in terms of shape. Metal hardness is equal to HV 280 and impact strength $KCU \approx$ 120 J/cm^2. Further increase of post-weld heating temperature from 860 to 1035 °C results in significant change of hardness value and impact toughness of high-temperature HAZ areas due to presence of coarse-grained martensite of 07Kh3GNM steel, obtained directly after first welding heating up to 1300 °C and complete cooling of the billets.

Particular change of strength properties at welding heating is observed in 14KhGNMDFB steel. This steel was studied in the state after normalizing with bainite structure and 6--8 vol.% of retained austenite. In the initial condition, its hardness was HV 320 and impact toughness KCU = 92 J/cm^2. Heating of the above steel up to the temperature below critical point A_{C1} and further cooling maintain the impact toughness on the level of initial metal, while increasing its hardness (see Figure 1, *e*). Higher heating in the interval of intercritical temperatures A_{C1}--A_{C3} results in a rather considerable lowering of impact toughness that for samples heated up to 760 and 830 °C is approximately equal to 30 % of KCU level of steel in the initial state. Further increase of heating temperature leads to restoration of impact toughness of 14KhNMDFB steel. However, while after heating up to 885 °C it is still lower than the level of KCU values in metal in the initial state, it exceeds this level after heating up to higher temperatures. Thus, heating up to 930 and 1320 °C increases impact toughness value up to 103 and 106 J/cm^2, correspondingly. As a result, steel acquires martensite structure with hardness HV 410--395.

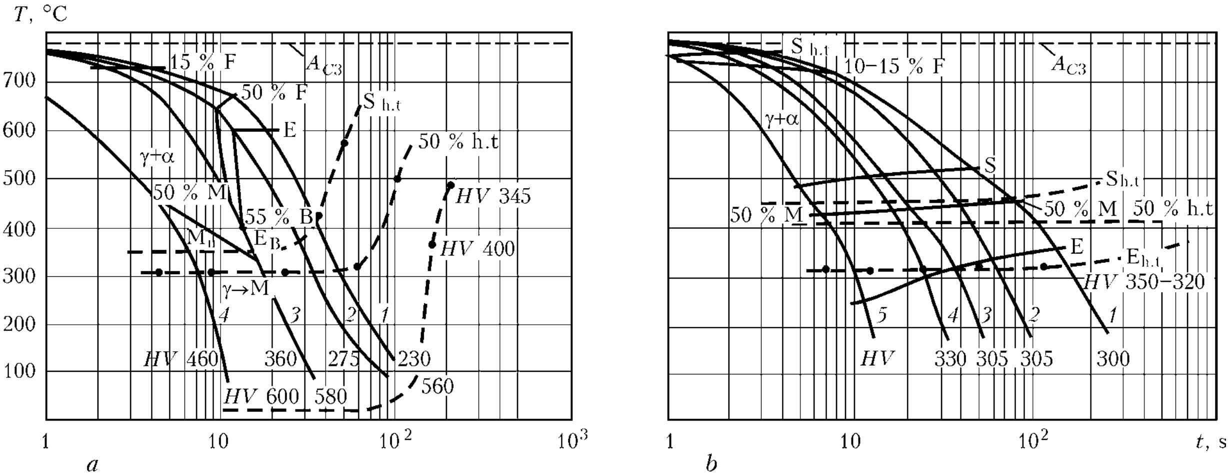

Figure 2. Diagrams of thermokinetic transformation of austenite of 40Kh (*a*) and 07Kh3GNM (*b*) steels obtained at different cooling rates (*1–5*): dashed curves ---- after sample heating up to 1300 °C; solid ---- after heating up to 1300 °C, cooling in air with rate of about 17 °C/s up to 200 °C and reheating up to 770 °C; h.t ---- heat treatment; S and E ---- start and end of structural transformation; B ---- bainite; F ---- ferrite; M ---- martensite

Post-weld heating of 14KhGNMDFB steel samples with martensite structure from 250 °C up to the temperature below 700 °C provokes noticeable change of metal hardness, but makes only an insignificant influence on impact toughness in comparison with these indices in hardened metal of high-temperature HAZ areas (see Figure 1, *e*). Thus, heating up to 615 °C decreases hardness to *HV* 350 with preservation of *KCU* equal to 106 J/cm^2. Effect of dispersion hardening becomes apparent after heating up to 680 °C. Steel hardness increases up to *HV* 375 after such heating, but impact toughness still remains on the level of hardened metal, being equal to 96 J/cm^2. Heating up to 755 °C results in an increase of hardness up to *HV* 400, and lowering of impact strength value to 52 J/cm^2. Further increase of post-weld heating up to 770 and 845 °C virtually does not lead to any change of hardness, but increases the value of impact toughness (*KCU* = 65 and 85 J/cm^2, respectively).

Thus, post-weld heating of high-temperature HAZ areas with martensite structure of steel alloyed with carbonitride-forming elements, in intercritical temperature interval causes an increase of metal hardness due to dispersion hardening and marked lowering of impact toughness. Therefore, for such steels it is rational to perform heating during post-weld heat treatment up to the temperature below temperature interval of dispersion hardening. Now, quenching of other steels from intercritical temperature interval leads to formation of ferrite-martensite metal structure with sufficient level of strength and ductility.

Thus, welding heating in intercritical temperature interval A_{C1}–A_{C3} has the most significant influence on impact toughness of investigated steels. During the indicated heating of steels, which do not contain such strong carbonitride-forming elements as vanadium, niobium, aluminium, the impact toughness significantly increases, and an adverse effect is observed in the case of their presence in steel composition.

Influence of cooling rate on transformation kinetics of austenite formed during post-weld heating in intercritical temperatures interval, was studied by means of heating--cooling of rigidly fixed samples by a procedure, described in [11]. Tubular samples were heated by passing current up to 1300 °C, cooled at the rate of $w_{550} \approx 17$ °C/s up to specified temperature, again heated in intercritical temperature interval with average temperature of about 100 °C/s and again cooled at different rate. Change of the temperature and physical properties at sample heating–cooling was registered with a loop oscillograph. Diagram of thermokinetic transformation of 40Kh steel austenite, formed at post-weld heating up to 770 °C, is given in Figure 2, *a*. The thermokinetic transformation of austenite after one time heating of 40Kh steel up to 1300 °C and cooling of samples at various rates is also shown here by a hatched line for comparison.

During post-weld heating up to 770 °C about 20 % of ferrite phase, formed from martensite at it fast heating, remains in 40Kh steel structure. Austenite newly formed during heating in the intercritical temperature interval has non-uniform carbon content due to high heating rate. Subsequent cooling of such an austenite-ferrite structure at the rate of 12.0–31.6 °C/s results in austenite decomposition. During cooling at the rate of 12 °C/s at 670 °C about 50 vol.% of austenite is preserved, and at 600 °C it completely decomposes by the pearlite mechanism into a ferrite-cementite mixture. Sample hardness after such a cooling is *HV* 230. Cooling at the rate of 15 °C/s does not lead to a change of transformation mechanism, just the temperature interval of phase transformation shifts downwards. Thus, the temperature of the presence of 50 vol.% of austenite is 630 °C, and transformation is over at 595 °C, while sample hardness rises to *HV* 275.

Increase of cooling rate up to 31.6 °C/s results in a significant change of kinetics of austenite transformation. In this case all three types of its transformation are already observed: pearlite, bainite and martensite. Temperature of the presence of 50 vol.% of austenite drops to 440 °C. Transformation is suspended at 390 °C and martensite formation starts at the temperature of 295 °C during cooling. Structure of sample metal after complete cooling consists of martensite (about 45 vol.%), as well as free ferrite and ferrite-cementite areas, formed by pearlite and bainite mechanisms. Hardness of metal, having such a structure, is equal to *HV* 360.

Cooling at the rate of $w_{550} \approx 100$ °C/s leads to complete depression of pearlite mechanism of austenite transformation, which starts at the temperature of 460 °C, when bainite forms from austenite. Martensite phase forms from more carbon-saturated austenite, it is located, primary, in the areas adjacent to the boundaries of former austenite grains, formed at initial heating of steel up to 1300 °C. Metal hardness after such a mode of post-weld heating and cooling is equal to *HV* 460.

Comparison of stability of overcooled austenite formed at one time heating up to 1300 °C and post-weld heating up to 770 °C shows that in the last case it is lower approximately by an order. This is accounted for by inhomogeneity of austenite formed by heating in intercritical temperature interval with preservation of ferrite and, possibly, carbide phases, being substrates at further austenite recrystallization, as well as extensive area of grains boundaries.

Post-weld heating of coarse-grained martensite of 07Kh3GNM steel up to 800 °C results in preservation of about 15 vol.% of untransformed α-phase. Bainite-martensite transformation of austenite takes place (Figure 2, *b*) at further cooling at the rate from 3.3 up to 33.3 °C/s.

With cooling rate increase in this range, the temperature of the start of bainite transformation decreases from 520 to 480 °C. A similar regularity is found at the temperature of the end of austenite transformation from 350 to 250 °C. Hardness of samples increases from *HV* 300 up to 330.

Comparison of diagrams of thermokinetic transformation of austenite, obtained at cooling with different rate after one time heating of 07KH3GNM steel samples up to 1300 °C [12] and for heating cycles up to 1300 °C, cooling up to 200 °C, reheating up to 800 °C and subsequent cooling, indicates their significant difference. Reheating of high-temperature HAZ area leads to increase of temperature of the start of its transformation at subsequent cooling of residual and newly formed austenite. Line of presence of 50 vol.% of austenite virtually coincides with the line of transformation start, obtained at austenite cooling after one time heating up to 1300 °C. Formation of ferrite phase and bainite, as well as high enough temperature of martensite transformation, increases HAZ metal resistance to cold crack formation after its post-weld heating in intercritical temperature interval.

Performed studies allowed establishing the optimum modes of local post-weld heating in welding of high-strength steels of various alloying systems. Such heating provides sufficient resistance of HAZ metal to cold crack formation and its high impact toughness.

1. Lebedev, Yu.M. (1999) Influence of steel composition on formation of HAZ structure of welded joints. *Avtomatich. Svarka*, **11**, 8–13.
2. Rykalin, N.N. (1951) *Calculations of thermal processes in welding*. Moscow: Mashgiz.
3. Goncharov, S.N., Gudnev, N.Z., Sterenbogen, Yu.A. et al. (1982) Effect of thermal cycle in twin-arc welding on resistance of 20KhGSNM steel to cold cracking. *Avtomatich. Svarka*, **7**, 14–15.
4. Metelev, A.V., Gorbachev, Yu.I. (1984) Control of twin-arc welding thermal cycle of hardenable steels. *Svarochn. Proizvodstvo*, **4**, 4–5.
5. Bursky, S.G., Dovzhenko, V.A., Sterenbogen, Yu.A. (1990) Resistance to cold cracking in HAZ of 14KhN3MDA type steel joints made by twin-arc narrow-gap welding. *Avtomatich. Svarka*, **2**, 20–24.
6. Sidoruk, V.S., Dudko, D.A., Gorbenko, N.V. (1985) Simulation of thermal cycle in heat-affected zone during electroslag welding by modulated current. *Ibid*., **7**, 12–15.
7. Dudko, D.A., Sidoruk, V.S., Ivashchenko, G.A. et al. (1990) Structure and hardness of HAZ metal in twin-arc welding by modulated current of steel 45. *Ibid*., **3**, 10–12.
8. Vagner, F.A. (1980) *Equipment and methods of pulse arc welding*. Moscow: Energiya.
9. Savitsky, A.M., Savitsky, M.M., Novikova, D.P. (2004) Influence of welding speed and duration of periodical cooling on structure formation in welded joints of hardening steels in arc welding with thermal cycling. *The Paton Welding J*., **8**, 39–43.
10. Kulik, V.M., Vasiliev, V.G., Grigorenko, G.M. et al. (2007) Phase and structural transformations in welding and arc treatment of 30KhGSA steel joints. *Ibid*., **9**, 6–10.
11. Lebedev, Yu.M., Kravchenko, L.P., Danilyuk, N.M. (1978) Procedure of modeling of welding thermodeformation cycles. *Avtomatich. Svarka*, **12**, 31–33.
12. Lebedev, Yu.M., Lazarev, V.N., Klejner, L.M. et al. (1989) Examination of weldability of low-carbon martensitic steel 07Kh3GNM. *Ibid*., **9**, 1–4.

POWER SUPPLY SYSTEMS BASED ON RESONANCE INVERTERS

E.N. VERESHCHAGO and **V.I. KOSTYUCHENKO**
Admiral Makarov National Shipbuilding University, Nikolaev, Ukraine

The paper gives a generalizing analysis of development and application of promising resonance power sources for arc welding and related processes. Shown are the examples of development of special power supply systems on their basis with a reduced level of high-frequency noise and improved reliability.

Keywords: *power system, arc welding, power source, air-plasma cutting, resonance topologies*

Manufacturing of semi-conductor electric power converters as the main functional sources of power supplies for welding and related processes and technologies is developing along the path of miniaturization, improvement of efficiency and reliability, reducing their influence on the mains, lowering their cost, etc. The above problems are solved with application of up-to-date local and foreign electronic components and new magnetic materials, advanced electric circuits and technique of power addition. Promising electric circuits ensure an increase of conversion frequency, without which it is impossible to increase the specific power of the source.

In the traditional circuits of high-frequency converters with square-wave voltage and current in order to ensure the optimum use of the frequency characteristics of the elements, electromagnetic compatibility with the mains, overvoltage and secondary breakdown protection of the semi-conductor devices, lowering the switching power losses and noise generated by the power sources (PS), these problems were solved by forming a favourable path of transistor and diode switching. Dissipative generating circuits, providing a delay between voltage drop and current front of the transistor at switching on and current drop and voltage front at its switching off, considerably lower the switching power losses in transistors.

On the other hand, their application has a number of disadvantages. First, formation of the switching path is accompanied by energy accumulation in the reactive elements, which then evolves in the form of heat on additional resistors. Secondly, their introduction limits the admissible values of the coefficient of transistor utilization by current and voltage, while the shape of transistor current remains practically square wave. Therefore, all the associated disadvantages are preserved, namely the high level of electromagnetic noise, overvoltages on semi-conductor devices, etc.

Alternatively, resonance topologies can be used [1–4]. This variant of pulsed PS is used in applications, which require high reliability, minimum weight and smallest dimensions, high efficiency and, what is most important, a lower level of generated noise. Resonance converters (RC) are based on circuits of traditional high-frequency voltage converters, into which resonance circuits are incorporated, which are formed by additional or parasitic reactive elements [1–4]. As current, or voltage on the key during the switching time are close to zero, switching on or off losses are eliminated, and for some modes both the kinds of losses, namely for switching on and off, are eliminated. Therefore, RCs can operate at much higher frequencies than the regular PWM converters.

RCs can be divided into the following groups: those with series resonance circuits and load switched on in series or in parallel to the resonance circuit elements; quasiresonance; E class; with soft switching. The Table gives the results of comparison of some topologies of pulsed PSc, which allow taking a compromise decision as regards selection of a suitable technology of the designed PS.

The Chair of Welding Engineering of the National Shipbuilding University gives a lot of attention to improvement of the principles of design of PSc for arc load. This paper gives descriptions of devices, which were designed with the authors' participation, and the technical characteristics of the developed devices

Results of comparison of some topologies of pulsed PSs

Type of pulsed PS	Cost	Weight	RF-noise	EMI-interference	Efficiency, %
Pulsed stabilizer with PWM	High	Small	High	High	70–80
Resonance converter	Same	Same	Medium	Medium	78–92
Quasiresonance converter	»	»	Same	Same	78–92

Figure 1. Appearance of PS for arc welding

give a certain idea of the main indices achievable for this class of semi-conductor energy converters.

Arc welding power source based on zero voltage switching circuit — ZVS. A functionally complete module of an all-purpose professional inverter of a welding system was developed for arc welding of steel materials 0.5–10 mm thick, and with the use of special accessories and materials — for argon-arc welding of stainless steel and copper alloys. The system can be used as part of automatic and semi-automatic welding machines, and it can be integrated into robotic, automated and mechanized complexes and devices. The optimized module simplifies design of multimodule PSc. Figure 1 shows the appearance of the arc welding power source.

The main technical characteristics of the self-sufficient single-phase module (open-circuit voltage is 90 V, open-circuit losses are not more than 10 W, ambient temperature range is from –20 to 40 °C, frequency range is from 25 to 150 kHz) are as follows:

Mains voltage, V	220 (+10 %; –15 %)
Open circuit voltage, V	not more than 90
Range of smooth adjustment:	
output current, A	20–160
output voltage, V	19–26
Duty cycle, %	60
Consumed power, kW	not more than 6
Efficiency at rated power, %	90
cos φ	0.85
Operating mode	TIG/MAG/MMA
Consumable electrode diameter, mm	1.5–3.25
Wire diameter, mm	0.6–1.0
Overall dimensions, mm	not more than 400 × 180 × 280
Weight, kg	not more than 8.5

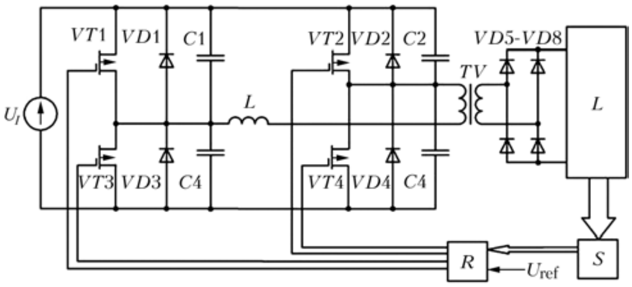

Figure 2. Diagram of frequency converter with a quasiresonance inverter (L — load; S — sensors; R — regulator, U_{ref} — reference voltage)

The base of the power source is a quasi-resonance converter with a «soft» switching with frequency method of output power adjustment in the inverter, providing high values of efficiency, power factor, reliability and impulse noise level [1].

Used as the power keys are high-voltage MOS-transistors of the new series L, meeting a whole number of additional requirements to ensure reliable operation of ZVS-converters manufactured by International Rectifier Company.

Simplified electric circuit of one of the proposed structures for powering an arc load based on a bridge inverter of ZVS-type is shown in Figure 2.

The power components of the quasi-resonance voltage converter with an AC choke generated output voltage according to the following expression [1]:

$$U_{0*} - I_r r_{\partial *} = U'_{1*}\gamma - 4L_{k*}f_* I_{r*} - U'_{1*}t_{rr}f_0 f_* - I_{r*}r_*, \quad (1)$$

where $U_{0*} = U_0/U_{r0}$; $I_{r*} = I_r/I_{r0}$ $f_* = f/f_0$; $L_{k*} = L_k f_0/R_{r0}$; U_{r0}, R_{r0} are the base (rated) voltage and equivalent load resistance corresponding to the operating mode with the rated load current I_{r0}; f_0 is the base value of modulation frequency; $R_{r0} = U_{r0}/I_{r0}$; $U_{1*} = U_1/U_{r0} = nU_1/U_{r0}$ is the relative (normalized) input voltage reduced to the secondary winding.

Power source internal resistance reduced to inverter output, is given by the following expression:

$$R_{L_k} = 2L_k/T,$$

where T is the pulse repetition rate; L_k is the inductance.

It is obvious that the higher the power source frequency ω, the higher inductance L_k, the steeper is the slope of the output characteristic and the more it differs from that of an ideal converter.

In the actual circuit, resistance r_c rises because of the resistance of the diodes, keys and resistance of copper of the transformer and choke windings. Stabilization of output current I_r in the stabilizer at destabilizing disturbances of output voltage U_1, arc voltage U_0, temperature, etc. is performed by changing the conversion frequency.

Frequency variation is performed according to the control action [3]:

$$\omega(t) = \omega_0 + \Delta\omega_{max}\overline{U}_*(t), \quad (2)$$

where $\Delta\omega_{max} = 2\pi\Delta f_{max}$ is the maximum frequency deviation at modulation (frequency deviation); $\overline{U}_*(t)$ is the rated input control signal equal to $U(t)/U_{max}$; U_{max} is the maximum value of the input signal.

Maximum level of current at the output will be obtained at $\omega_{min} = \omega_0$, and minimum level at $\omega_{max} = \omega_0 + \Delta\omega_{max}$. Range of adjustment D of modulation frequency in this case is given by the following expression:

$$D = \frac{I_{\min}}{I_{\max}} = \frac{\omega_{\max}}{\omega_{\min}}.$$

Having divided the left and right parts of expression (2) by ω_0, we get

$$\frac{\omega(t)}{\omega_0} = \frac{\omega_0}{\omega_0} + \left(\frac{\omega_{\max}}{\omega_0} - \frac{\omega_0}{\omega_0}\right)U_*(t).$$

Hence,

$$\omega(t) = \omega_0[1 + (D - 1)U_*(t)].$$

In the steady-state mode modulation frequency f and input signal value ($u = U$) are related to each other by a linear dependence

$$f = f_0 + k_m k_c U = f_0 + k_m k_s k_c (I_r - I_s), \tag{3}$$

where k_m, k_s, k_c are the transfer constants of voltage controller generator (frequency modulator), current sensor and control device, respectively; I_s is the setting current.

In the steady-state mode the setting current ($i_s = I_s$) is equal to the initial load current:

$$I_s = I_{r0}.$$

In relative values equation (3) has the following form:

$$f_* = 1 + \frac{k_m k_c U_{\max}}{f_0} U_* = 1 + \frac{k_m k_c k_s I_{r0}}{f_0}(I_{r*} - I_{s*}) = 1 + \frac{(D-1)k_c k_s I_{r0}}{U_{\max}}(I_{r*} - I_{s*}), \tag{4}$$

where $k_m = f_0(D - 1)/U_{\max}$.

Substituting expression (4) into (1), we obtain a relationship determining the output current of a stabilizer with a closed-loop feedback circuit:

$$I_{r*}^2 - I_{s*}I_{r*} + \frac{r_* - r_{d*} + 4L_{k*}}{a} I_{r*} - \frac{U'_{1*}\gamma - U_{0*}}{a} = 0, \tag{5}$$

where $a = 4L_{k*}\dfrac{k_m k_c k_s I_{r0}}{f_0}$.

Load current is determined as a positive root of expression (5):

$$I_{r*} = \frac{I_{s*} + \dfrac{r_{\partial*} - r_* - 4L_{k*}}{a}}{2} + \sqrt{\left(\left(I_{s*} + \frac{r_{\partial*} - r_* - 4L_{k*}}{a}\right)/2\right)^2 + \frac{U'_{1*}\gamma - U_{0*}}{a}}.$$

Approximating expression (5) by two first terms of the power series, we get

$$I_{r*} = I_{s*} + \frac{r_{\partial*} - r_* - 4L_{k*}}{a} + \frac{U'_{1*}\gamma - U_{0*}}{I_{s*}a + r_{\partial*} - r_* - 4L_{k*}}, \tag{6}$$

where the condition of convergence of the series is

$$\left|\frac{U'_{1*}\gamma - U_{0*}}{a}\right| \le \left(I_{s*} + \frac{r_{\partial*} - r_* - 4L_{k*}}{a}\right)^2.$$

Static adjustment error Δ_{st} of stabilizer current, the power circuit of which is made by the diagram of Figure 2, has the following form:

$$\Delta_{st} = |I_{s*} - I_{r*}| = \frac{r_{\partial*} - r_* - 4L_{k*}}{a} + \frac{U'_{1*}\gamma - U_{0*}}{I_{s*}a + r_{\partial*} - r_* - 4L_{k*}}. \tag{7}$$

As is seen from expressions (6) and (7), the accuracy of maintaining the load current increases with increase of transfer constants k_m and k_c of frequency modulator, and of amplifier, respectively. At $k_m k_c = \infty$ adjustment static error is zero. At a finite value of $k_m k_c$ the accuracy of maintaining the current is influenced, for instance, by arc voltage. Adjustment error increases with U_0 decrease, as well as with decrease of inductance L_{k*}, current I_{s*} and load voltage U_{r*}.

It follows from expression (7) that in the compensation stabilizer changes of the value of any parameter, determining I_r, including voltage U_0, lead to output current instability. In order to assess the influence of these changes let us use the sensitivity of output current to a change of any parameter P (parameter included into control of adjustment characteristics, or describing the operation of frequency modulator) in the stabilizer, for instance $(\partial I_r/\partial P)_0$. Then, the total change of output current ΔI_r at an aggregate effect of destabilizing factors will be given by the following expression:

$$(\Delta I_r)_0 = \sum_P (\partial I_r/\partial P)_0 \Delta P / (r_{\partial*} - r_* - 4L_{k*} - 2aI_{r*}^0 + aI_{s*}^0). \tag{8}$$

It follows from formula (8) that in order to reduce the forced (steady-state) component of the error, it is necessary to increase $k_c k_m$. However, at $k_c k_m$ increase the stability margin decreases, the system moves closer to stability limit, and the transient process becomes oscillatory to a greater extent (transient process characteristics deteriorate).

Formation of static and dynamic characteristics of the power source–arc system is performed under the effect of delayed negative load current feedback. Current feedback signal acts through the «insensitivity zone» link. In an approximated piecewise-linear form the equation of the static characteristic of the nonlinear link in the circuit of negative current feedback is expressed as follows:

$$x_2 = \begin{cases} 0 & \text{at } x_1 \le b; \\ k(x_1 - b) & \text{at } x_1 > b; \quad k = \operatorname{tg}\alpha. \end{cases}$$

It is obvious that the converter external characteristic in the general form has three characteristic

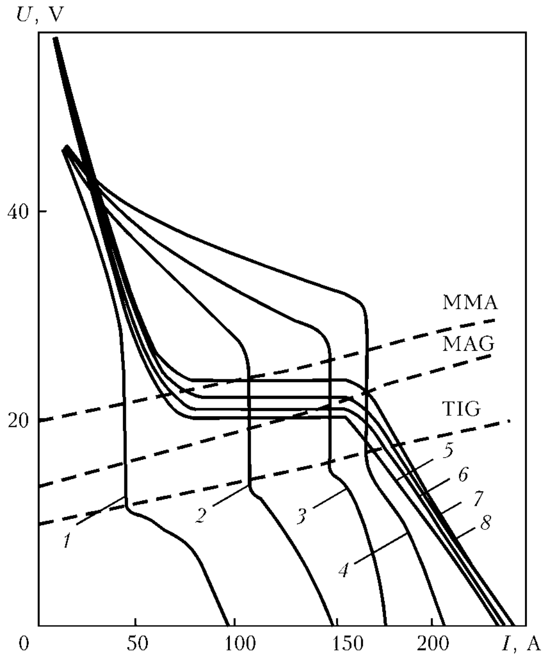

Figure 3. Experimental external characteristics of the power source: *1–4* — I_s = 424, 102, 142 and 160 A; *5–8* — U_s = 20, 21, 22 and 24 V, respectively

sections: I — small load section, characterized by an insignificant voltage drop at increase of load current (voltage stabilization); section II of output current stabilization, in which the slope of the working section changes from zero to a unity and an abrupt drop of output voltage occurs; section III, in which the converter moves into a non-controlled mode, characterized by a smooth decrease of output voltage at increase of load current (limitation of maximum current right down to the load short-circuiting mode). Figure 3 shows experimentally measured PS external characteristics at different values of output voltage and current [1].

The developed PS allows realizing load power on the level of 5 kW. In design of more powerful PSs their parallel operation for a common load is envisaged, the more so, since the use of the considered principle of construction of the power components provides an increase of load power in the most simple way by connection of additional modules without the need to use special means for equalizing the current and power between the modules.

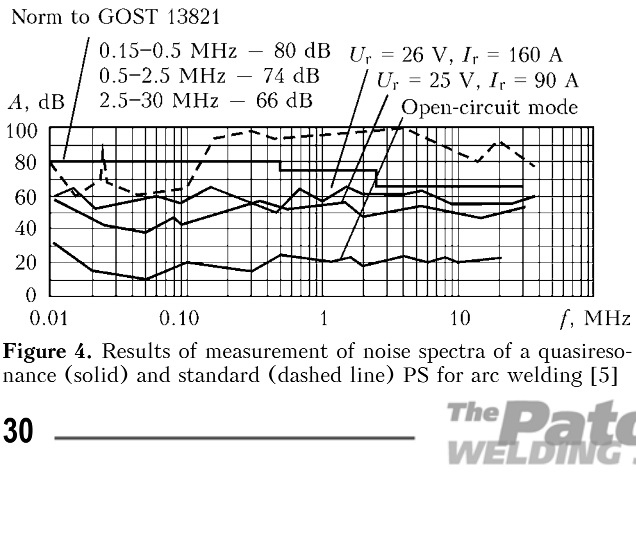

Figure 4. Results of measurement of noise spectra of a quasiresonance (solid) and standard (dashed line) PS for arc welding [5]

In the realized PS the following advantages of the frequency method of adjustment and combined modulation were confirmed:

• practically complete absence of through currents (impulse noise) due to unblanked and smooth switching on–off of the switching transistors and rectifier diodes;

• possibility of increasing the switching frequency up to 100 Hz;

• lowering of static and dynamic losses in the transistors and diodes provided the efficiency > 92 %.

Inverter PS for welding, for instance, with stick electrodes with MP control, has a complex-combined external VAC ensuring realization of the functions of «hot start», arc boosting, selection of the slope of VAC working section in the range from 0.4 up to 2.0 V/A, depending on the specific conditions of welding and electrode type, rigidity of the external characteristic of 0.01 V/A.

The system also ensures a smooth adjustment of current in the range of 20–160 A; lowering of open-circuit voltage U_0 to 12 V at long-time breakdowns (more than 0.6–1.0 s); maintaining the set current at mains voltage fluctuations; protection from electrode sticking at short-circuiting for more than 0.5 s, etc.

An important advantage of the new PS with a completely digital control system relative to the traditional one, is the possibility of a smooth variation of output VAC of the source to make it close to an ideal one.

Figure 4 shows that the technology used in PS development allows an essential lowering of the noise level. For the considered PS the noise level at the output and in the power circuit does not exceed 65 dB in the entire frequency range.

Power supply units (PSU). *PLASMA-2 PS* (Figure 5). A practical application of power sources operating for the arc gap, were devices of power supply for plasma ignition of fuel [2]. In practical development of PSU for plasma technologies, alongside the main quality indices (efficiency, reliability, weight), the following additional ones were also taken into account: power voltage and its scatter; frequency range and stability; ambient temperature and possible

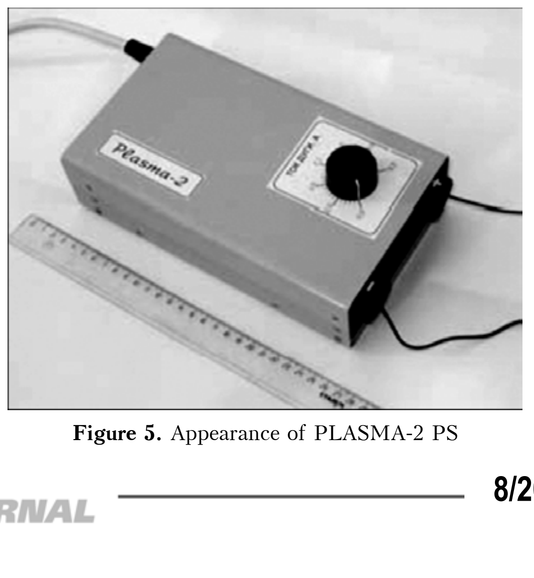

Figure 5. Appearance of PLASMA-2 PS

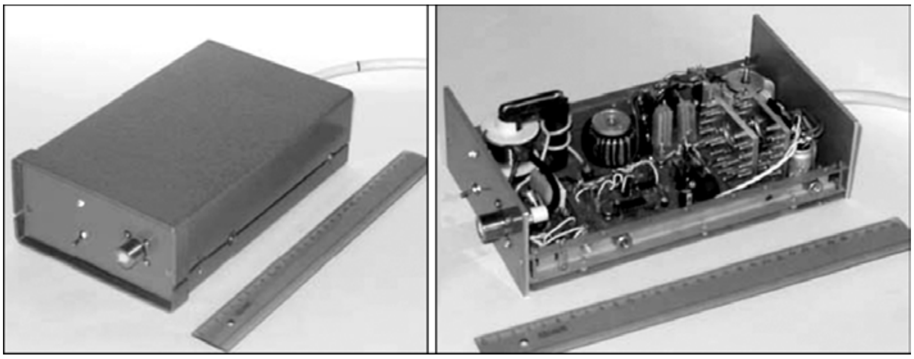

Figure 6. Appearance of PLASMA-3 PS

cooling methods; power factor; specific weight; design requirements (overall dimensions, impact and vibrational overloads, standard and tropical versions); operation cycles, and service life. Each of the above indices is of a fundamental importance and can change the technical characteristics of the designed device.

Power units for systems of plasma ignition of fuel were made to have the circuit of quasi-resonance high-frequency transistor inverters with switching at zero current or voltage [2, 4].

Main technical characteristics

Kind of plasma medium	air
Pressure gradient of plasma medium, MPa	(1--6)--10
Plasma medium consumption, g/s	0.1--0.5
Kind of arc current	DC
Open-circuit voltage, V	600±40
Arc working voltage, V	150±30
Short-circuit current, A	7.5±1.0
Range of arc current adjustment, A	1.5--7.5
Operating mode	repeated-short-term
Power unit life, switching	not less than 10000

PLASMA-3 PS (Figure 6) is designed for power supply to ignition systems of gas turbine engines from 27 V on-board mains, as well as simultaneous operation with VPT-5 (VPL-8) plasmatron.

Main technical characteristics

Power circuit voltage, V	27 (+10 %; --20 %)
Kind of output current	DC
Open-circuit voltage, V	600±40
Rated arc working current, A	2.5
Arc working voltage, V	150--270
Overall dimensions, mm	not more than 250 × 160 × 80
Weight, kg	not more than 2.0
Operating mode	repeated-short-term

PS circuit is based on two-step converter built with field transistors of new L series of International Rectifier Company, which forms 50 Hz AC pulses in the matching transformer windings.

PLASMA-4 PS. «PLASMA-4» unit can be applied to determine the main power characteristics of air micro-plasmatrons and life testing of plasma ignitions (Figure 7).

Main technical characteristics

Mains voltage, V	1--220
Open-circuit voltage, V	not more than 700
Arc current range, A	2--20
Maximum consumed power, kV·A	7
Weight, kg	not more than 8
Overall dimensions, mm	not more than 400 × 180 × 280

Power unit for air-plasma cutting. Development of power units based on bridge converters with transistor quasi-resonance inverters with phase control, providing soft transistor switching (power key switching at zero voltage values — ZVS) is of practical interest for power supply to powerful air plasmatrons [3].

A fragment of electric circuit of power components of an improved ZVS with an adaptive structure for a converter with full-wave rectifier and L-filter for the case of arc load operation with output current varying in a broad range, is shown in Figure 8.

Converter control system is based on ATmega 16 microprocessor [3, 4]. In addition to improvement of the accuracy of the process unit operation, new topology of the power components with microprocessor control significantly (by 15–20 %) improves the accuracy and quality of the cut out blanks specified by GOST 14792--80 (EN 60791--1) and similar standards of Germany, France and other countries, reduces consumption of rapidly-wearing parts of the plasmatrons not less than 2 times, ensures self-diagnostics of the condition and protection of the entire controlled complex, digital indication of the real and set values of current and voltage of the arc and interfacing with higher level computer.

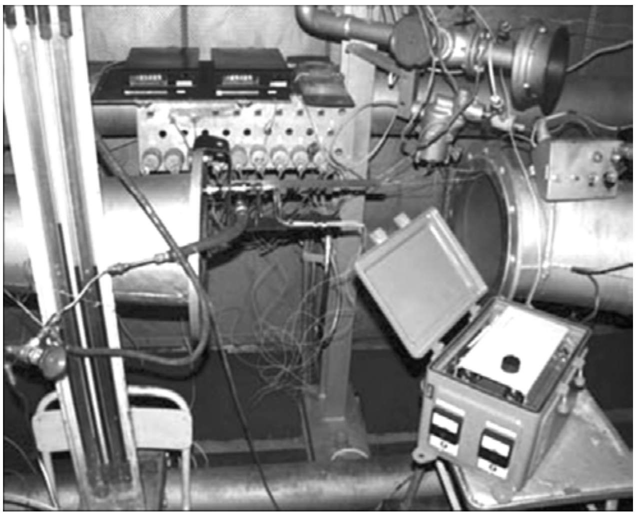

Figure 7. Appearance of a bench for testing systems for plasma ignition of fuel

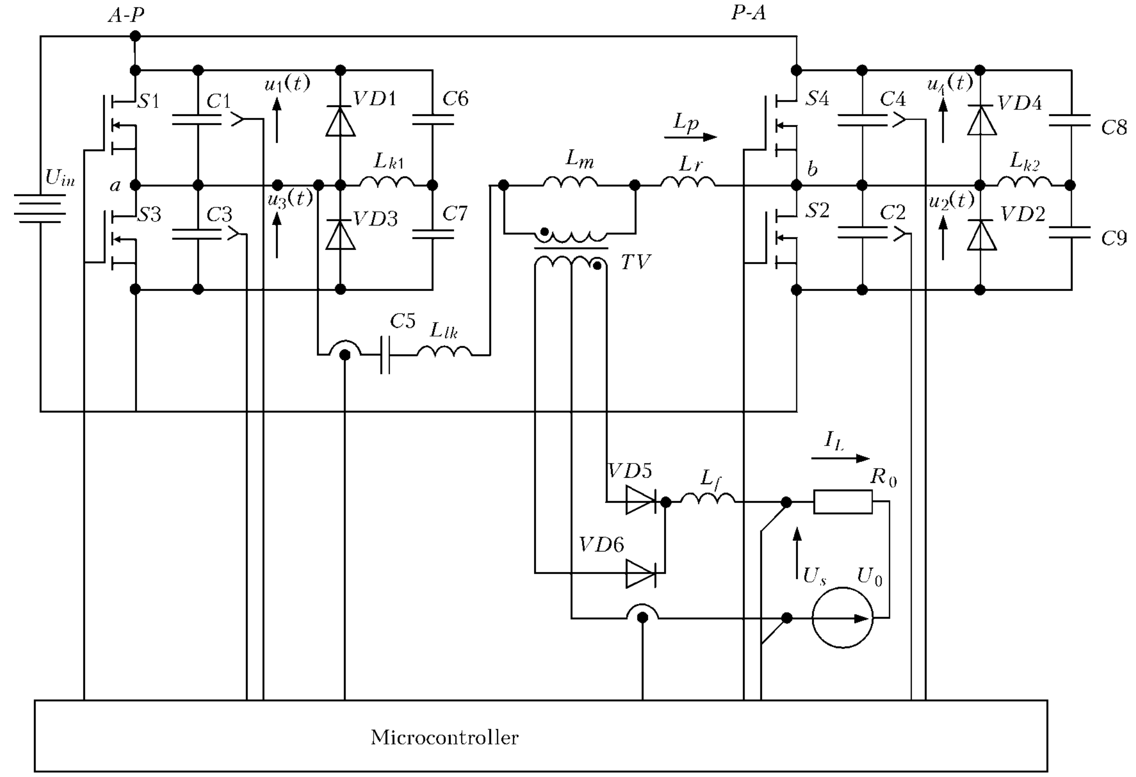

Figure 8. Diagram of power components of the developed PS

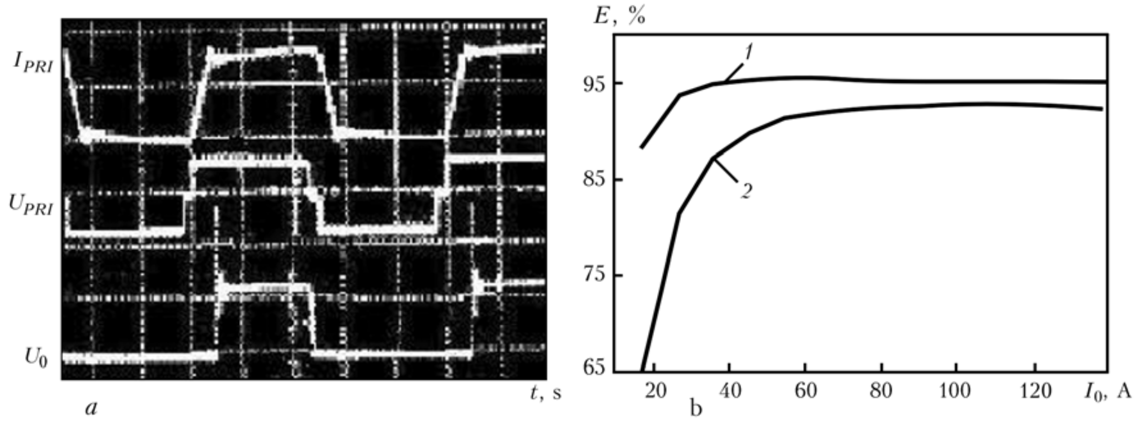

Figure 9. Oscillograms (m_t = 7.2 μs/div) of primary voltage U_{PRI} (m_U = 1000 V/div), primary current I_{PRI} (m_I = 15 A/div), rectified voltage U_0 (m_U = 200 V/div) (*a*) and dependence of efficiency *E* of the conventional (*1*) and ZVS-FB-converter (*2*) on load current (*b*)

Figure 10. Appearance of PLASMA 110i HF PS

Oscillograms given in Figure 9 show the advantages of the new technology application: operating mode becomes more symmetrical, thus promoting a lowering of losses in the power components and allows a considerable (3–5 times) lowering of the level of electromagnetic noise. Voltage surges in the oscillograms are practically absent. Figure 9, *b* shows that converter efficiency turns out to be increased and practically independent in the range of currents from 20 % up to the rated value. Figure 10 gives the appearance of transistor PLASMA 110i HF PS. Specific bulk power of the converter was 160 W/dm^3.

Main technical characteristics

Voltage, V/phase number/frequency, Hz ... 380/3/50–60
Kind of current .... direct
VAC CC

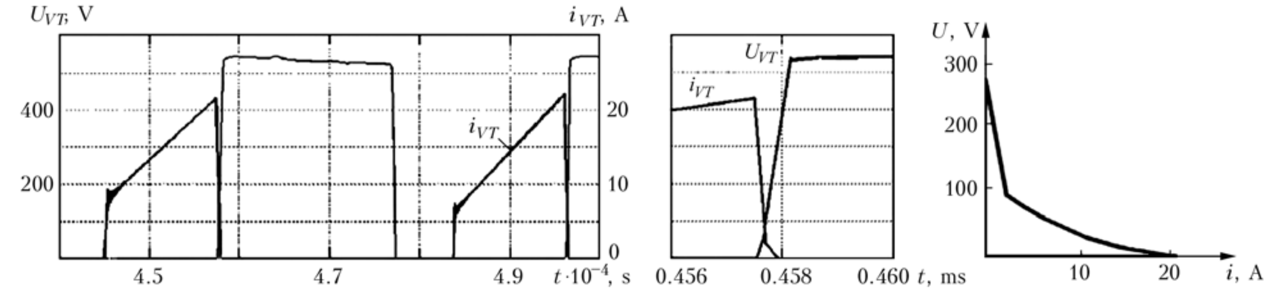

Figure 11. Process of switching in the inverter and paths of transistor working point movement

Maximum consumed power, kW	20
Current adjustment range, A	20--100
Maximum open-circuit voltage, V	250
Duty cycle, %	100
Maximum cut thickness, mm:	
quality cut	25
severing cut	35
Efficiency, %	85
Power factor	0.95
Overall dimensions, mm	710 × 285 × 485
Weight, kg	28

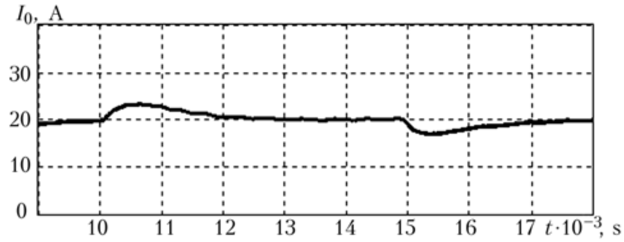

Figure 12. Transient processes in the system «in the large» (R_n = = 5 Ohm; R_{n1} = 5 Ohm; i = 20 A)

Experimental studies of the interaction of current regulator with the actual technological load showed that the transition to a high conversion frequency provides a high stability of the arc discharge at output circuit inductance below 300 μH. Short response time of the regulator ensures a fast increase of current at arc discharge excitation, while the high steepness of the current limitation section (> 40 V/A) ensures reduction of current fluctuations at the change of the air flow velocity.

During the switching process in the inverter, the transistor working point moves at a maximum distance from the limit of the region of transistor safe operation, so that dynamic losses are decreased and reliability is increased (Figure 11).

The modified module incorporated into the quasiresonance converter for powering the plasmatron in ZVS mode provided a 15--25 dB lowering of the emitted radio-noise, generated during the instrument operation in different operating modes compared to standard ZVS-converter, while the relative voltage level of the generated radio-noise did not exceed the norms in keeping with GOST 13281 in the entire frequency range. This was promoted by absence of the influence of current of reverse restoration of antiparallel diodes and lower du/dt level, which are characteristic for this application. An additional improvement of spectral composition can be achieved when using higher-capacity snubber capacitors.

In order to analyze the current regulator dynamic properties, processes occurring in the system at jumplike variations of the load were considered. Result of transient process simulation «in the large» in a system with an optimized regulator [3, 4] is shown in Figure 12. The stabilized current converter provides the set static accuracy of the system, stability and desired aperiodic nature of the process of output current drop-build-up at load jumps. Figure 12 gives the parameters of the transient process: maximum overregulation $\Delta I_{0\max} = 4$ A, process duration $t_{pr} = 2 \cdot 10^{-3}$ s. Comparison of the main characteristics shows the good prospects for application of the new topology of power components as an intermediate frequency link for powering the plasmatron.

PLASMA 110i HF PS was awarded the Diploma of the All-Ukrainian Competition-Exhibition «Best Local Product 2008».

In conclusion it should be noted that improvement of the principles of construction of transistor converters of electric power parameters, regarding the power units as power supply system elements, provision of electromagnetic compatibility with the mains and electric power users in these systems has a considerable influence on circuit design solutions and, eventually, on their technical characteristics.

Thus, results of scientific and engineering developments on creation of special power supply systems on the basis of resonance transistor inverters, with maximum allowance for the features of technological loads, showed the high potential of the accepted approach to development of PSs with a high efficiency, high density per a unit of power, a reduced level of high-frequency noise and increased reliability, operating for arc loads.

1. Vereshchago, E.N., Kvasnitsky, V.F., Yavishev, D.I. (2005) Power source of welding arc on the base of ZVS-circuit. *Tekhn. Elektrodinamika*, **6**, 24--28.
2. Vereshchago, E.N., Feldsher, I.F., Kostyuchenko, V.I. (2006) A new power source for plasma treatment of parts. *Vestnik Dvigatelestroeniya*, **4**, 16--19.
3. Vereshchago, E.N., Kvasnitsky, V.F., Kostyuchenko, V.I. (2008) Quasi-resonance power source PLASMA 110i HF for plasma cutting. *Svarochn. Proizvodstvo*, **6**, 37--41.
4. Vereshchago, E.N., Kvasnitsky, V.F., Miroshnichenko, L.N. et al. (2000) *Circuit design of inverter power sources for arc load*: Manual. Nikolaev: UGNTU.
5. Korotynsky, A.E., Kopylenko, E.A., Pavlenko, G.V. et al. (2005) Evaluation of parameters of electromagnetic compatibility of arc welding equipment. *Svarochn. Proizvodstvo*, **11**, 9--12.

EXPERIENCE OF EFFECTIVE ORGANISATION OF TRAINING OF SPECIALISTS OF WELDING PRODUCTION FOR SHIPBUILDING

A.M. KOSTIN
Admiral Makarov National Shipbuilding University, Nikolaev, Ukraine

The positive experience of regional centre for training specialists of welding production for shipbuilding is described.

Keywords: *welding production, personnel training, shipbuilding*

The integration of Ukraine into European Community, including the field of training the specialists of welding production complies with the adopted principles of Bologna system accounting for the gained international experience and branch practice inside the country [1]. In this relation the experience of the Admiral Makarov National Shipbuilding University (NSU) represents an interest. This University was approved in 1996 by common Decree of Ministry of Education and Science and Ministry of Industry of Ukraine as a leading organization in training personnel of all levels in shipbuilding welding production. At NSU together with shipbuilding plants of South of Ukraine the association «Shipbuilding Training Center of Welding» (STCW) was founded, the co-founders of which were «Vadan Yards Okean», State Enterprise «Zarya-Mashproekt», «Khersonsky Sudostroitelny Zavod», «Zavod imeni 61 Kommunara», «Chernomorsky Sudostroitelny Zavod» and NSU. The association is an independent legal organization and conducts its activity on the principles of self-sustaining and self-management. The supreme direction body of STCW is the Board of Trustees. Apart from this the Chair organized two branches at the leading enterprises of the city: «Vadan Yards Okean» and «Zarya-Mashproekt», to expand practical training of engineers and their adaptation to industrial conditions. The chiefs of the Chair branches are Yu.V. Solonichenko, Technical director, and Yu.V. Butenko, Chief welder. The enterprises are the basic ones to carry out all kinds of training among the students.

The foundation of new effective organizational structure allowed the Chair to expand significantly the list of performed works and cooperation area with leading enterprises of the region. In particular, beginning since 1997 STCW together with German Welding Association of the land Meklenburg-Vorpommern (SLV) within the scope of international program «Transform» started retraining of leading specialists of welding production of enterprises of the South of Ukraine with issue of a certificate «European Welding Engineer», and since 2000 the training on the program «International Welding Engineer» is performed. The realizing of this program allowed the teachers of the Chair to improve their qualification and to receive the appropriate certificates [2].

The association carries out also the training and attestation of welders in accordance with NPAOP 0.00-1.16--96 (Permission 019.05.48.80.42.0) and Russian Marine Navigation Register (RMNR) regulations (Enterprise Certification Certificate 05.00035.160). For these purposes the training class for twelve welding stations and attestation laboratory are equipped at the Chair of Welding Engineering, where complete training and attestation of welders is performed with issue of qualification certificates with the right to manufacture, mount, reconstruct and repair objects and equipment in compliance with all acting standard documents in Ukraine (NPAOP, SNiP, DBN, DSTU). The attestation base of STCW is also an official regional test center of Nikolaev department of RMNR, with which the Chair has as fruitful cooperation. The training and attestation are performed practically on all welding methods. For this purpose a constant acting attestation commission was founded with chairmen: Yu.V. Butenko, Chief welder of «Zarya-Mashproekt» (Nikolaev), Yu.M. Konashchuk, Chief welder of CNGS Engineering (Simferopol), A.N. Vorobiov, Chief welder of Odessky Priportovy Zavod, A.M. Kostin, Senior lecturer of NSU. STCW trains specialists of the first and second level on NDT of welds. The protocols of welder's attestation tests are recognized practically by all classification societies and is a basis to issue certificates in accordance with requirements of classification societies (GL, LR, BV).

As the experience of work showed it is reasonable for enterprises to carry out attestation of welders at the common basis disposing considerable material and scientific potential. The independent expert evaluation completely excludes the influence on attestation results and gives possibility to estimate welders qualification objectively. Using this approach the personnel of the Chair is always conscious of production problems which in general has positive influence on studying process. The existing attestation base fosters attraction of funds for repair and modernization of equipment, studying classes and rooms, allows students to master the working profession of welder, here all welding consumables are purchased by STCW. Some students successfully pass qualification tests and get basic certificates of electric welder, which allows work on the profession during industrial practice.

In the frames of attestation-test work the Chair constantly carries out practical seminars, consultations and lectures on development and implementation into production of new welding consumables, basic and auxiliary welding equipment inviting the leading specialists of our country and from abroad. In the recent years on the basis of the Chair such companies as KZESO, SELMA, «Arksel», «Amiti», «Messer Cutting & Welding», «Boehler», «Abicor Binzel», ESAB, «Drahtzug Stein», «MezhGosMetiz» and other propagate their production on regular basis. The works on the trend are carried out attracting students, who obtain new knowledge directly from developers in active and interesting way.

The specialists of the Chair, being independent experts, systematically participate in estimation of quality of manufacture of single parts, assemblies and objects, perform certification of welding technologies in accordance with DSTU 3951–2000 and RMNR regulations, provide consultations and carry out classes for workers and engineer-technician personnel directly at enterprises without work interruption. The training as a rule is conducted as regards to definite products with a detailed discussion of existing problems. The possibility of joint scientific work and introduction of progressive technical and technological solutions into production arises. One of the most significant examples in this trend is a joint development of plasma cutting source Plasma 110i HF by NSU and SPE «UkrTertMash», which was awarded diploma at all-Ukrainian exhibition and competition «The best domestic goods 2008» in the nomination «Shipbuilding» [3] or, for example, the power source VDU1202, developed by «Amiti», with combined external characteristic in complex with automatic machine TS77 which allows using solid wire in automatic mode under flux to produce butt joints of thickness from 16 up to 40 mm into slot gap without edge preparation [4]. Still there are plenty examples.

In the recent years the fruitful mutually benefitial cooperation was established with our constant partners such as SELMA, KZESO, «Vadan Yards Okean», «Zarya-Mashproekt», Nikolaev department of RMNR and other. The enterprises regularly invite our graduates for a work and send their workers for a study by correspondence. The study is performed according to the working area of regional enterprises, the considerable part of diploma projects is performed on their order. The Chief welders of enterprises are actively involved in studying process, they regularly attend defense of diploma projects, that make their choice of graduates for widening the welding departments personnel easier. The mentioned enterprises, except of active cooperation in the area of personnel training, render considerable material aid to Chair of Welding Engineering. Just in the recent years the Chair has received new equipment, materials and aid from sponsors at the sum of more than 100 thou UAH. The aid is not interrupted even under conditions of total economic crisis.

The Chair keeps close relations with graduates working at enterprises of Nikolaev, Kherson, Simferopol, Kerch, Odessa and many other cities, involve them into participation in practical seminars, cooperation in the frames of STCW working plan, the most gifted are invited to post-graduate courses. STCW undertook the functions of regional coordinator and consolidated efforts of enterprises in the area of personnel training of all levels for the needs of welding production. The expansion of the Chair activity consolidates the relations of teaching personnel with successfully working enterprises which positively influence its image.

As the experience showed the complex approach to the problem of personnel training on the basis of close relation with enterprises of different forms of property, the creation of branches of the Chair on the basis of leading industrial enterprises of the region, common organization of regional center of personnel training provide the modernization of material-technical and methodical base on training of welding specialists of all levels for the needs of different branches of industry.

1. Zhuravsky, V.S., Zgurovsky, M.Z. (2003) *Bologna process: main principles of entry to Europe space of higher education*. Kiev: Politekhnika.
2. Kvasnitsky, V.F., Kostin, A.M., Romanchuk, N.P. et al. (2006) Efficient organizational structures for training welding specialists for ship building. *The Paton Welding J.*, **4**, 39–40.
3. (2008) Universal quasi-resonance power source of new class for plasma cutting: Admiral Makarov National Shipbuilding University. Winners of competition 2008 for Best National Good of Year. http://www.krashiy.com/main/ukr/nominations2008/nid=25&pid=1119&id=8264
4. Dragan, S.V., Yaros, Yu.A., Yaros, O.O. et al. *Rectifier for submerged-arc welding and surfacing*. Pat. 30840 Ukraine for utility model. Publ. 11.03.2008.

PECULIARITIES OF STRUCTURE OF METAL DEPOSITED ON EDGES OF SINGLE-CRYSTAL BLADES MADE FROM NICKEL SUPERALLOYS

K.A. YUSHCHENKO[1], **B.A. ZADERY**[1], **A.V. ZVYAGINTSEVA**[1], **V.S. SAVCHENKO**[1], **I.S. GAKH**[1] and **O.P. KARASEVSKAYA**[2]

[1]E.O. Paton Electric Welding Institute, NASU, Kiev, Ukraine
[2]G.V. Kurdyumov Institute for Metal Physics, NASU, Kiev, Ukraine

Peculiarities of crystallography and structure of metal deposited on free edges of single-crystal blades made from heat-resistant alloy JS-26 are considered. Their dependence upon the crystallographic orientation of the initial metal has been established. It is shown that, in general, inheritance of the crystallographic orientation and changes in the structural state of the initial metal by the deposited metal in cladding obeys the same qualitative mechanisms as in welding.

Keywords: *electron beam cladding, filler metal, single crystals, heat-resistant nickel superalloys, crystallographic orientation, shape of solidification front, thermal gradient, direction of preferred solidification, dislocation density*

As shown by systematisation of service damages on GTE blades conducted by the authors of this article, as well as the data of studies [1--3], most defects occur within the edge portion of a blade. The major part of them (50--90 %) takes place in the leading edge, while the rest of them --- in the end part and trailing edge. Such damages are repaired mainly by arc or plasma cladding, or with the electron beam. In the blades produced by the directed solidification method, the edge to be repaired consists of a single, bi- or tricrystal. Crystallographic orientation of the edge to be clad is determined by location of a defect.

It is well known that structure of the weld metal in welding of single-crystal nickel-base superalloys is determined, in the first turn, by the crystallographic orientation of the initial metal and by the welding direction [4--9].

Differences in structure of the welds and clad metal are caused by a specific character of the thermal-deformation cycle, shape of the molten metal pool solidification front and other peculiarities. In this connection, the purpose of this study was to investigate the effect of an initial crystallographic orientation of substrate of a single crystal being clad on the degree of its inheritance by the deposited metal, as well as peculiarities of structural changes in the initial single crystal.

In order to obtain comparable results to exclude the impact on structure by natural fluctuations and conditions of growth and cladding of samples of different supplies, the investigations were conducted on bicrystals, and only the check ones --- on single crystals.

Initial 60×80 mm billets of nickel superalloy JS-26 were made in the process of growth of single-crystal plates 6--8 mm thick by the method of high-speed directed solidification. Chemical composition of the alloy was as follows, wt.%: 0.8--1.2 V, 4.3--5.6 Cr, 0.8--1.2 Ti, 0.8--1.4 Mo, 10.9--12.5 W, 8.0--10.0 Co, 4.5--8.0 Al, 1.4--1.8 Nb, 0.22--0.27 Mn, 0.9--1.1 Fe, 0.13--0.18 C. One of the crystals was chosen so that its crystallographic orientation was close to the direction of high-symmetry axes. Cladding was performed layer-by-layer on the edge of a plate using the same filler metal as the initial alloy by the electron beam method. Height of a layer deposited per pass was 1.5--2.0 mm. Up to three layers were deposited in the experiments (Figure 1). Values of the cladding parameters were limited by a requirement to provide the quality formation of the deposited metal (absence of rolls, fusion with the base metal (BM), and smooth surface geometry), as well as the absence of cracks.

The investigations showed that the sensitivity to cracking of single crystals of the alloy in cladding on the edge was determined by height of the deposited layer, quantity of cladding passes, initial crystallographic orientation and structure.

Cracks were very scarce in the case of the deposited metal up to 1 mm high. Increase in the height of the deposited metal, like the quantity of the passes, increased the probability of cracking. The unfavourable crystallographic orientation for inheritance, which did not coincide with the high-symmetry axes of the initial single crystal (as well as the presence of high-angle grain boundaries in it) led to distortion of the initial structure, formation of stray grains and cracks. However, no cracks were formed in the case of a small (less than 6°) disorientation of grains, «soft» thermal cycle (cladding speed 10--20 m/h, preheating to 400--600 °C) and small height of the deposited metal. In the presence of high-angle grain boundaries, the cracks might initiate not only in the deposited metal, but also in the HAZ metal, at some distance from the fusion line. This can be associated, to a major degree, with peculiarities of distribution of thermal stresses, rather than with structural changes (refinement of the γ-phase, etc.). Also, it should be noted that in cladding the probability of cracking is much lower than

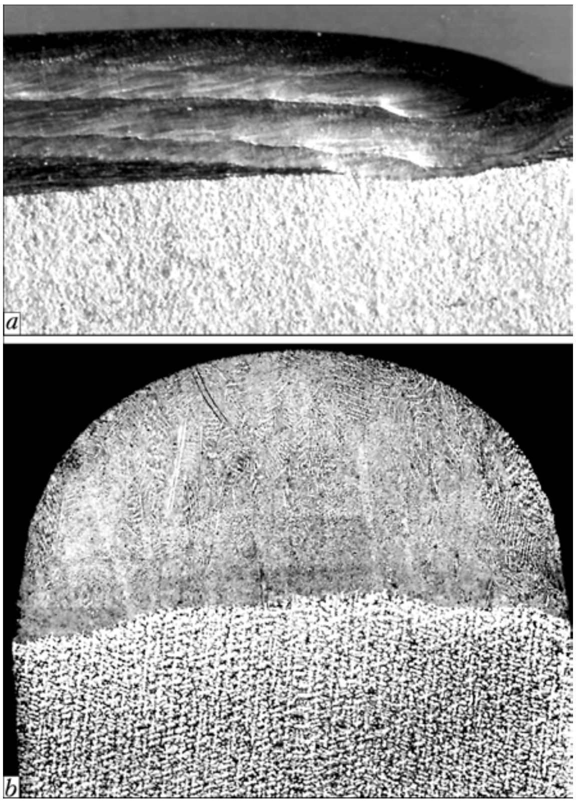

Figure 1. Appearance (*a* ---- ×5) and macrosection (*b* ---- ×25) of three-layer cladding on sample edge (cladding direction [013], cladding plane (100), and section plane (031))

in butt welding, which seems to be associated with peculiarities of distribution of welding stresses across the section of a joint, their values, more favourable shape of the solidification front (see Figure 1), and, hence, perfection of structure of the deposited metal.

The investigations were carried out on longitudinal and transverse sections by the optical metallography and X-ray diffractometry methods. Distribution of the intensity of scattered X-rays near the reciprocal lattice points was evaluated. Regions were examined by irradiation of the surface area measuring 0.3 × 2.0 mm with a reflex located in a direction normal to the plane of the deposited metal, by gradually passing from BM to the deposited metal, the irradiated (examined) area remaining parallel to the fusion line (sample edge). 36 regions were examined on the surface of a sample 10 mm wide. The displacement step was 0.28 mm. The main point of the procedure is described in more detail in studies [7--9].

It can be seen from examination of the pole figures (Figure 2) that orientations of surfaces of the plate and deposited metal (edge being clad) in crystal II of the examined sample are identical and correspond with an accuracy of up to 2° to orientation <100>. In crystal I, orientation of the plate is (013) and that of the deposited metal surface (edge) is <100>. Therefore, the surfaces of the crystals being clad are planes of zone <100>. Morphology of the crystalline structure and crystallography of the clad samples of crystals I and II are shown in Figures 3 and 4. It can be seen from the Figures that the initial crystallographic orientation at a meso-level is inherited very closely at a

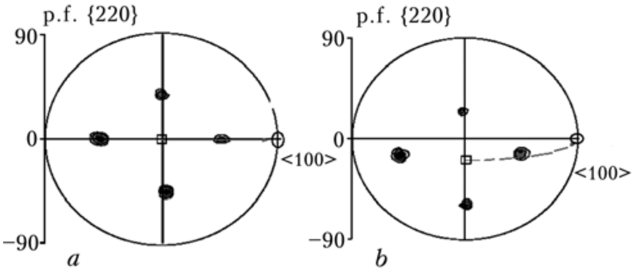

Figure 2. Pole figures {220} for crystals II (*a*) and I (*b*) (square ---- orientation (001)). Cladding direction in crystal II ---- <010> and crystal I ---- <013>, section plane in crystal II ---- {001}, in crystal I ---- {031}

substantial refinement of elements of the weld structure.

As seen from Figure 5, positions of maxima of distribution of $I_{q\parallel}$ of the reflection in BM and deposited metal coincide, i.e. the values of lattice parameters of the γ- and γ′-phases persist [10]. Width of the reflection in the deposited metal grows, compared to BM, by 10--15 % in crystal I, and by 4 % (within the error limits) in crystal II. Therefore, imperfection (dislocation density) of metal structure in cladding on asymmetrically oriented crystal I is much higher than on symmetrically oriented crystal II. However, this increase (difference) is much lower than in welding [8, 9].

The shape and width of distributions of $I_{q\perp}$ of the reflection in BM (Figure 6, *a, e*) are typical for the grown single crystals, i.e. they are smooth in all azimuthal directions, and the iso-intensity lines are elliptical. As seen from Figure 6, *a*, reflection (024) for crystal II is located exactly on a vertical line (355° ---- instrument coordinates in Figure 6; therefore, devia-

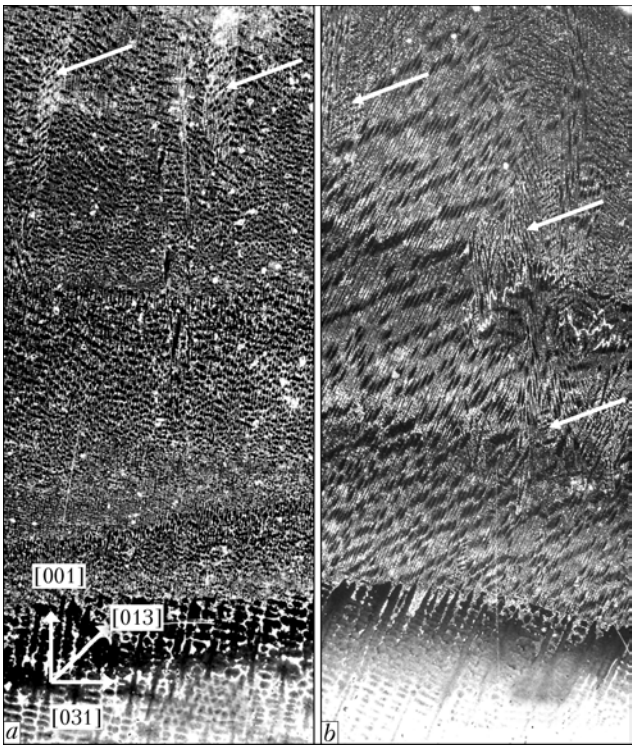

Figure 3. Microsections (×50) and crystallography of clad samples (dark field) of crystal I: *a* ---- longitudinal section; *b* ---- transverse section (arrows ---- stray grains in deposited metal)

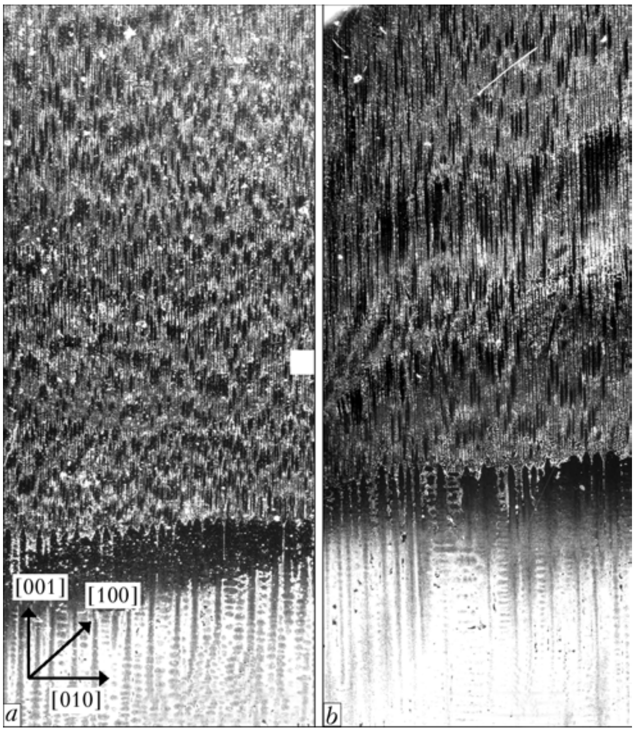

Figure 4. Microsections (×50) and crystallography of clad samples (dark field) of crystal II: *a* ---- longitudinal section; *b* ---- transverse section

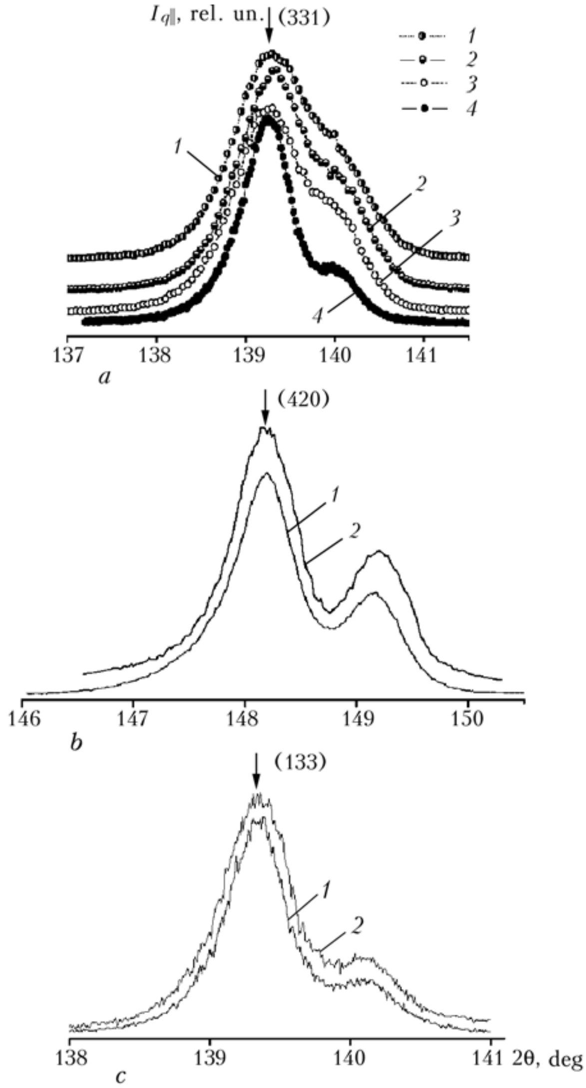

Figure 5. Distribution of intensity $I_{q\|}$ in different regions of a welded joint (*a*): *1* ---- weld metal near FZ; *2* ---- weld axis; *3* ---- HAZ; *4* ---- BM; in deposited metal (*b, c*) (*b* ---- crystal I, reflection (420)); *c* ---- crystal II, (133): *1* ---- BM; *2* ---- deposited metal. Orientation of fusion surface in the welded joint ---- {011}, and in the deposited metal ---- {100}

tion from the vertical is 5°). Arrow in Figure 6, *a* indicates the cladding direction on a section along the fusion line. In HAZ, a change from the initial elliptical shape of distribution of $I_{q\perp}$ can be seen on the iso-intensity lines. Broadening in the cladding direction (Figure 6, *b*) is observed in parallel to the fusion line. It grows in the fusion zone (FZ) (Figure 6, *c*), i.e. there is a turn about the direction normal to the cladding surface. Isolated reflections of a low intensity can be seen in the deposited metal, this being indicative of the presence of stray grains (see Figure 3). Width of the iso-intensity lines in layers which are closest to BM are maximal (Figure 6, *c*). In the layers which are distant from BM (Figure 6, *d*), at an observed broadening in the direction parallel to the fusion line, the width of the reflection decreases normal to the fusion line. Since broadening of the reflex reflects direction of preferred stresses in the sample plane, it can be concluded that substantial longitudinal stresses take place near the fusion line, and that they decrease at the deposited metal surface.

In contrast to crystal II, crystal I has reflection (311) on the vertical (359° ---- instrument coordinates in Figure 6, therefore, deviation from the vertical is 1°). Like in crystal II, in HAZ of crystal I the iso-intensity lines of distribution of $I_{q\perp}$ broaden in a direction parallel to the fusion line, and the elliptical lines transform into the round ones. A turn about a direction normal to dendrites in BM is seen in FZ (Figure 6, *g*), i.e. the broadening projection on the sample plane is normal to the projection of dendrites on the same plane. The reflection of other orientation deviating from the main reflex mainly in a direction of its broadening can be seen even on the fusion line (Figure 6, *g*). Localised, asymmetrical regions of an increased intensity can be seen in distribution of $I_{q\perp}$ in the deposited metal, in the layers adjoining BM, with the reflection width increasing in different directions (Figure 6, *g*), which is also characteristic of the welds. Broadening in different directions, i.e. in a direction normal to the projection of direction of dendrites on the sample plane, as well as in the other directions, is observed in the iso-intensity curves in the layers located at a distance from BM (Figure 6, *h*). Therefore, residual stresses are locally heterogeneous in crystal I, in contrast to crystal II with their homogeneous distribution. Most probably, this is the effect of the asymmetry of crystallographic orientation of the initial single crystal with high-symmetry axes.

It should be noted that, along with a very clear inheritance of the initial crystallographic orientation of the examined single crystals by all the layers of a multilayer cladding (see Figures 3 and 4), one can also see the following peculiarities, which are not that

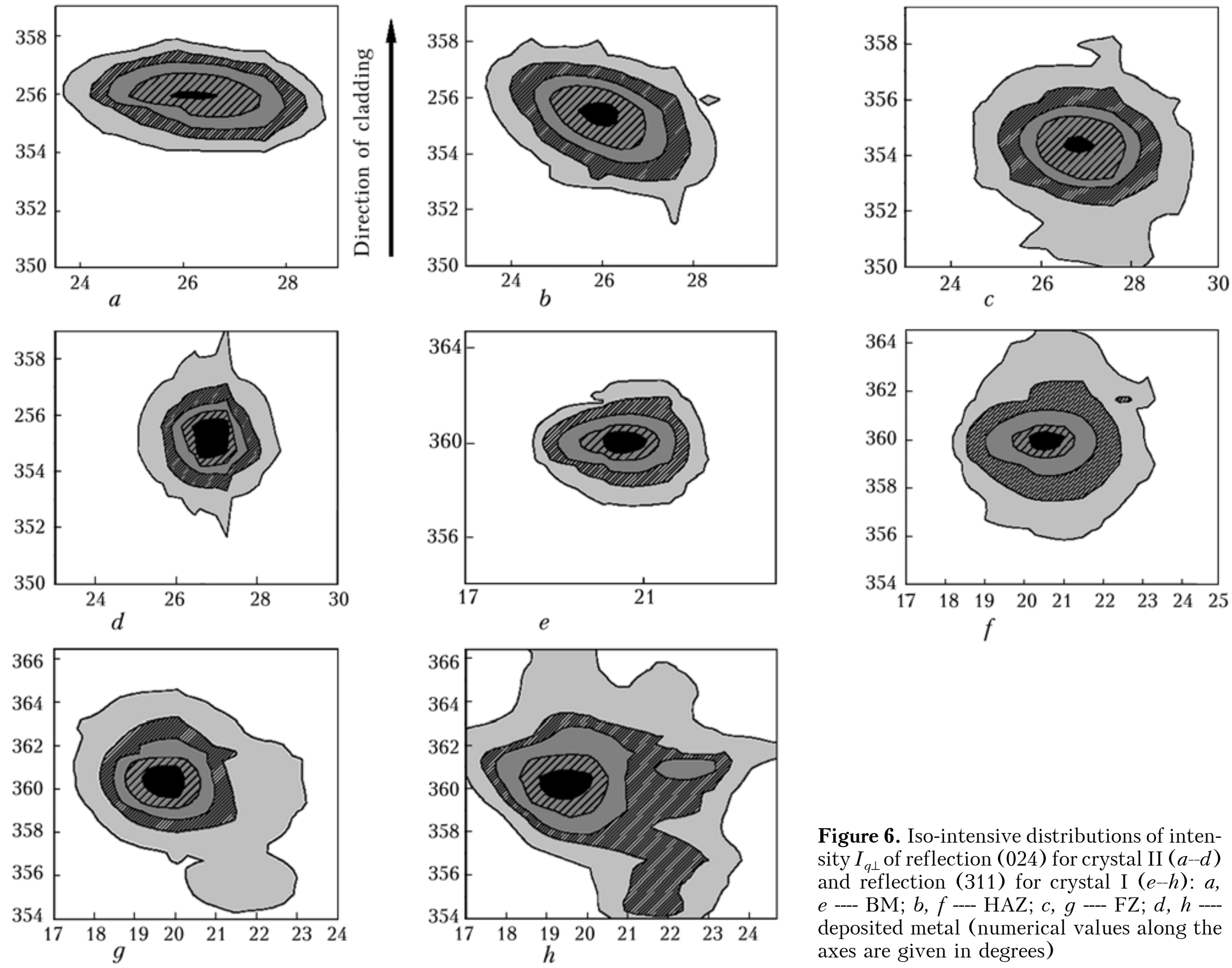

Figure 6. Iso-intensive distributions of intensity $I_{q\perp}$ of reflection (024) for crystal II (*a*–*d*) and reflection (311) for crystal I (*e*–*h*): *a, e* ---- BM; *b, f* ---- HAZ; *c, g* ---- FZ; *d, h* ---- deposited metal (numerical values along the axes are given in degrees)

significant numerically, but are important for understanding of the inheritance mechanism.

Claddings on crystals I and II (Figure 7, *a*) are characterised by a change of 1.5° in orientation in the plane of a section located near FZ. Then, with distance from the fusion line, orientation of the deposited metal becomes close to that of BM. A turn in crystals I and II is approximately identical, but character of this change near FZ is different. The turn in the FZ of crystal II (orientation in the section plane is (001))

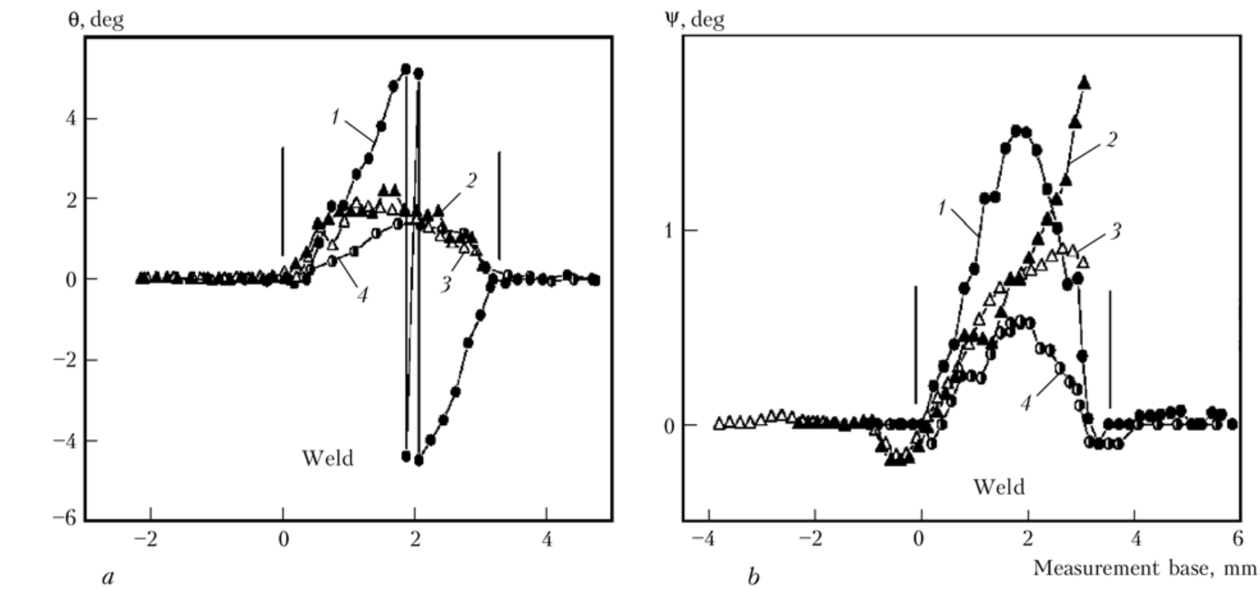

Figure 7. Change in orientation across the section of plate in the welded joint and deposited metal with respect to the fusion surface (*a*) and welding or cladding direction (*b*): *1* ---- fusion surface {110} (15–18° to {310}); *2* ---- {310}; *3* ---- {100}; *4* ---- {100}; «0» ---- FZ of the deposited metal and weld; width of the welds and height of the claddings is approximately 3 mm

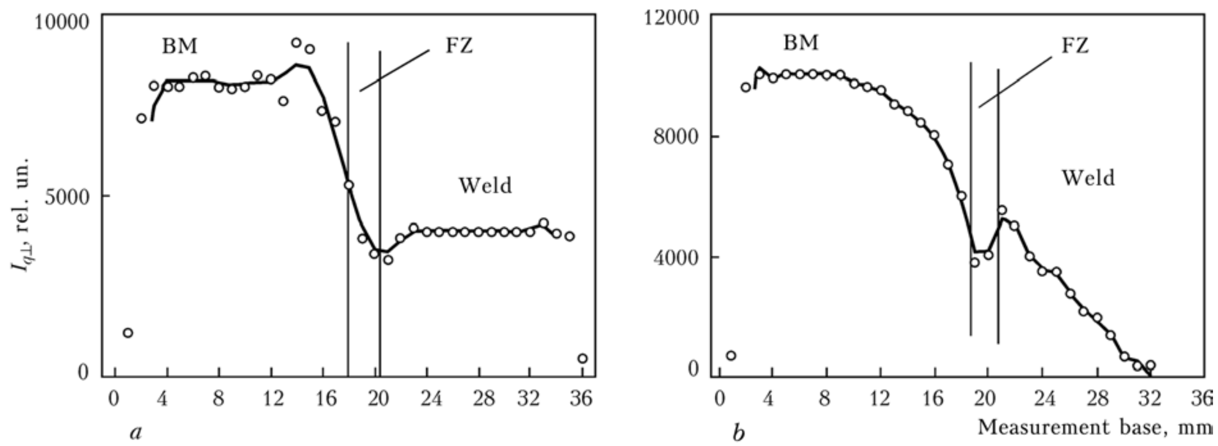

Figure 8. Change in distribution of maximal intensity $I_{q\perp}$ in height of a cladding for crystal I, reflection (420) (*a*), and for crystal II, reflection (113) (*b*)

is smooth, whereas in crystal II (orientation (013)) it is stepwise, with local heterogeneities and fragmentation of crystal appearing in distribution of intensity $I_{q\perp}$ (Figure 8). Most probably, the turn is associated with non-coincidence of the thermal gradient direction with normal to the sample surface (edge) and, hence, the shape of the weld pool solidification front. This leads to a gradual change in orientation in the clad zone for crystal II, and to a stepwise one for crystal I, which seems to be also associated with crystallography of the samples, which is symmetrical for sample II and asymmetrical for sample I.

A change in orientation of the deposited metal relative to the sample surface also takes place in crystals I and II (see Figure 7, *b*). The turn in crystal II is approximately 1°, and in crystal I it is approximately 2°. The change in orientation in crystal II begins from FZ, and in crystal I — from HAZ. The turn in HAZ seems to result from an increased dislocation density (which can be seen from the distribution of intensity $I_{q\perp}$) under the effect of welding stresses. It is likely that the initial crystallographic orientation and turn (2°) are the causes of fragmentation of the crystal (formation of stray grains and local heterogeneity in the distribution of $I_{q\perp}$). Decrease in the change of orientation at the external edge with respect to BM can be seen in crystal II, whereas in crystal I the turn on the external edge of the sample grows.

Apparently, the ratio of direction of the maximal thermal gradient (weld pool shape) to direction of the preferred growth is a key factor affecting peculiarities of structure formation in the deposited metal.

There is a large difference in intensity $I_{q\perp}$ in the deposited metal between crystals I and II (see Figure 8). In crystal II the intensity in the deposited metal at a substantial distance from BM is constant (although it is lower than in BM). In crystal I the intensity in the deposited metal gradually decreases with distance from BM. The following peculiarities can be distinguished in behaviour of the intensity: the intensity of reflection in the deposited metal is much lower (2 times) than in BM (crystal II). Dip of the intensity occurs at an interface between BM and the first layer of the deposited metal. Absolute values of the intensity of reflections may decrease also as a result of refinement of the structure [11], as when the structural components become smaller, and diffraction of radiation on them leads to an irreversible escape of X-ray from the interval of diffraction angles [10, 12]. Examination of microstructure of the deposited metal showed a 5--10 times decrease in distance between dendrites.

It should be emphasised that intensity $I_{q\perp}$ in the deposited metal on crystal II decreases approximately 2 times and remains unchanged in the entire height of the deposited metal. In crystal I with the same refinement of dendrites in the deposited metal, the intensity continuously decreases, which may be related to fragmentation of crystal and appearance of stray grains within the irradiated volume. Stray grains in the deposited metal of crystal I grow in number towards the end in height. This corresponds to the presence of local heterogeneities and formation of stray reflections, in addition to the main ones, in distribution of $I_{q\perp}$ for crystal I. Therefore, the considered character of the change is determined by the fact how close the orientation of the solidification front is to the direction of the preferred growth of the crystal (to what extent they coincide).

Probably, the observed structural and crystallographic changes in height of the deposited metal are also associated with successive intrusion of dendrites with an unfavourable crystallographic orientation, and increase in the quantity of stray grains is related to overcooling of the surface of the deposited metal because of evaporation.

Analysis of the results of investigation of structural changes in the process of cladding on edges of heat-resistant nickel alloy single crystals allows a conclusion that inheritance of the initial structural states and crystallography by the deposited metal obeys the same qualitative mechanisms as in welding [7--9, 12]:

- single-crystallinity and general crystallographic orientation persist;
- clear dependence of inheritance of the initial structural state upon the asymmetry of crystallography of the initial metal (substrate) and cladding (welding) direction takes place;

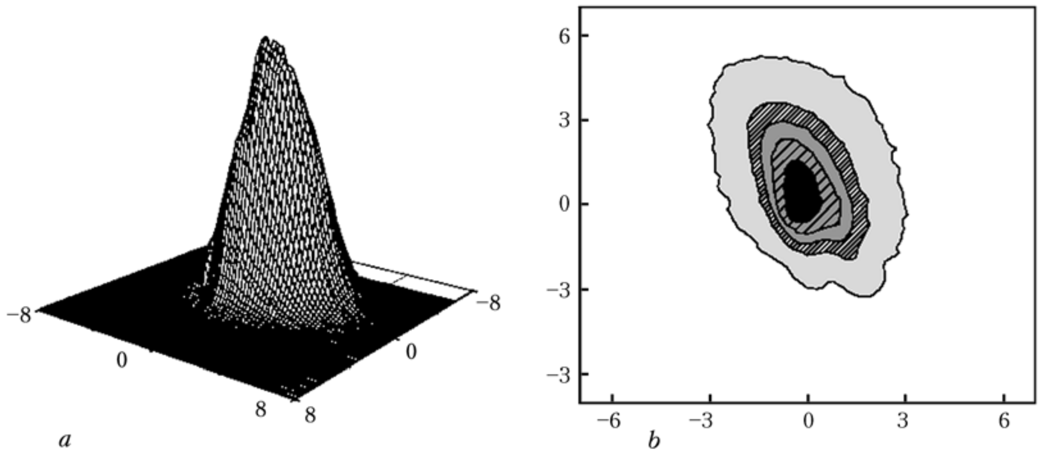

Figure 9. Three-dimensional (*a*) and iso-intensive (*b*) distribution of intensity $I_{q\perp}$ of reflection (311) in the initial material (numerical values along the axes are given in degrees)

• structural components substantially decrease in size, and dislocation density grows in the deposited metal (weld);

• lattice parameters of the γ- and γ′-phases remain almost unchanged (within the error limits) in all regions (see Figure 5);

• formation of cracks in the deposited metal during cladding, like during welding, seems to be promoted by formation of the local stress zones related to the heterogeneous distribution of dislocations.

The following takes place at an edge in the deposited metal because of a flatter shape of the solidification macro front and, hence, more unidirectional heat removal, as well as lower welding stresses compared with the welds:

• more uniform distribution of dislocations (Figures 6 and 10);

• 2–3 times decrease in deviation of crystallographic orientation of the deposited metal from the initial one (see Figure 7);

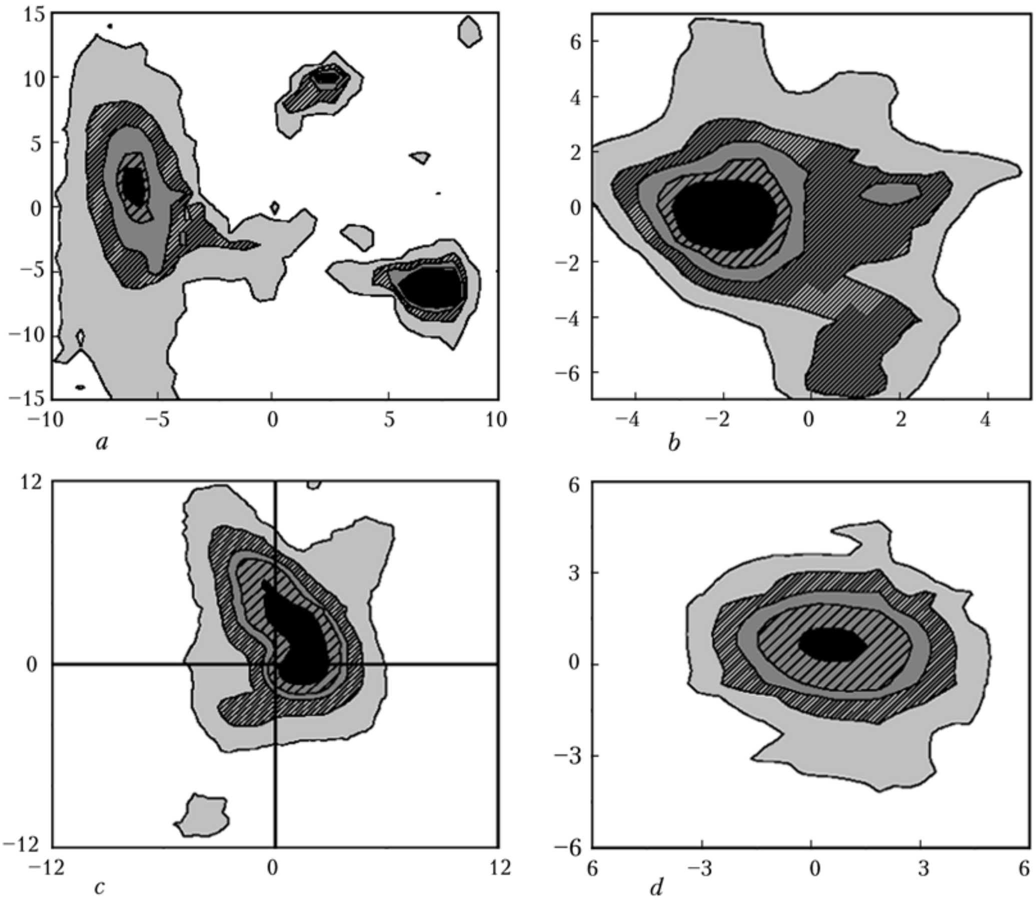

Figure 10. Distribution of intensity $I_{q\perp}$ of reflections (311) in the weld zone (*a*, *c*) and in cladding (*b*, *d*) at different fusion surfaces: *a*–*c* ---- {310}, *d* ---- {100} (numerical values along the axes are given in degrees)

• 8--10 times decrease in the quantity of stray grains at deviation of crystallographic orientation of the clad edges from the direction of high-symmetry axes (Figures 9 and 10);

• growth of dislocation density: for the welds made at low welding speeds (about 10–20 m/h) the dislocation density grows 6–8 times, and at high welding speeds (about 60--80 m/h) it grows 15–20 times, compared with the initial one (see Figures 5, 6, 9 and 10).

CONCLUSIONS

1. The quality of cladding on edges of single crystals of heat-resistant nickel alloys is determined by geometry of the deposited metal, absence of cracks, degree of deviation of crystallographic orientation of the weld from the initial substrate, presence of stray grains, and density, concentration and distribution of dislocations.

2. The sensitivity to cracking depends primarily upon the cladding speed, bead height and crystallographic orientation of the initial metal and weld.

3. The degree of deviation of crystallographic orientation from the initial one, formation of stray grains, density and distribution of dislocations at an almost flat solidification macro front depend mainly upon the crystallographic orientation of the initial single crystal, direction of making of the weld relative to the high-symmetry axes, and perfection of its single-crystalline structure.

4. Inheritance of crystallographic orientation of the initial metal at a sufficiently perfect single-crystalline structure takes place at the investigated parameters and conditions of cladding on edges of single crystals of heat-resistant nickel alloys.

5. Cladding on edges of single crystals of casting heat-resistant nickel alloys of the JS-26 type is recommended to perform on a material oriented close to the high-symmetry axes by using the 1.0--1.5 mm thick filler metal of the same chemical composition, at a height of metal deposited per pass equal to no more than 2 mm. The recommended cladding speed is 10–15 m/h.

1. Smolin, A.A., Sporyagina, N.M. (1976) Evaluation of mechanical damageability of compressor rotor in service. In: *Resource and reliability of gas turbine engines*. Moscow: TsIAM.
2. Ilchenko, G.A., Andreev, V.I., Guseva, T.P. (1979) Analysis of service defects and problems of repair of gas turbine engine blades. In: *Proc. of 9th Conf. of Junior Scientists of NIAT*. Moscow: NIAT.
3. Kablov, E.N. (2001) *Cast blades of gas turbine engines. Alloys, technology, coatings*. Moscow: MISIS.
4. Pollock, T.M., Murphy, W.H. (1996) The breakdown of single-crystal solidification in high refractory nickel base alloys. *Metall. Mater. Transact. A*, **27**, 1081--1094.
5. Park, J.-W., Baby, S.S., Vitek, J.M. et al. (2003) Stray grain formation in single crystal Ni-base superalloy welds. *J. Appl. Phys.*, 94(**6**), 4203--4209.
6. Gaumann, M., Bezencon, S., Canalis, P. et al. (2001) Single crystal laser deposition of superalloy. *Sci. and Technol. of Adv. Materials*, **49**, 1051--1062.
7. Zadery, B.A., Kotenko, S.S., Polishchuk, E.P. et al. (2003) Peculiarities of crystalline structure of welded joints in single crystals. *The Paton Welding J.*, **5**, 13--20.
8. Yushchenko, K.A., Zadery, B.A., Karasevskaya, O.P. et al. (2006) Structural changes in welding of single crystals of nickel superalloys in crystallographically asymmetric position of the welding pool. *Metallofizika i Nov. Tekhnologii*, 28(**11**), 1509--1527.
9. Yushchenko, K.A., Zadery, B.A., Zvyagintseva, A.V. et al. (2008) Sensitivity to cracking and structural changes in EBW of single crystals of heat-resistant nickel alloys. *The Paton Welding J.*, **2**, 6--13.
10. (1961) *Radiography in physical materials science*. Ed. by Yu.A. Bagaryatsky. Moscow: Metallurgizdat.
11. Ovsienko, D.G., Sosnina, E.I. (1956) On production of single crystals of predetermined orientation from melts. *Fiz.-Khimich. Mekhanika Materialov*, **2**, 16--18.
12. Yushchenko, K.A., Zadery, B.A., Savchenko, V.S. et al. (2008) Welding and cladding of heat-resistant nickel alloys with single-crystal structure. *The Paton Welding J.*, **11**, 191--196.

EFFECT OF CONCENTRATION OF HARD PARTICLES ON GAS-ABRASIVE WEAR RESISTANCE OF COMPOSITE ALLOY

A.P. VORONCHUK
E.O. Paton Electric Welding Institute, NASU, Kiev, Ukraine

Effect of the concentration of hard particles on wear resistance of composite alloys is considered. The selectivity of wear of composite alloys is shown. Calculation of wear resistance of a composite alloy has been made by using the additivity rule, and comparative data on this alloy have been obtained by experiments.

Keywords: *arc cladding, cladding composite alloys, hard particles, wear resistance, concentration of particles, gas-abrasive wear*

Effect of the concentration of hard particles on wear resistance of cladding composite alloys is insufficiently studied. Achievement of a different and specified concentration of hard particles in the matrix during cladding of composite alloys involves difficulties. This is associated with the fact that hard particles, e.g. tungsten carbides, sink in the weld pool, their distribution in it being very non-uniform. Therefore, the concentration of tungsten carbide particles in the initial charge is assumed to be the concentration of these particles in a composite alloy [1]. However, this assumption is inadmissible for induction cladding.

Special model samples with a preset concentration of hard particles in the wear plane were made for the experiments described below. A recess was turned in a billet of steel 45, which was filled with one layer of special 1.0 mm beads of alloy VK8. Gaps between the beads were filled with a powder of a binding nickel alloy of the Colmonoy type, having the following chemical composition, wt.%: 15 Cr, 4.5 Si, 4.0 Fe, and 3.75 B. A sample was heated up to melting of the binding alloy between two graphite electrodes by using projection resistance machine MR-8001. The required concentration of the VK8 particles in the wear plane was provided by grinding of the composite layer to a certain depth. This caused a change in cross section diameter of a bead in the wear plane. However, this change was small and not exceeded the range within which the value of wear depends but insignificantly upon the particle size [2, 3]. Samples of three concentrations of the particles were produced in this way, vol.%: 30–32, 49–53, and 73–77. Microhardness of the alloy matrix was 4200–5860, and that of the VK8 particles was 20780–22140 MPa.

The tests were carried out by using the OB-876 machine under the following conditions: jet attack angle — 30°, abrasive — quartz sand, and excessive pressure ahead of the nozzle — 0.24 MPa. Wear was evaluated from the loss of weight of the samples and by plotting profilograms of the worn-out surface. Relative wear resistance of the composite alloy was determined by comparing it with wear of annealed low-carbon steel. The kinetics of wear of the composite alloy can be considered by conducting tests (at a constant consumption of an abrasive) depending upon the test time determined by the consumption of the abrasive. Here two approaches can be used to analyse the wear process. With the first approach, the relative wear resistance after each measurement is determined as

$$\varepsilon = \frac{\Delta m_r}{\Delta m_c}, \tag{1}$$

where Δm_r and Δm_c are the losses of weight of a reference sample and sample of the composition tested from the beginning of the test up to a given measurement.

Relative wear resistance ε is determined on the basis of the total losses of weight of the samples during the total test time. Figure 1 shows a change in relative wear resistance ε depending upon the consumption of the abrasive for compositions with a different concentration of the VK8 particles. Some decrease in ε takes place at the beginning of the tests. Then, as the test time increases, the relative wear resistance reaches some constant value, which depends upon the concentration of a wear-resistant component of the alloy. Increase in the concentration of the wear-resistant component in the alloy is accompanied by increase in ε. Some decrease in ε in the initial period of the tests is related, most probably, to exposure of the VK8 particles and bombardment of their side faces at a high attack angle, this leading to an accelerated wear of the particles.

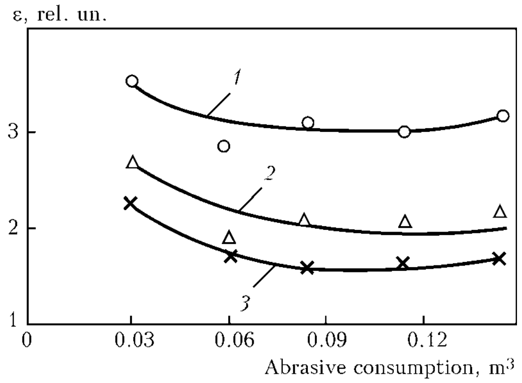

Figure 1. Dependence of total relative wear resistance ε upon the consumption of abrasive at different concentrations of particles in the composition: *1* — 75; *2* — 52; *3* — 30 %

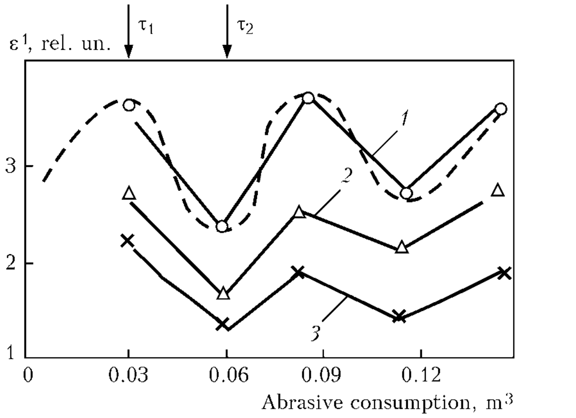

Figure 2. Dependence of discrete relative wear resistance ε^1 of the composite alloy upon the consumption of abrasive at different concentrations of the VK8 particles: *1* –– 75; *2* –– 52; *3* –– 30 %; dashed curve –– theoretical

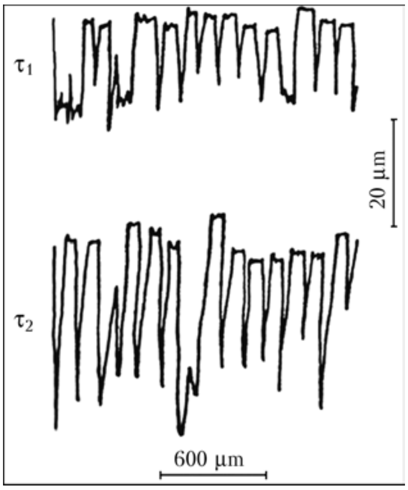

Figure 3. Profilograms of worn-out surface of the composite alloy with concentration of the hard particles equal to 75 vol.% (τ_1 and τ_2 –– see Figure 2)

The kinetics of wear of the composition can also be considered discretely during separate time periods. In this case, relative wear resistance ε^1 is determined as follows:

$$\varepsilon^1 = \frac{m_{n-1,\,\mathrm{r}} - m_{n,\,\mathrm{r}}}{m_{n-1,\,\mathrm{c}} - m_{n,\,\mathrm{c}}}, \qquad (2)$$

where $m_{n-1,\,\mathrm{c}}$ and $m_{n-1,\,\mathrm{r}}$ are the weights of samples of the composition and reference sample in previous weighing, respectively; and $m_{n,\,\mathrm{c}}$ and $m_{n,\,\mathrm{r}}$ is the same in subsequent weighing.

Variation of ε^1 with time is of a cyclic character (Figure 2). This character of variations in ε^1 should be attributed to the selectivity of wear of the composition. Consider one cycle. The first to wear is a comparatively less wear-resistant matrix, and ε^1 of the composition decreases. Then the projecting reinforcing particles prevent the matrix from further destruction, and mostly they start wearing out. The value of ε^1 grows. Gradually, with wear of the reinforcing particles, the favourable shadow effect for the matrix diminishes, and the intensive wear of the matrix recommences, the cycle is repeated. The character of the cycle (deviation of ε^1 from an average value, cycle duration, etc.) depends upon the concentration of the reinforcing particles, difference in physical-mechanical properties of the matrix, and different ability of the composition components to resist wear at different attack angles used during the tests. The fact that the intensity of wear of the matrix grows in a time period (see Figure 2) is proved by the profilograms of the worn-out surface shown in Figure 3. Valleys in the profilogram correspond to a depth of wear of the composition matrix. The lower the concentration of the reinforcing particles, the larger is the depth of the valleys. Thus, at an abrasive consumption of 0.06 m^3, the mean depth of the valleys for samples with the concentrations of the VK8 particles equal to 75, 52 and 30 % was 21.2, 30.9 and 35.4 μm, respectively.

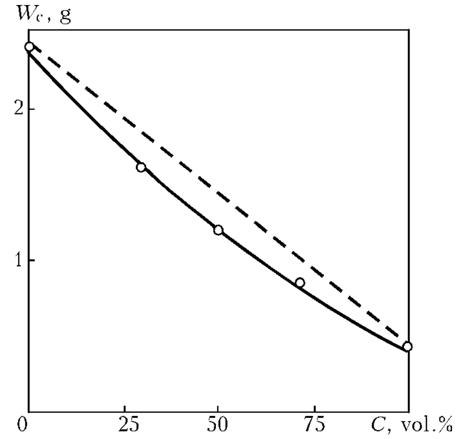

Figure 4. Effect of concentration of hard particles on wear of composite alloys: solid curve –– experimental data; dashed curve –– calculation using equation (*3*)

Determine whether wear W_c of the «hard particle–matrix» composition obeys the additivity rule:

$$W_\mathrm{c} = W_r C_r + W_\mathrm{m}(1 - C_r), \qquad (3)$$

where W_r and W_m are the values of wear of the particles and matrix, respectively; and C_r is the volume content of the particles in the composition.

The model samples, i.e. matrix and sintered alloy VK8, were subjected to gas-abrasive wear at an attack angle of 30°. Quartz sand was used as an abrasive, and low-carbon steel was used as a reference, like in the previous experiments. The test results are shown in Figure 4.

According to the experimental data, wear of the matrix (alloy of the Colmonoy type) was 2.74 g, and that of the VK8 hard particles was 0.46 g. Wear of composite alloys with content of the hard particles equal to 30 vol.% was 1.62 (experiment) and 1.916 (calculation). Wear of composite alloys with 52 vol.% content of the hard particles was 1.24 (1.396), and that with 75 vol.% –– 0.91 (0.947).

Therefore, the difference between the experimental and calculated results for wear is about 12 %. The calculation of wear of the composite alloy by using the additivity rule leads to substantial errors caused by the selectivity of wear of the composition components.

1. Klejs, I.R., Stupnitsky, A.M., Pirogov, S.Ya. (1977) Wear of composite tungsten carbide based alloys caused by a sliding jet of abrasive. *Avtomatich. Svarka*, **5**, 60–61.
2. Yuzvenko, Yu.A., Zhudra, A.P., Frumin, E.I. et al. (1972) Peculiarities of gas-abrasive wear of composite alloys. *Ibid.*, **8**, 35–38.
3. Yuzvenko, Yu.A., Zhudra, A.P., Frumin, E.I. (1973) Abrasive wear of composite alloys. *Ibid.*, **7**, 62–63.

THESES FOR SCIENTIFIC DEGREES

E.O. Paton Electric Welding Institute of the NAS of Ukraine

V.V. Kurenkova (E.O. Paton Electric Welding Institute) defended on the 17th of June 2009 her thesis for the Candidate of Technical Sciences Degree on subject «High-Temperature Brazing of Casting Heat-Resistant Nickel Alloys Using Boron- and Silicon-Containing Filler Metal». The thesis is dedicated to investigation of materials science aspects of producing brazed joints on casting heat-resistant nickel alloys for repair of heat-loaded parts of gas turbine engines and power units. One of the problems of repair brazing is low ductility of the seam and seam--substrate diffusion zone, which is caused by heterogenisation of structure and precipitation of central-axis or interdendrite boride/carboboride eutectics in the brazed seam metal during solidification.

The goal of the thesis is to develop a method for neutralisation of the negative effect of boron in composite filler metal NiCoCrAl--2.5 % B + Rene-142 used as a charge by adding to it 15--25 wt.% of filler metal Ni--12 % Si of the eutectic composition. Diffusion of boron into the alloys being brazed was decreased, liquidus temperature of the complex filler metal was lowered by 60 °C, and high homogeneity of the seam metal in short-time (10--25 min) high-temperature (1200--1230 °C) brazing in vacuum was achieved by using a mutual effect of boron and silicon (as two interstitial elements) and partial diluting the filler metal melt with nickel. Precipitation of dispersed carboboride phases uniformly distributed in the seam, the volume content of which after heat treatment was f = 4.2--5.9 %, and shape of the carbide particles close to the globular one provided increase in the technological ductility and strength of the brazed joints.

Adding powder of filler metal Ni--12 % Si to composite filler metal NiCoCrAl--2.5 % B + 60 wt.% Rene-142 excludes formation of boride eutectics γ-Ni + + CrB, the formation of which leads to decrease in heat resistance of the brazed seam and brittle fracture of the joints below the yield point. Alloying with silicon decreases the level of internal stresses of the crystalline lattice of matrix solution of the filler metal, while boron, according to the X-ray diffraction examination data, precipitates mostly in the form of dispersed inclusions Ni_3B along the boundaries of the γ/γ'-phases during solidification of the seam.

Systematic investigations were carried out to study microstructure, phase composition, strength and ductility of metal of the brazed joints on alloys ChS70VI, VJL12U, JS26VI and NK.

Quality factor ($\sigma_{tBJ}/\sigma_{tBM}$) at 20 °C was 0.92--1.0, depending upon the type of alloys being brazed. It was established that width of the technological gap (or natural capillary) within a range of 50--950 μm has no effect on strength of the brazed joint on alloy JS26NK at room temperature with a minimal width of the mutual diffusion zone at an interface with the metal brazed. Depth of a reliable brazed seam in the bulk of a blade was 4 mm. Long-time strength at 900 °C slightly decreased with increase in the gap width. At a long-time high-temperature load effect, diffusion of boron into the base metal after 22 h reached 3 mm on the brazed joints formed by using a boron-containing filler metal. In the case of using a boron- and silicon-containing filler metal, after 68 h of long-time tests the diffusion zone did not exceed 120 μm.

100 h gas-dynamic tests were conducted (at the Institute for Strength Problems of the NAS of Ukraine) on fragments of shutters of alloy VJL12U with the cracks repaired by brazing (thermal cycle time τ = 90 s; T_{max} = 1000 °C). No fracture of fragments of the shutters was detected, thus proving fitness of the repaired parts for further operation.

E.O. Paton Electric Welding Institute of the NAS of Ukraine

V.D. Poznyakov (E.O. Paton Electric Welding Institute) defended on the 24th of June 2009 his doctoral thesis on subject «Weldability of High-Strength Steels in Repair of Durable Structures». The thesis is dedicated to investigation of peculiarities of formation of structure and welding stresses in joints on high-strength steels with tensile strength of 350--800 MPa, which were welded under rigid restraining conditions, evaluation of the effect of this factor on changes in mechanical properties and resistance of these joints to brittle, delayed and fatigue fractures, and development of theoretical principles and practical measures providing increase of the technological and service strength of the repaired metal structures.

The character of variations in strength properties of HAZ of high-strength steels under conditions of continuous heating–cooling of metal according to the welding thermal cycle was studied. It was shown that an intensive decrease of 600–800 MPa to 90--130 MPa in yield stress and strength of the high-strength steels heated above the A_{c3} temperature occurred in a temperature range of 400--780 °C. At the same time, elongation and reduction in area of metal increased by 40--50 %, the metal transforming into the thermal plastic condition. Strength properties of the metal monotonously increased during the cooling process. Dramatic changes in yield stress (with an intensity of up to 45--65 MPa/°C in formation of bainite, and 120--145 MPa/°C in formation of martensite) took place in the initial period of structural transformations. Strength at this moment reached the ultimate values for specific steels and cooling conditions. Formation of the above structures was accompanied by increase in volume of the metal, this causing its increase to a level the relative values of which might change from 0.18 to 0.47 %, depending upon the chemical composition of steel and cooling rate of specimens. The set of the generated data made it possible to widen notions on the kinetics of development of temporary stresses within the heat-affected zone of structurally unstable high-strength steels. It was experimentally proved that dislocation structure and properties of the deformed metal changed under the effect of residual stresses, the value of which amounted to $0.8\sigma_{0.2}$ of this metal. It was shown that this process is related to development of low-temperature plastic deformation, generation of dislocations and evolution of the dislocation structure. Intensive interaction of dislocations promotes formation of new sub-grains and fragmentation of structure. Fragments become finer with increase in load, and their disorientation grows. The combination of these factors leads to an 8--12 % increase in values of microhardness and yield stress of the metal. Formation of local regions with an increased dislocation density favours development of brittleness of the metal, as a result of which its cold resistance decreases by 25--40 %. Welding stresses have a stronger effect on cold crack resistance of welded joints. The degree of this effect depends upon the composition and properties of the base and deposited metals, as well as upon the saturation of welds with diffusible hydrogen. It was shown that at moderate ($w_{6/5} \leq 10$ °C/s) cooling rates and a limited content of diffusible hydrogen in the deposited metal equal to 4 ml/100 g, the probability of initiation of cold cracks in rigidly restrained welded joints on steels with C_{eq} = = 0.35--0.40 % would be minimised if $\sigma_{res} \leq 0.9\sigma_{0.2}$, and with C_{eq} = 0.45–0.55 % and C_{eq} = 0.60–0.70 % ≈ ≈ $0.7\sigma_{0,2}$ and $0.5\sigma_{0.2}$, respectively. It was proved that increase in cooling rate $w_{6/5}$ of welded joints to 25 °C/s and hydrogen content to 16 ml/100 g causes the need to reduce residual stresses, which are permissible in terms of formation of cold cracks, 1.7–1.9 times at C_{eq} = 0.35--0.55 %, and 2.5 times at C_{eq} = = 0.60--0.70 %.

It was experimentally found that the level of transverse and longitudinal stresses can be lowered, the latter by 20--25 %, due to welding by the block method with a layer-by-layer peening of the deposited metal, as well as due to adjustment of the composition of welding consumables and limitation of welding parameters.

It was established that resistance of welded joints to fatigue and brittle fracture after the first and second repair could be restored in full. No substantial changes in structure of the weld and HAZ metals were observed. They occur after numerous (not less than 3-fold) thermal and force effects on the metal, which take place in repair and cyclic loading of the welded joints and show up in an increased heterogeneity of structure. Tensile strength of T-specimens decreased as a result of such changes after the third repair by 30--50 %, and after the fourth repair it decreased almost twice. A marked decrease in values of K_{Ic} and δ_c (more than by 30 %) occurred after the fourth repair. Factors determining the insufficient strength of the low-alloy and high-strength steel joints repaired by welding were analysed. It was shown that fatigue life of the T-joints could be increased more than twice by employing the welding technology based on the use of the combined welds, where the root and filling layers are made with traditional welding consumables for the given steels, providing the required strength and cold resistance, and a cover (cladding) layer is made with the consumables allowing decrease in the stress raiser in the weld to base metal transition locations, or with austenitic-martensitic consumables with a lower (below 200 °C) temperature of beginning of martensitic transformation, favouring formation of compressive stresses in the welds.

PETRANIEVSKY READINGS (DEVOTED TO 70th ANNIVERSARY OF CREATION OF UONI-13 ELECTRODES)

International scientific and technical conference «Welding Consumables» took place at FSUE «Central R&D Institute of Materials» in St.-Petersburg on May 18–22. It was dedicated to an outstanding event in the history of welding science and engineering — 70th anniversary of creation of a range of high quality UONI-13 electrodes in this Institute (former R&D Institute-13). This product played an excetionally important role in production of armored defense vehicles, artillery and in military shipbuilding during the Great Patriotic War and the post-war period in all branches of machine- and shipbuilding, in construction of electric power stations, bridges, pipelines, in transport, etc. At present time indicated electrodes and their modifications make up a significant part of output of high quality electrodes for welding highly loaded structures for critical applications in Russia and other countries of the post-Soviet space.

130 specialists, institute professors and post-graduate students, including 2 Academicians and 2 Corresponding Members of the RAS and NAS of Ukraine, 14 General Directors of enterprises-manufacturers of welding consumables, 13 professors and doctors as well as 37 candidates of science in engineering took part in the Conference activities or were co-authors of papers. 38 papers on topical issues of improvement of welding consumables, their production and development of raw material sources, as well as arc welding technologies were made at the Conference. Many-sided and highly productive activity of Konstantin V. Petran was broadly covered in the detailed paper «Konstantin Vatslavovich Petran — prominent Russian scientist in the welding field» by Yu.M. Belov and V.B. Vikhman.

Competition among young scientists and post-graduates for the best papers on the works, which are of scientific and practical importance for development of welding engineering, was conducted within the framework of the Conference.

In the light of present achievements in the area of development and improvement of welding consumable manufacture in CIS, increase of requirements to their quality for improvement of performance and safe operation of welded structures, from one side, as well as taking into account the critical state in most of the areas of machine-building and expansion of foreign manufacturers into the CIS market of welding consumables, from the other side, Conference participants developed a range of recommendations on improvement of welding consumables quality and competitiveness.

A collection of papers of Conference materials was issued, which includes 38 papers of leading specialists of Russia and Ukraine in area of welding consumables manufacture and development of welding practices. Different aspects of development, production and application of electrodes, fluxes and flux-cored wires as well as new sources of minerals for their production are considered.

The number of papers was dedicated to simulation during development of welding consumables, investigation metallurgical processes, peculiarities of heating, cooling and structure formation in welded joints.

A lot of attention was given to international and Russian standardization in the field of welding, certification of welding consumables and international system of quality management in welding engineering, including manufacture of welding consumables.

TO CENTENNIAL OF BIRTH OF G.V. RAEVSKY

Georgy Vladimirovich Raevsky, a well-known scientist in the field of welded structures, Doctor of Science in engineering, laureate of Lenin Prize and State Prize of the USSR, would celebrate his 100th anniversary on July 7. After graduation from the Dnepropetrovsk Institute of Transportation Engineers in 1932, he started his engineering activity in «Dneprostroj» management, leading the engineering operations in mounting of open-hearth, blast-furnace shops and some other facilities of «Zaporozhstal». He was invited in 1934 to work in Moscow in «Promstrojproekt» Institute, where for two years he was involved in project work of the second stage of Magnitostroj. Since 1963 and up to the end of his life Georgy V. Raevsky had been succefully working at the E.O. Paton Electric Welding Institute on development of different structures, first as a senior researcher and since 1939 as Laboratory Head and later as Department Head. In the prewar years comprehensive investigations of railway car welded structures were carried out with direct participation of G.V. Raevsky under the leadership of Evgeny O. Paton, academician of AUAS, which resulted in development of a new design of welded railway car that allowed a significant metal saving. During the Great Patriotic War, Georgy V. Raevsky was in Nizhny Tagil in the Urals together with Institute. In this period under the leadership of academician E.O. Paton and with participation of G.V. Raevsky important work on improvement of technological effectiveness of tank bodies was carried out, scheme of production line for welding of T-34 tank body in assembled form was proposed and developed. This allowed a significant widening of the volumes of automatic submerged-arc welding application in tank production and noticeably shortening the time of their construction.

Method of industrial production of outsized welded tanks for oil and oil products storage by the coiling technique, yielding a significant technical and economic effect, that was proposed by G.V. Raevsky in 1944, developed and widely introduced under his leadership together with other organizations of Minmontazhspetsstroj of USSR and Ukr. SSR, received worldwide recognition. New technology created favorable conditions for improvement of structure quality, reduction of labor consumption and cost of tank construction, significant shortening of construction time. In 1958 G.V. Raevsky, as work supervisor, and a group of other specialists of the national economy, was awarded the Lenin Prize for development and implementation of the industrial method of construction of oil tanks from flat panels coiled into rolls. The task of industrial cost-effective method of manufacture of a number of outsized thick-walled welded cylindrical structures was solved with the technology of temporary deformation developed at the E.O. Paton Electric Welding Institute by the suggestion of G.V. Raevsky. During investigations aimed at improvement of welded structure reliability, a package of works on improvement of the design and manufacturing technology of welded rotating cement and other furnaces was carried out at the E.O. Paton Electric Welding Institute at the suggestion of Georgy V. Raevsky, that allowed using the industrial method of production of furnace body shells on the basis of the method of temporary deformation, developing a new support system on pneumocushions, that prevents support overloading, finding a new solution of support unit with usage of welded band. G.V. Raevsky is one the authors of the development of welded pressure vessels of a new design, so called multilayer coiled vessels. Investigations of new design with participation of G.V. Raevsky showed its significant advantage over the vessels with a solid wall in terms of production simplicity and service reliability, and this became the base for establishing the fabrication of multilayer apparatuses for large-capacity chemical and petrochemical productions in the USSR. In 1976 G.V. Raevsky was awarded the State Prize of the USSR for work on establishment of industrial production of the multilayer variant of pressure apparatuses in the USSR.

G.V. Raevsky is the author of more than 150 scientific works, author of more than 30 important developments; he has over 50 foreign patents. He was a member of academic councils of the E.O. Paton Electric Welding Institute and Kiev Construction Engineering Institute, member of editorial board of «Avtomaticheskaya Svarka» journal. His work was marked by governmental awards.

His pupils, colleagues and all those who knew him, will always keep the blessed memory of Georgy V. Raevsky, an outstanding person and scientist.